THE RNA-BINDING PROTEIN, IMP, GENERATES NEURAL DIVERSITY IN THE *DROSOPHILA* TYPE 2 NEUROBLAST LINEAGE

by

JORDAN ALISSA MUNROE

A DISSERTATION

Presented to the Department of Biology
and the Division of Graduate Studies at the University of Oregon
in partial fulfillment of the requirements
for the degree of
Doctor of Philosophy

March 2024

DISSERTATION APPROVAL PAGE

Student: Jordan Alissa Munroe

Title: The RNA-Binding Protein, Imp, Generates Neural Diversity in the *Drosophila* Type 2 Neuroblast Lineage

This dissertation has been accepted and approved in partial fulfillment of the requirements for the Doctor of Philosophy degree in the Department of Biology by:

Judith Eisen	Chairperson
Chris Doe	Advisor
Tory Herman	Core Member
Cris Neill	Core Member
Scott Hansen	Institutional Representative

and

Krista Chronister	Vice Provost for Graduate Studies

Original approval signatures are on file with the University of Oregon Division of Graduate Studies.

Degree awarded March 2024

© 2024 Jordan Alissa Munroe

This work is licensed under a Creative Commons
Attribution-NonCommercial-NoDerivs (United States) License.

DISSERTATION ABSTRACT

Jordan Alissa Munroe

Doctor of Philosophy

Department of Biology

March 2024

Title: The RNA-Binding Protein, Imp, Generates Neural Diversity in the *Drosophila* Type 2 Neuroblast Lineage

Neural diversity generated during development is required to produce a fully functioning nervous system. Thousands of neurons precisely target their axons to the relevant post-synaptic partners to create neural circuits that generate proper sensory and motor behavior at the organismal level. A lack of neural diversity can cause improper circuit formation. In *Drosophila*, temporal patterning within neural stem cells aids in the correct regulation and generation of neurons. *Drosophila* neural stem cells, or neuroblasts (NBs), within the central brain express opposing temporal gradients of the RNA-binding proteins, Imp and Syp. Here I show that a subset of central brain NBs, known as type 2 NBs (T2NBs) all express Imp in a high-to-low expression pattern early in *Drosophila* neurogenesis, while Syp expression is dependent upon the T2NB lineage.

Unique to T2NBs, compared to other *Drosophila* neuroblasts, is the generation of intermediate neural progenitors (INPs) which are necessary for expansion of neural number and diversity in the *Drosophila* central complex (CX), an adult brain structure required for celestial navigation. Upon their generation, I have shown that newborn INPs express equivalent Imp and Syp levels as T2NBs and form high-to-low expression gradients throughout the INP lineage. However, Imp levels increase in old INPs where I show it is required for the proper generation of

E-PG and PF-R neurons in the CX. Loss of Imp in old INPs causes morphological defects while Imp overexpression causes abnormal neurite morphology. Finally, I highlight Imp's minor role in post-mitotic morphogenesis of PF-R and P-FN neurons in the adult CX. Loss or overexpression of post-mitotic Imp causes only minor changes in PF-R and P-FN neuropil volume.

This dissertation includes previously published co-authored material.

Supplemental Video 3.1 Imaris reconstruction of T2NBs in larval brain

CURRICULUM VITAE

NAME OF AUTHOR: Jordan Alissa Munroe

GRADUATE AND UNDERGRADUATE SCHOOLS ATTENDED:

University of Oregon, Eugene
Boise State University, Boise

DEGREES AWARDED:

Doctor of Philosophy, Biology, 2024, University of Oregon
Bachelor of Science, Biology, 2018, Boise State University

PUBLICATIONS:

Munroe, J.A. & Doe, C. Q. (2023). Imp is expressed in INPs and newborn neurons where it regulates neuropil targeting in the central complex. *Neural Development*. (Accepted).

Hamid A, Gutierrez A, Munroe J, Syed MH. (2023). The Drivers of Diversity: Integrated genetic and hormonal cues regulate neural diversity. *Semin Cell Dev Biol*. 2:23-35. doi: 10.1016/j.semcdb.2022.07.007.

Munroe, J. A., Syed, M. H., & Doe, C. Q. (2022). Imp is required for timely exit from quiescence in Drosophila type II neuroblasts. *PLOS ONE*, *17*(12), e0272177. https://doi.org/10.1371/journal.pone.0272177

LaFoya B, Munroe JA, Albig AR. (2019). A comparison of resveratrol and other polyphenolic compounds on Notch activation and endothelial cell activity. *PLOS ONE*. 14(1), e0210607. doi: 10.1371/journal.pone.0210607.

LaFoya B, Munroe JA, Pu X, Albig AR. (2018). Src kinase phosphorylates Notch1 to inhibit MAML binding. *Scientific Reports*. 8(1):15515. doi: 10.1038/s41598-018-33920-y.

LaFoya B, Munroe JA, Miyamoto A, Detweiler MA, Crow JJ, Gazdik T, Albig AR. (2018). Beyond the Matrix: The Many Non-ECM Ligands for Integrins. *Int J Mol Sci*. 19(2):449. doi: 10.3390/ijms19020449.

LaFoya B, Munroe JA, Mia MM, Detweiler MA, Crow JJ, Wood T, Roth S, Sharma B, Albig AR. Notch: A multi-functional integrating system of microenvironmental signals. *Developmental Biology*. 418(2):227-41. doi: 10.1016/j.ydbio.2016.08.023.

ACKNOWLEDGMENTS

I wish to express sincere thanks and appreciation to my mentors, Dr. Chris Doe and Dr. Allan Albig. Chris has been an amazing mentor throughout my PhD, and without him and his expertise and guidance none of this work would exist. He truly made my time in grad school a positive experience and helped me to become the scientist I am today. I would also like to thank Dr. Allan Albig, who accepted me into his lab as a confused undergraduate and first sparked my love of science.

I would also like to extend my greatest appreciation to my fellow Doe lab members, Kristen Lee and Heather Pollington. The help and support I received from you in lab truly advanced my research. You also made lab a stellar place to be, and I will miss Baywatch very much.

I would not have been able to complete this research without the support of my cohort members and best friends: Elizabeth Vargas, Zac Bush, Ethan Shaw, Kona Orlandi, and Michael Shavlick. I would never have survived grad school without you, and thank you for taking every Fireball shot I ever put in front of each of you. We solved some unknown knowns, but the known unknowns remain a mystery.

Finally, I would like to thank my family most of all. My parents Mark and Heidi and my brother Tommy, I am the person I am today because of you, and this work is as much yours as it is mine. I will never be able to thank you enough or express how grateful I am to have you as my family. The life lessons you have all taught me, and will continue to teach me, have fueled me to never settle and always push to accomplish my goals. I love you! **To Mom and Dad: *Modern Family*, season 4, episode 2, 3:37 – 4:30.**

This work is dedicated to my parents, Heidi Munroe and Mark Munroe, and my brother Tom Munroe. Without your love, support, and belief in me this work would not have been possible. To my always enthusiastic and supportive grandmothers George-Ann Wilson, Gaylene Munroe, and Joyce Hunzeker. To my grandfathers, Tom Wilson and Dave Munroe, you both saw the beginning of my grad school experience, and I wish you were both here to see the end. I love and miss you very much. Finally, to Nermal, who was with me for every experiment, every late-night analysis marathon, all the good times and the bad, you're forever my ray of sunshine. Meow.

TABLE OF CONTENTS

Chapter Page

LIST OF FIGURES

Figure Page

Figure Page

LIST OF TABLES

Table Page

CHAPTER I

INTRODUCTION

Reproduced with permission from Munroe, JA, Syed MH, and Doe CQ. 2022. *Plos One*

Reproduction with permission from Munroe, JA and Doe, CQ. 2023. *Neural Development*

Introduction:

Neuronal diversity is essential for proper behavior and function for most metazoans. Loss of, or an increased number of key cell types in the nervous system can result in neurodegeneration and cause impaired sensory and motor function. For example, a lack of diversity in motor neurons can result in amyotrophic lateral sclerosis (ALS) followed by severe spinal muscular atrophy (Kanning et al., 2010). More recent discoveries in neurodegenerative diseases, such as Alzheimer's disease and Parkinson's disease, which are largely asymptomatic during development, are linked to changes in neural diversity (Lu & Vogel, 2009). With a vast genetic toolkit and conserved mechanisms in their neurodevelopmental programs, *Drosophila melanogaster* has emerged as an excellent model for studying the generation and maintenance of neural diversity.

Outer radial glial cells in primates:

The human neocortex contains 16 billion molecularly diverse cells, largely generated during development (Pollen et al., 2015; Siletti et al., 2023). A subset of mammalian neural stem cells, radial glial cells (RGs), arise from the neural epithelium and begin to proliferate and differentiate to generate the large and diverse cell number of a fully developed cortex (Hansen et al., 2010; Pollen et al., 2015). In the developing rat brain, RGs will line the cerebral ventricles within the ventricular zone (VZ, vRGs), reviewed in Pollen (2015). vRGs will extend processes

to the cerebral ventricles and form adherens junctions to the cerebral ventricles for signal transduction via the cerebrospinal fluid, which is essential for proliferation (Pollen et al., 2015). The progeny of vRGs will migrate to the subventricular zone (SVZ) and maintain apical processes to the ventricles and basal processes to the pial (Hansen et al., 2010).

The VZ and SVZ are both present in developing mammalian brains, but the expansion of the outer subventricular zone (OSVZ) is a key evolutionary development that allowed for the enlargement of the neocortex and is unique to primates (Fietz et al., 2010; Hansen et al., 2010; Lewitus et al., 2013; Pollen et al., 2015). RGs specific to the OSVZ are known as outer RGs (oRGs) and are molecularly distinct from other RGs, are located within a separate brain layer from vRGs in the neocortex, and they lack apical adherens junctions (Hansen et al., 2010; Pollen et al., 2015). oRGs migrate into the OSVZ immediately prior to cell division and then begin to generate intermediate, transit-amplifying progenitors that expand neural number and diversity, leading to the enlarged neocortex (Hansen et al., 2010; Pollen et al., 2015).

Type 2 neuroblasts in *Drosophila*:

Similar to oRGs, type 2 neuroblasts (T2NBs) in *Drosophila melanogaster* generate intermediate progenitors that expand both neural number and diversity in the central brain (Bello et al., 2008; Boone & Doe, 2008; Bowman et al., 2008). Out of the ~100 neural stem cells in each lobe of the larval brain, there are also 8 T2NBs that will each asymmetrically divide to self-renew and bud off a smaller intermediate neural progenitor (INP) (Figure 1.2) (Bello et al., 2008; Boone & Doe, 2008; Bowman et al., 2008; Riebli et al., 2013). In each brain lobe, six T2NBs are located medially (DM1-6), while the remaining two are more lateral (DL1,2) (Bello et al., 2008). Once generated, an INP will go through its own asymmetrical cell division to self-renew and

generate a smaller progenitor known as a ganglion mother cell (GMC) (Bello et al., 2008; Boone & Doe, 2008; Bowman et al., 2008). Finally, this GMC will divide to generate sibling neurons (Bello et al., 2008; Boone & Doe, 2008; Bowman et al., 2008). This is different than type 1 neuroblasts (T1NBs) which do not generate an INP, but instead self-renew and generate a series of GMCs (Figure 1.2) (Bello et al., 2008; Boone & Doe, 2008; Bowman et al., 2008). T2NBs and INPs will continue this division pattern throughout neurogenesis, with T2NBs dividing 40-60 times and each INP dividing 4-6 times and generating 8-12 pairs of cells (Bello et al., 2008; Homem et al., 2013). This allows each T2NB to produce ~500 cells, contributing ~8,000 cells to the *Drosophila* brain (Riebli et al., 2013).

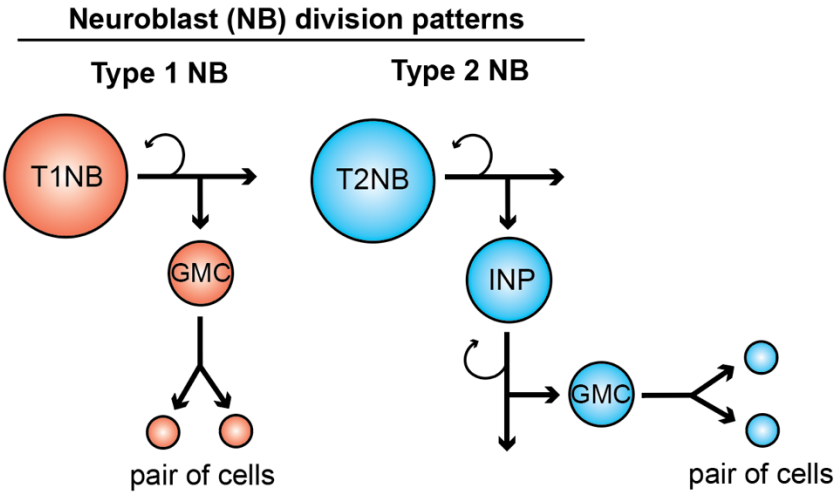

Figure 1.1. *Drosophila* type 1 and 2 neuroblast division patterns. T1NBs (red) generate a ganglion mother cell (GMC) that will produce a pair of cells, while T2NBs (blue) generate a series of intermediate neural progenitors (INPs) that will each produce a GMC followed by a pair of cells.

In comparison, each T1NBs only divides ~150 times (Riebli et al., 2013). While T2NB lineages can produce a large number of cells, regulation is required to prevent tumorigenesis. The translational repressor Brain tumor (Brat) and the homeodomain transcription factor

Prospero (Pros) are required at different stages within the T2NB lineage to prevent tumor growth (Bowman et al., 2008; Choksi et al., 2006; Hakes & Brand, 2020). Brat is required in INPs to promote differentiation and Pros expression prevents GMCs from reverting to a neural progenitor identity (Bowman et al., 2008; Choksi et al., 2006). Pros is also required to induce quiescence in NBs at the end of neurogenesis (Lai & Doe, 2014; Yang et al., 2017). With proper proliferation and differentiation, T2NBs will populate a key brain structure known as the central complex (CX) (Walsh & Doe, 2017; Wang et al., 2014; Wolff et al., 2015; Yu et al., 2013), a highly conserved region analogous to the mammalian basal ganglia (BG) (Givon et al., 2017; Pfeiffer & Homberg, 2014; Strausfeld & Hirth, 2013). Both the BG and the CX have similar developmental gene expression programs and both regions contain prominently GABAergic and dopaminergic neurons (Pfeiffer & Homberg, 2014). It is also thought that the CX is analogous to the mammalian cerebellum since both brain regions play roles in motor coordination (Strausfeld & Hirth, 2013).

Temporal patterning in neuroblasts:

As larval T2NBs exit quiescence at the beginning of larval neurogenesis (Figure 2.1) they transition through different temporal factors in a process known as temporal patterning (Syed et al., 2017). T2NBs have an early (0-60h after larval hatching or ALH; all times subsequently will be in hours after larval hatching) and late (60-120h) stage characterized by expression of early and late temporal transcription factors (TTFs) (Figure 1.3). Early factors are the transcription factors Castor, Chinmo, and Seven-up, and the RNA-binding proteins Insulin-like growth factor-II mRNA-binding protein (Imp) and Lin-28 (Figure 1.3) (Syed et al., 2017). Early factors have varying expression patterns within the 0h – 60h expression window (Syed et al., 2017). The late

factors include the TTFs Broad and E93, and the RNA-binding protein Syncrip (Syp (Figure 1.3) (Syed et al., 2017). The expression of the hormone ecdysone receptor (EcR) at 60h causes the shift from early to late in T2NBs via ecdysone signaling (Syed et al., 2017). Ecdysone hormone is present throughout larval development, however the EcR is not expressed until ~60h, and results in the inhibition of early factor Imp, and the promotion of later factor Syp (Syed et al., 2017). The RNA-binding proteins, Imp and Syp, are particularly interesting due to their known involvement in cell cycle regulation (Samuels et al., 2020; Yang et al., 2017) and the generation of neural diversity (Liu et al., 2015; Ren, et al., 2017) in other *Drosophila* stem cell populations, yet the roles of Imp and Syp in T2NBs is not completely understood.

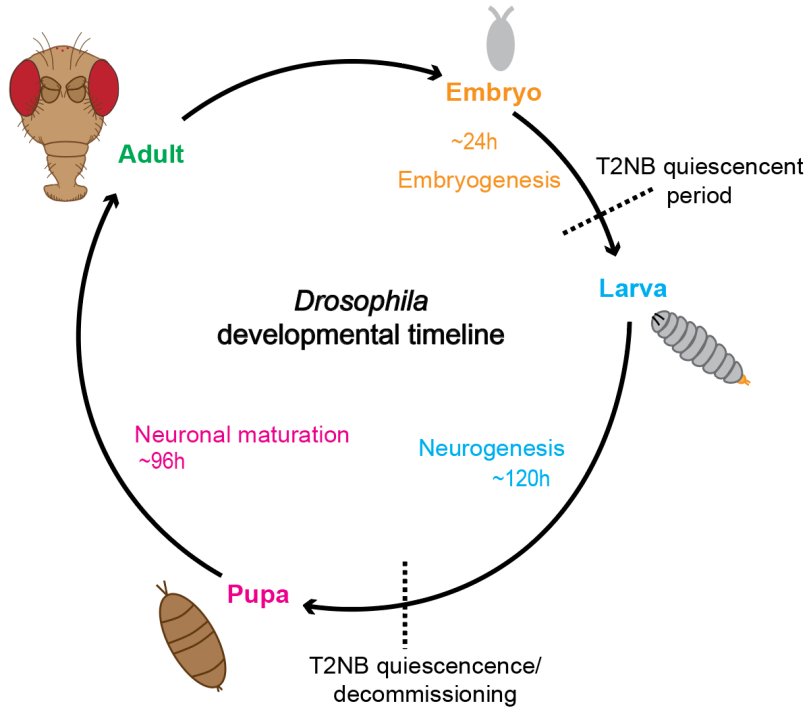

Figure 1.2. *Drosophila* developmental timeline. Development from embryogenesis to adulthood, takes ~10 days. Embryogenesis (orange) lasts for ~24h before entering neurogenesis during larval life (blue) for ~120h. Pupation (pink) follows larval life and allows neuronal maturation for ~96h to occur before an adult (green) *Drosophila* emerges. T2NBs enter a period of quiescence at the end of embryo genesis and enter final quiescence then final decommissioning at the end of neurogenesis.

Imp and Syp are expressed in opposing temporal gradients (Figure 1.3) (Liu et al., 2015; Ren, et al., 2017; Samuels et al., 2020; Syed et al., 2017). In T2NBs, as well as other sets of neural stem cells known as mushroom body neuroblasts (MBNBs) and antennal lobe anterodorsal neuroblasts (ALad1s), Imp is expressed in a high-to-low temporal protein gradient upon T2NB exit from quiescence (Liu et al., 2015; Ren, et al., 2017; Samuels et al., 2020a; Syed et al., 2017). Imp begins neurogenesis ~0-36h with high protein levels, reaching its lowest expression level ~60h, and remains low through the remainder of neurogenesis (Liu et al., 2015; Ren, et al., 2017; Syed et al., 2017). In contrast, Syp begins larval life with low protein expression levels and begins to increase at ~60h, when Imp levels are low (Liu et al., 2015; Ren, et al., 2017; Syed et al., 2017). In the adult *Drosophila* brain, the mushroom body (MB), a structure important for olfactory memory and learning, is made up of three cell types, all generated by MBNBs (Lee et al., 1999; Liu et al., 2015). These three MB cell types, γ, αβ, and α'β', are all generated within specific temporal windows defined by high/low Imp and Syp expression levels. From 24-60h γ cells are produced, followed by α'β' production from 60-84h, and lastly αβ neurons are generated from 84h to 36h after pupa formation (APF) (Liu et al., 2015). High Imp/low Syp expression levels early in neurogenesis generate γ neurons, low Imp/low Syp during mid-neurogenesis generates αβ, and finally low Imp/high Syp late in development defines α'β' neurons (Lee et al., 1999; Liu et al., 2015). In addition to MBNBs, Imp is expressed in the ALad1 type 1 neuroblast lineage to define an early subset of progenies consisting of 12 neuron types (Liu et al., 2015). In this NB lineage, the early generation window is 24-50h and the late temporal window is 50-84h ALH (Liu et al., 2015). Previous work has shown that different types of CX neurons are generated at specific stages of the INP lineage from

T2NBs, but it is not completely understood how this neural diversity is generated (Sullivan et al., 2019; Walsh & Doe, 2017).

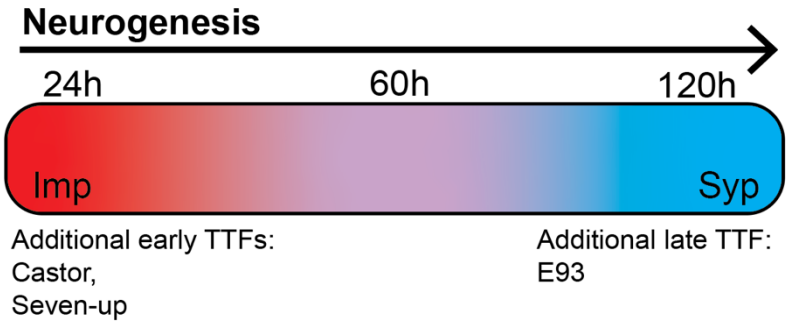

Figure 1.3. Imp/Syp temporal patterning in T2NBs during neurogenesis. Imp (red) shifts from high-to-low expression early (0-60h) in neurogenesis, and Syp (blue) shifts from low-to-high expression late (60-120h) in neurogenesis.

After the exit from quiescence, Imp promotes proliferation and differentiation through the stabilization RNA targets like *myc* and *chinmo* (Dillard et al., 2017; Liu et al., 2015; Ren, et al., 2017; Samuels et al., 2020), while late expression of Syp promotes the nuclear accumulation of Prospero, leading to cell cycle exit (Yang et al., 2017). While much work has gone into characterizing Imp's expression pattern in T2NBs and its role in proliferation, it is not known if, similar to T2NBs, INPs also proceed through temporal patterning of Imp and Syp as they continue to divide (Bayraktar & Doe, 2013). INPs newly generated from T2NBs, termed young INPs will age to mid and then old INPs with each division and transition through the temporal patterning program: Dichaete > Homeobrain > Grainyhead > Eyeless > Scarecrow (Bayraktar & Doe, 2013; Tang et al., 2022). Young INPs and old INPs each specify different cell types, contributing more diversity to neurogenesis (Sullivan et al., 2019; Tang et al., 2022).

Temporal patterning of neuroblasts is not specific to central brain neuroblasts (T2NBs, MBNBs, and ALad1s), but is also seen in T1NBs in the ventral nerve cord (VNC) and the optic lobe neuroblasts (reviewed in Pollington (2023)). The VNC, analogous to the mammalian spinal cord, is generated during embryogenesis. T1NBs in the VNC sequentially transition through the TTFs Hunchback (Hb) > Krüppel > Pdm1/2 > Castor (Pollington et al., 2023). Temporal patterning in the VNC neuroblasts is critical for proper neurogenesis, and misexpression of the early TTF Hb can lead to an increased number of cells generated during the Hb window at the expense of cells generated by later TTFs (Isshiki et al., 2001; Tran & Doe, 2008). Similar temporal factors can be found in mammals. For example, Ikaros, similar to Drosophila Hb, specifies early born neurons (Doe, 2017; Mattar et al., 2015). Optic lobe neuroblasts (OLNBs), located in the medulla, will sequentially transition through their own temporal program Homothorax > Klumpfuss > Eyeless > Sloppy paired 1/2 > Dichaete > Tailless This sequence of TTFs decides downstream TFs that specify different types of optic lobe neurons (Suzuki et al., 2013).

Drosophila central complex:

The CX is required for *Drosophila* celestial navigation (Figure 1.4) (Pfeiffer & Homberg, 2014; Walsh & Doe, 2017; Wolff et al., 2015; Yu et al., 2013). Celestial navigation allows *Drosophila* to orient themselves within their environment based on the sun, moon, and polarized light (Warren et al., 2019). Wild type flies have an arbitrary heading orientation to a fictive sun, while silencing of specific CX neurons causes a loss of arbitrary heading and results in only frontal headings (Giraldo et al., 2018). The CX consists of six areas of dense synaptic connection, known as neuropils, which are the protocerebral bridge (PB), fan-shaped body (FB),

ellipsoid body (EB), noduli (N), gall (G), and the round bodies (RB). They are connected in different combinations by different types of neurons (Figure 1.4) (Walsh & Doe, 2017; Wolff et al., 2015; Yu et al., 2013). For example, E-PG neurons have dendrites in the EB and axons in the PB and G, while PF-R neurons have dendrites in the PB and FB and axons in the RB (Wolff et al., 2015). This gives each type of CX neuron a unique and distinct morphology and set of synaptic connections that are largely generated by the T2NB lineage (Sullivan et al., 2019; Walsh & Doe, 2017; Yu et al., 2013). Young INPs generate a different CX cell type, P-FN neurons (dendrites in the PB and axons in the FB and N) (Sullivan et al., 2019).While Imp is required in the MBNB and ALad1 lineages to generate neural diversity, it is unclear if its role remains the same in INPs from the T2NB lineage.

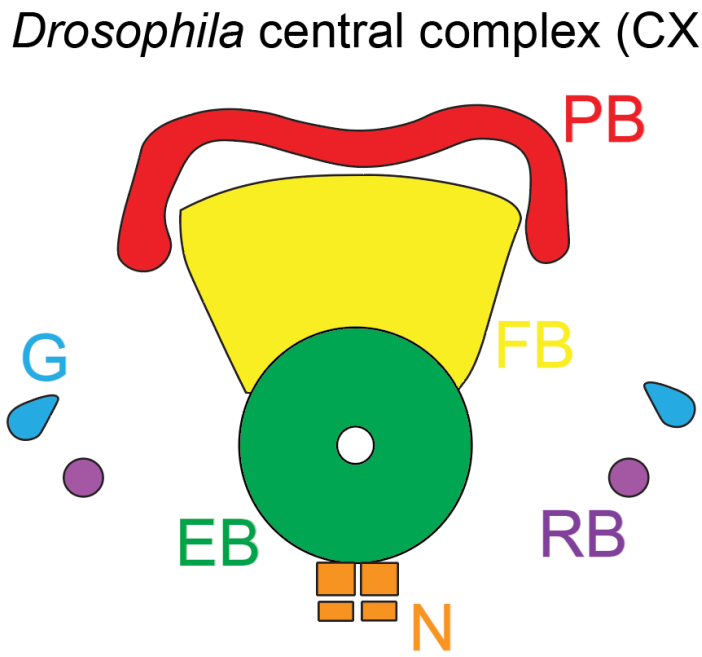

Figure 1.4. *Drosophila* central complex (CX) neuropils. Six main neuropils make up the adult *Drosophila* CX: the protocerebral bridge (PB, red), fan-shaped body (FB, yellow), ellipsoid body (EB, green), noduli (N, orange), gall (G, blue), and round bodies (RB, purple).

Imp and Syp in mammals:

Imp and its mammalian homologues, IMP-1, -2, and -3, are members of the Vg1 RBP/ Vera, IMP-1,2,3, CRD-BP, KOC, ZBP-1 (VICKZ) protein family, which are involved in a wide array of RNA localization, trafficking, and stabilization processes across the animal kingdom (Samuels et al., 2020a; Yisraeli, 2005). IMP1-3 consist of two RNA recognition motifs (RRMs) and four hnRNP K homology (KH) domains, while *Drosophil*a Imp only has four KH motifs (Nielsen et al., 1999). Samuels et al 2020 was able to identify several Imp mRNA targets in *Drosophila*, including *ytr*, *imp*, *jim*, *pros*, *myc*. In mammals, only a few targets of IMP1-3 have been discovered, *β-actin*, *Vg1*, *c-myc*, *IGF2*, *H19*, *tau*, and *CD44* (Vikessa et al., 2006). The overlap of *myc* as a target of Imp in *Drosophila* and mammals suggests that Imp plays similar roles across the animal kingdom.

The mammalian orthologue of Syp is heterogeneous nuclear ribonuclear protein Q (hnRNP Q), expressed throughout the mammalian brain (Tratnjek et al., 2017), which plays roles in sorting microRNAs (miRNAs) (Hobor et al., 2018; Santangelo et al., 2016), regulating myeloid leukemia stem cells (Vu et al., 2017), and synapse formation (Titlow et al., 2020). Both human and *Drosophila* Syp contain three conserved RRMs, and an additional N-terminal unit for RNA recognition (NURR) for targeting mRNA and miRNA targets (Hobor et al., 2018). However, the diversity and complete list of Syp targets is not known, and it is hypothesized that combinations of these RRMs allow Syp to target multiple RNAs (Hobor et al., 2018).

Post-mitotic roles of Imp and Syp:

Once cells are generated, RNA-binding proteins have a common role in axonal and dendritic pathfinding (Olesnicky et al., 2014; Ravanidis et al., 2018; Vijayakumar et al., 2019).

As expected, Imp plays a new role post-mitotically in defining cellular morphology. In MBNB generated γ neurons, Imp is required for axon pathfinding through the formation of ribonucleoprotein (RNP) granules (Vijayakumar et al., 2019). Removal of the prion-like domain (PLD) in Imp results in a shortening of adult γ axons, causing a loss of branching and polarized growth (Vijayakumar et al., 2019). Additionally, both Imp and Syp are required in immature motor neurons (MNs) to define proper cell morphology in *Drosophila* (Guan et al., 2022). The neuroblast lineage Lin A/15 generates 29 different MNs with unique morphologies (Guan et al., 2022). This is partially due to combinations of different TF codes that will determine MN morphology (Guan et al., 2022). Imp and Syp assist in generating and maintaining these TF codes in immature MNs prior to morphological differentiation via the opposing expression patterns and is crucial for the axon connectome (Guan et al., 2022).

Dendrite development also requires RNA-binding proteins (RBPs), largely for mRNA silencing and transport to dendrite arborizations (Olesnicky et al., 2014). Dendritic morphologies and arborizations are often complex and it is believed that RBPs play major roles in their development. Zip-code binding protein 1 (ZBP1), an RBP from the same family as Imp, can be found in mammalian ribonucleoprotein (RNP) granules and dendritic processing bodies (P-bodies), both structures known to be involved in dendrite morphogenesis (Perycz et al., 2011). In rat hippocampal neurons, ZBP1 is required for proper dendrite morphology via the transport of β-actin, and changes in ZBP1 expression resulted in dendritic morphological defects (Perycz et al., 2011).

Current research

Despite the amount of work that has gone into characterizing the expression pattern and roles of the RNA-binding proteins Imp and Syp, there are still several questions concerning Imp's role in neuroblasts. In this work I show the multiple roles that Imp plays in generating neural diversity in the T2NB lineage. At the progenitor stages I found that a base level of Imp is required for T2NB timely exit from quiescence, that Imp and Syp have their own unique expression patterns in individual T2NB lineages and in the INP lineage that follows, and finally that Imp is required in old INPs and newborn neurons for the proper generation of E-PG and PF-R neurons. Additionally, I found that Imp's roles extends into differentiated CX neurons and plays a minor post-mitotic role in determining PF-R and P-FN morphology. Based on this work, I can conclude that Imp is required at multiple stages in the T2NB lineage to generate neural diversity.

Bridge:

In this chapter I described how the T2NB lineage generates neural number and diversity throughout *Drosophila* development, and I discuss how the T2NB lineage is unique compared to other NB lineages due to the generation of intermediate neural progenitors (INPs). T2NB lineage populates the adult central complex (CX), a brain region constructed of six neuropils interconnected by different types of neurons. I describe how the RNA-binding proteins Imp and Syp are expressed in opposing temporal gradients in the T2NB during neurogenesis to regulate proliferation and differentiation. Throughout this work, I am to elucidate the role and expression patterns of Imp throughout the T2NB lineage and its requirement for the generation of neural diversity in adult CX.

In the next chapter describe Imp's role in regulating T2NB exit from quiescence, and I hypothesize that a base level of Imp is required for T2NB exit from quiescence. I also observe that the Imp expression gradient is maintained in T2NBs, even when Imp is knocked down or overexpressed.

CHAPTER II

IMP IS REQUIRED FOR TIMELY EXIT FROM QUIESCENCE IN *DROSOPHILA* TYPE 2 NEUROBLASTS

Reproduced with permission from Munroe, JA, Syed MH, and Doe CQ. 2022. *Plos One*

Introduction

The generation of neuronal diversity is essential for proper brain assembly and function. This is particularly true for the primate cortex, which derives from a specialized neural stem cell called outer radial glia (oRG). These stem cells are thought to have driven cortical expansion and diversity during evolution (Fietz et al., 2010; Hansen et al., 2010; Noctor et al., 2004), but how they regulate their proliferation remains incompletely understood.

One way to help understand oRG lineages is to use model organisms that contain neural stem cells with lineages similar to oRGs, which can be used to generate testable hypotheses for investigating primate oRG lineages. In *Drosophila*, there is a small pool of 16 neural stem cells in the brain (eight stem cells per brain lobe), called type 2 neuroblasts (T2NBs), that undergo a lineage similar to primate oRGs to generate neurons (Bello et al., 2008; Boone & Doe, 2008; Bowman et al., 2008) (Figure 2.1A). In primates these oRGs generate neurons of the cortex; in *Drosophila* the T2NBs generate neurons of the adult central complex (CX), a region important for navigation, sleep, and sensorimotor integration (Turner-Evans & Jayaraman, 2016). Like oRGs, T2NBs undergo repeated asymmetric divisions to produce a series of transit amplifying cells called Intermediate Neural Progenitor (INPs), which themselves undergo a more limited division pattern to generate a series of ganglion mother cells (GMCs) which undergo a single terminal division to produce pairs of neurons and/or glia (Figure 2.1A, left) (Bello et al., 2008; Boone & Doe, 2008; Bowman et al., 2008).

Neuronal diversity is generated at each step in the T2NB lineage. T2NBs change gene expression over time as they generate distinct INPs, with some genes limited to early lineage expression such as insulin-like growth factor II mRNA-binding protein (Imp), Chinmo, and Lin-28; other genes are only expressed late in the lineage such as the RNA-binding protein Syncrip (Syp), Broad, and E93 (Ren, Yang, et al., 2017; Syed et al., 2017). These genes are called candidate temporal transcription factors (TTFs) or temporal identity factors due to their potential role in specifying different neuronal fates based on their time of birth. Subsequently, each individual INP undergoes a TTF cascade to generate molecularly distinct GMCs (Abdusselamoglu et al., 2019; Bayraktar & Doe, 2013; Tang et al., 2022). Thus, the T2NBs appear to be an excellent model for understanding oRG lineages in primates.

Another important aspect of T2NB lineages is how their pattern of proliferation is regulated to generate large populations of neurons without tumorigenesis. T2NBs begin their lineage in the embryonic brain, followed by a period of quiescence at the transition from embryo to first larval instar (L1), and then proliferation resumes between 12-30 hours after larval hatching (Álvarez & Díaz-Benjumea, 2018; Walsh & Doe, 2017); subsequently all times refer to hours after larval hatching. This is similar to the pattern of proliferation-quiescence-proliferation exhibited by most other embryonic larval neuroblast lineages (Chell & Brand, 2010; Lai & Doe, 2014). Previous work has shown that neuroblast quiescence is achieved through the accumulation of nuclear Prospero (Pros) (Lai & Doe, 2014; Maurange et al., 2008), and upon exit from quiescence each T2NB will generate ~60 INPs that produce hundreds of neurons and glia throughout larval development (Bayraktar & Doe, 2013; Bello et al., 2008; Boone & Doe, 2008; Bowman et al., 2008; Yang et al., 2017; Yu et al., 2013). Previous work has shown that Syp recruits the mediator complex and Pros to drive the mushroom body (MB) NBs into decommissioning (Yang et al.,

2017). This terminal exit from the cell cycle is also driven by the loss of proliferation and differentiation due to low Imp expression (Samuels et al., 2020; Yang et al., 2017). High Imp expression in early larval life promotes neuroblast proliferation via the stabilization of *myc* and *chinmo* RNAs as well as inhibition of the mediator complex (Liu et al., 2015; Ren et al., 2017; Yang et al., 2017). This makes Imp an attractive candidate for studying how T2NBs initiate exit from quiescence. Here we focus on the role of Imp in regulating neuroblast proliferation in T2NB lineages, where we identify a novel role for Imp in promoting T2NB exit from quiescence.

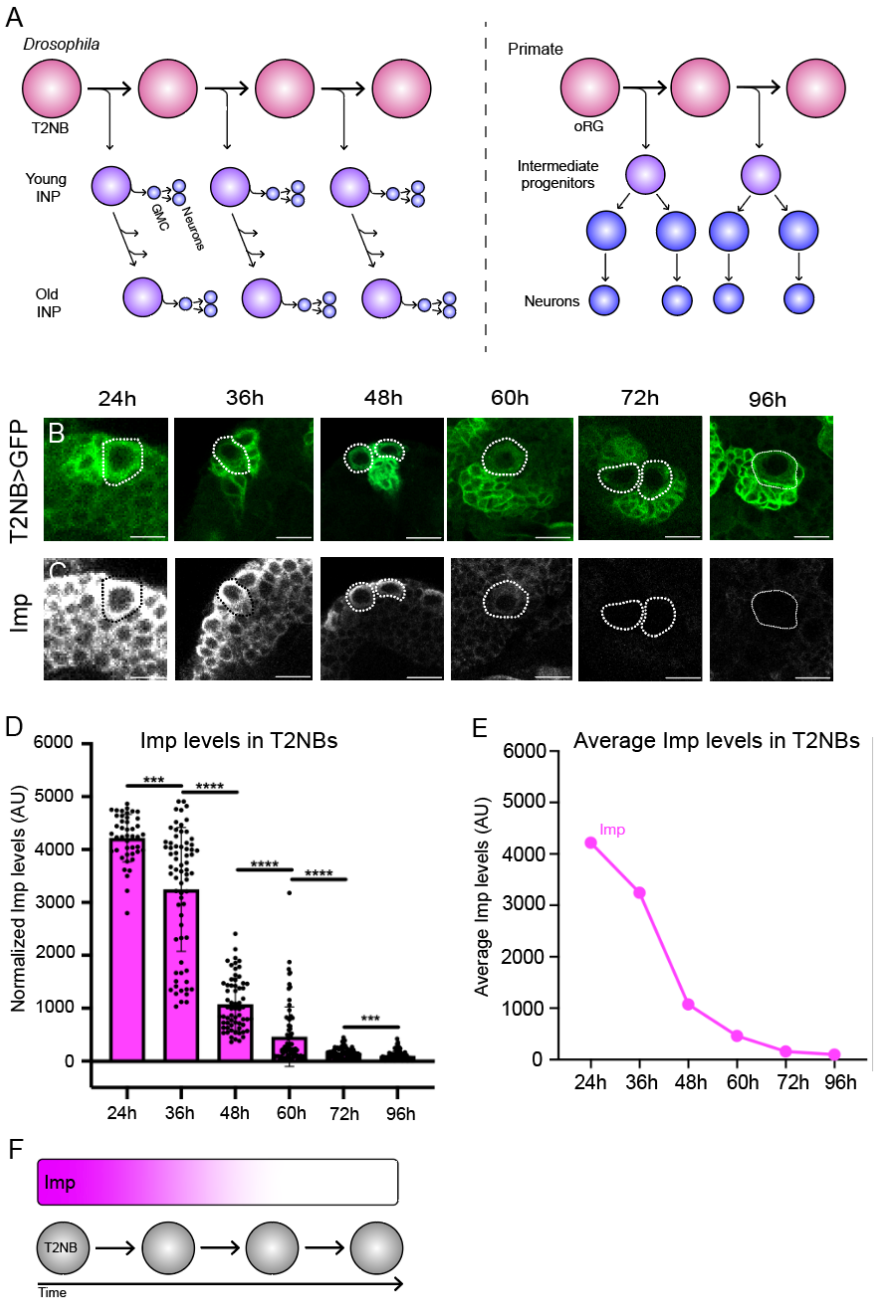

Figure 2.1. Quantification of the Imp gradients in type 2 neuroblasts.
(A) T2NBs (left) adapted from Boone (2008), Bowman (2008), and Bello (2008). and outer radial glial lineage (right) adapted from Liu (2017).
(B,C) Imp protein forms a high-to-low gradients in T2NBs during larval life (hours are time after larval hatching in this and the following figures). T2NBs are identified by expression of *pnt-Gal4 UAS-GFP*. Scale bar, 20µm.
(D, E) Quantification of Imp protein levels (see methods for details) for all n's (D) for the average levels (E). n=5 brains, each data point is one T2NB.
(F) Summary.

Results

Type 2 neuroblasts exhibit a high-to-low Imp protein gradient overtime.

Previous work has shown that Imp forms a high-to-low RNA and protein gradient in all assayed neuroblast populations (Liu et al., 2015), but at just a few timepoints. Here we used *Pointed-Gal4* (*pnt-Gal4*), which is expressed in all T2NBs, crossed to *UAS-GFP* to identify T2NBs and co-stained for Imp at 12h intervals throughout larval stages, from 24h to 96h after larval hatching; note that all times subsequently refer to hours after larval hatching (Figure 2.1B). We found that Imp protein forms a gradient from high to low over the first 60h of larval life, becoming virtually undetectable from 72-96h (Figure 2.1B-F). We conclude that Imp levels drop continuously in T2NBs during larval life.

Imp^{RNAi} and Imp^{OE} have opposing effects on the timing of the Imp protein gradient in type 2 neuroblasts

To alter the Imp protein gradient, we performed Imp^{RNAi} in T2NBs. We used *pnt-Gal4 UAS-imp^{RNAi}* to reduce Imp protein levels specifically in T2NB lineages. We found that Imp^{RNAi} in T2NBs significantly reduced Imp protein levels, although an Imp protein gradient persisted, effectively shifting the Imp gradient to earlier times in development (Figure 2.2A,C-E). In contrast, overexpression of Imp (Imp^{OE}) within T2NB lineages results in higher levels of Imp, without abolishing its gradient, effectively shifting the Imp gradient to later times in development (Figure 2.2B-E). We conclude that Imp^{RNAi} or Imp^{OE} reduces or increases Imp protein levels, respectively, and thus they are effective tools for manipulating Imp protein levels in T2NBs.

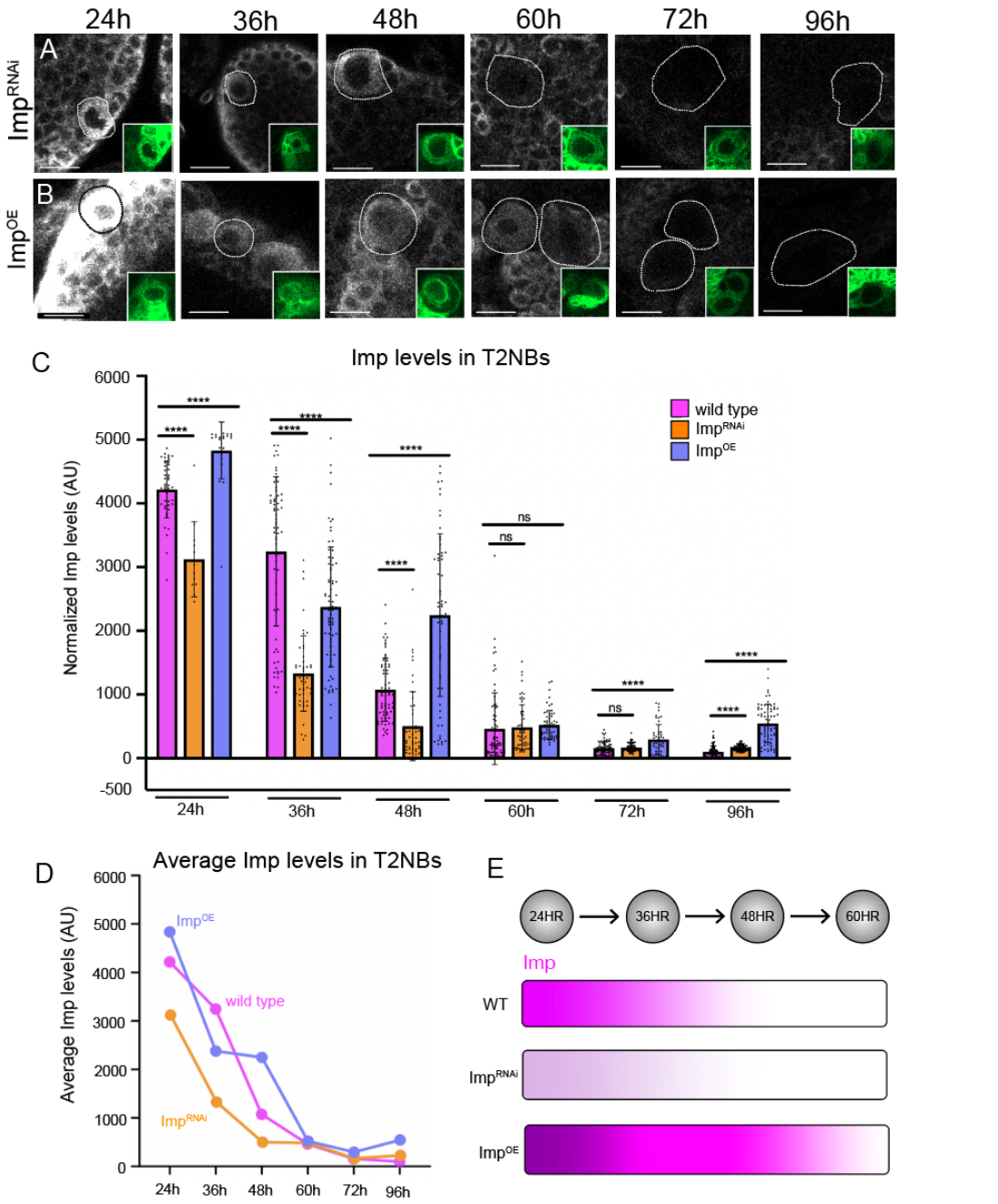

Figure 2.2. Imp^{RNAi} and Imp^{OE} result in reduced or increased Imp protein levels. Wild type Imp levels are shown in Figure 1.
(A) Imp^{RNAi} within T2NBs (inset: *pnt-Gal4 UAS-GFP*) leads to lower Imp protein levels without disrupting the protein gradient; quantified in C. Scale bar, 20µm.
(B) Imp^{OE} within T2NBs (inset: *pnt-Gal4 UAS-GFP*) leads to higher Imp levels without disrupting the gradient; quantified in C. Scale bar, 20µm.
(C, D) Quantification of Imp protein levels in T2NBs in wild type, Imp^{RNAi}, and Imp^{OE}. (C) Histogram showing all n's; (D) graph showing average values. n=5 brains, each point is one T2NB.
(E) Summary.

pnt-Gal4 UAS-GFP can be used to selectively label proliferating type 2 neuroblasts

Imp has been shown to promote neuroblast proliferation, and the decline in Imp levels in late larva contributes to termination of neuroblast proliferation [21,22]. Here we asked a related question: does reduction in Imp levels in T2NB delay exit from quiescence? Proliferating versus quiescent T2NBs can be distinguished by expression of *pnt-Ga4 UAS-GFP*, Deadpan (Dpn) and Cyclin E (CycE): proliferative neuroblasts in interphase are GFP+Dpn+CycE+ whereas quiescent neuroblasts are GFP-Dpn+CycE- (Chell & Brand, 2010; Lai & Doe, 2014). We found that *pnt-Gal4 UAS-GFP* was only expressed by proliferating T2NBs (Figure 2.3A; quantified in 2.3C), and no quiescent neuroblasts expressed *pnt-Gal4 UAS-GFP* (Figure 2.3B; quantified in 2.3C). This allowed us to quantify how many of the 16 T2NBs were proliferating, and infer the remainder were quiescent (see below). We conclude that *pnt-Gal4 UAS-GFP* can be used to identify proliferating T2NBs (Figure 2.3D).

Imp is required for timely exit from quiescence in type 2 neuroblasts

High Imp expression early in larval development promotes neuroblast proliferation, while late, low Imp expression leads to neuroblast decommissioning (Samuels et al., 2020a; Yang et al., 2017a). We wanted to know if high Imp expression early in larval life promoted T2NB exit from quiescence. To answer this question, we decreased Imp levels specifically in T2NB lineages and quantified the number of proliferating T2NBs at intervals from 24h to 96h. We used *pnt-Gal4 UAS-GFP* to identify proliferating T2NBs, *UAS-Imp*^{RNAi} (to reduce Imp levels), and Dpn to mark all neuroblasts (proliferating or quiescent). In wild type, at 24h ~8 of the 16 T2NBs are *pnt-Gal4 UAS-GFP*+ and thus have exited quiescence, with the remainder still in quiescence. By 36h, all 16 T2NBs have exited quiescence and are proliferative (Figure 2.4A,B). In contrast,

following Imp^{RNAi}, only ~2 T2NBs have exited quiescence at 24h, and it takes until 72h for all 16 T2NBs to exit quiescence and become proliferative (Figure 2.4A,B). We also wanted to see if Imp^{RNAi} delayed exit from quiescence in specific T2NB lineages – e.g. the pair of lateral DL neuroblasts

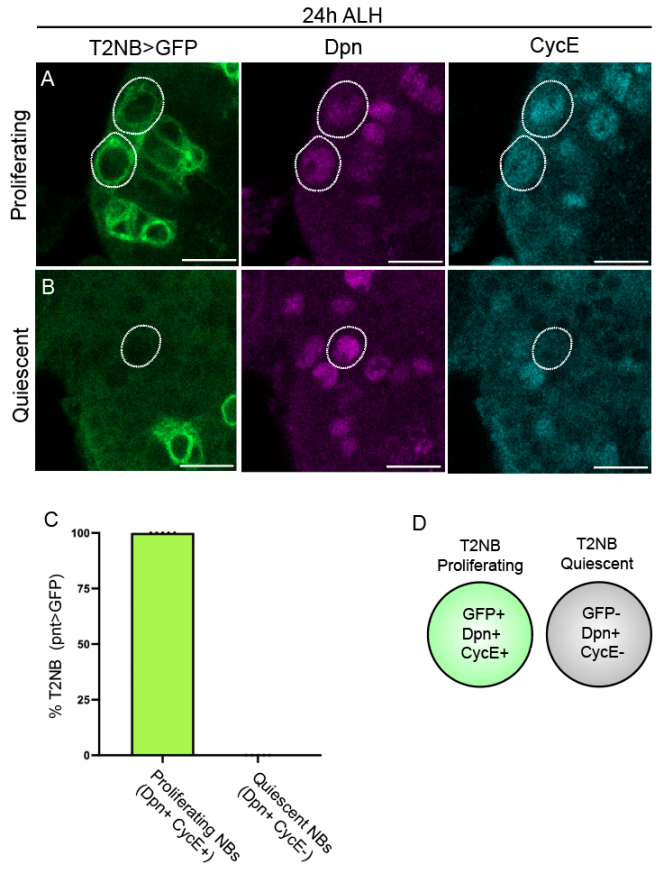

Figure 2.3. *Pointed-Gal4 UAS-GFP*+ T2NBs have exited quiescence and are proliferative.
(A) T2NBs are circled and identified by pnt-Gal4 UAS-GFP (green), Dpn (magenta), and reconfirmed as proliferative by CycE (cyan) at 24h. Scale bar, 5µm.
(B) *Pnt-Gal4 UAS-GFP* (green) and CycE (cyan) are not expressed in quiescent T2NBs, but Dpn (magenta) is still present. Quiescent cells (circled) are identified based on the position in the brain. Scale bar, 5µm.
(C) Histogram of the cells that are Dpn+. One hundred percent of T2NBs that are positive for GFP (*pnt-Gal4 UAS-GFP*) are Dpn+ and CycE+, while 0% of cells are GFP-, Dpn+, CycE-. n=5 brains, eac that point represents one brain.
(D) Summary.

or dorsomedial DM neuroblasts – but each class had an indistinguishable time of exit from quiescence. We conclude that Imp promotes exit from quiescence in T2NBs.

To determine if higher levels of Imp could drive precocious exit from quiescence, we used *pnt-Gal4* to drive *UAS-Imp* specifically in T2NB lineages. This manipulation results in significantly more Imp protein in T2NBs (Figure 2.2), but overexpression of Imp does not induce precocious exit from quiescence in T2NBs (Figure 2.4C,D). We conclude that Imp is necessary but not sufficient to drive T2NB exit from quiescence.

Because Imp promotes exit from quiescence, we asked whether quiescent T2NBs have low Imp and proliferating T2NBs have high Imp levels. Interestingly, we observed comparable levels of Imp in proliferating T2NBs (Figure 2.4E, first column; quantified in 2.4F) and quiescent T2NBs (Figure 2.4E, second column; quantified in 2.4F). Because Imp and Syp can cross-repress each other (Liu et al., 2015), we assayed Syp levels in proliferating and quiescent T2NBs. As expected, we found Syp to be expressed at lower levels than Imp in both proliferating and quiescent T2NBs (Figure 2.4E, third and fourth columns; quantified in 2.4F). Previous work has shown little to no Syp expression in early T2NBs; the very low levels of Syp seen here may be due to more sensitive acquisition methods than used previously (Syed et al., 2017). Interestingly, Syp levels in quiescent T2NBs were slightly higher than Syp levels in proliferative T2NBs (Figure 2.4F), showing a correlation between higher Syp levels and neuroblast quiescence. We conclude that Imp is expressed in quiescent neuroblasts and is necessary but not sufficient for timely exit from quiescence (Figure 2.4G).

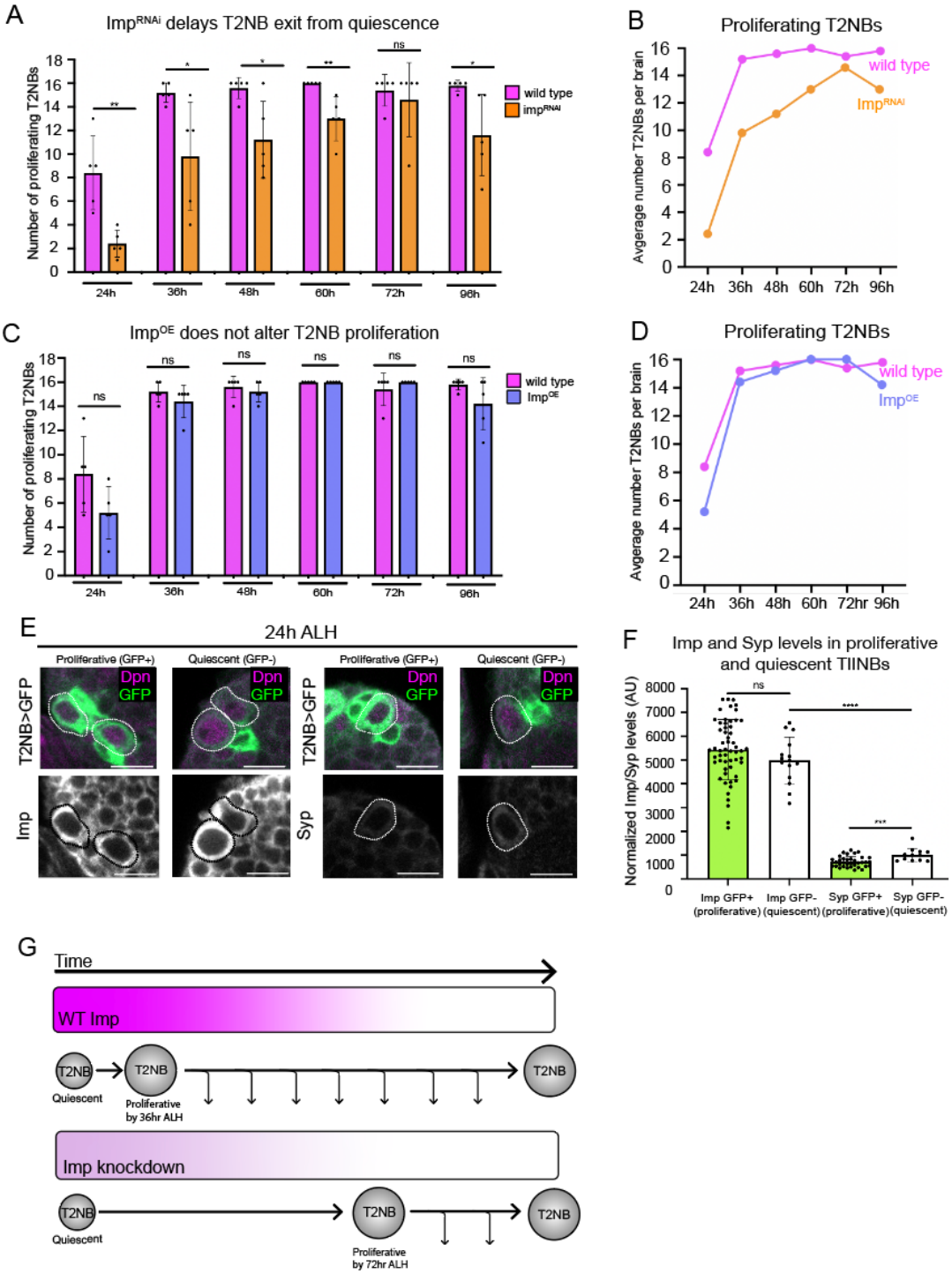
A
Imp^RNAi delays T2NB exit from quiescence
Number of proliferating T2NBs
wild type
imp^RNAi
24h
36h
48h
60h
72h
96h
B
Proliferating T2NBs
Avgerage number T2NBs per brain
wild type
Imp^RNAi
C
Imp^OE does not alter T2NB proliferation
Imp^OE
D
Proliferating T2NBs
E
24h ALH
Proliferative (GFP+)
Quiescent (GFP-)
T2NB>GFP
Dpn
GFP
Imp
Syp
F
Imp and Syp levels in proliferative and quiescent TIINBs
Normalized Imp/Syp levels (AU)
Imp GFP+ (proliferative)
Imp GFP- (quiescent)
Syp GFP+ (proliferative)
Syp GFP- (quiescent)
G
Time
WT Imp
T2NB
Quiescent
Proliferative by 36hr ALH
Imp knockdown
Proliferative by 72hr ALH

Figure 2.4. Imp is required for timely exit from quiescence in T2NBs.
(A, B) Quantification of proliferating T2NB numbers (expressing *pnt-Gal4 UAS-GFP*) over larval life in wild type and Imp^{RNAi}. Note that there is a maximum of 16 T2NBs per brain. In wild type, all NBs have exited quiescence/resumed proliferating by 36h as shown by *pnt-Gal4 UAS-GFP* expression. Imp^{RNAi} delays exit from quiescence and the full complement of 16 proliferating T2NBs is not achieved until 72h as shown by *pnt-Gal4 UAS-GFP* expression. n=5 brains, each data point represents one brain.
(C,D) Quantification of proliferating T2NB numbers (*pnt-Gal4 UAS-GFP+*) across larval development for the wild type and Imp^{OE}. There is no difference in exit from quiescence between wild type and Imp^{OE} genotypes.
(E) Imp levels are the same in quiescent and proliferating T2NBs, while Syp levels are lower in proliferating T2NBs. Proliferating T2NBs (circled; first and third columns) are identified by expression of *pnt-Gal4 UAS-GFP* (green), Dpn (magenta), and lack of Asense (not shown). Quiescent T2NBs do not express *pnt-Gal4 UAS-GFP* (green) but can be identified as Dpn+ (magenta) and lack of Asense. n=5 brains, each data point represents one brain.
(F) Quantifiation of Imp and Syp levels in quiescent and proliferating T2NBs at 24h. n=5 brains, each data point is one T2NB.
(G) Summary.

Discussion

It is well documented in previous studies that Imp is expressed in a temporal gradient in many central brain neuroblasts (Liu et al., 2015; Ren et al., 2017; Samuels et al., 2020a; Syed et al., 2017). In this study we have confirmed the Imp gradient in T2NBs from 24h – 96h and have quantified Imp levels in wild type as well as after Imp^{RNAi} knockdown or Imp^{OE}. While both knockdown and overexpression show significant changes in Imp levels, the Imp gradient is maintained throughout larval life in all cases. Interestingly, at 36h Imp^{OE} levels are lower than WT control levels, but only at this timepoint. This suggests a post-transcriptional 'homeostatic' mechanism that reduces Imp levels when they are experimentally increased. A possible explanation for this is Imp targeting by microRNA *let-7*. *let-7* targets Imp in *Drosophila* male testis and is present in MB NBs where it targets the temporal transcription factor Chinmo, which is also present in T2NBs (Toledano et al., 2012; Wu et al., 2012). Thus, *let-7* may regulate Imp in T2NBs and should be explored in future work.

At 24h wild type larval brains show ~8-10 T2NBs active, and all 16 T2NBs (8 neuroblasts per brain lobe) are active and proliferating by 36h. Imp knockdown results in only ~2-4 T2NBs at 24h and all 16 T2NBs are not proliferating until 72h. This late exit from quiescence shows that Imp is necessary for timely exit from quiescence. Previous studies have shown that high levels of Imp in T2NBs are required to maintain large neuroblast size and proliferative activity through the stabilization of *myc* RNA, and overexpression of Imp in neuroblasts can extend proliferation (Samuels et al., 2020a; Yang et al., 2017a). Our results add to these findings by showing that Imp is required for T2NB timely exit from quiescence. Additionally, Imp knock down in T2NBs promotes early exit from cell cycle at the end of larval life (Yang et al., 2017a). Imp^{OE} in T2NBs did not change the rate at which T2NBs exit from quiescence. Thus, Imp is necessary but not sufficient for exit from quiescence. These findings suggest that a minimum level of Imp is required for the exit from quiescence. A potential mechanism for this would be a negative feedback loop driven by over-expression of Imp, which could lead to over-proliferation if not regulated. Again, a candidate factor for regulation of Imp levels as T2NBs exit quiescence is *let-7*.

It is interesting that Pnt-Gal4 is not expressed in quiescent neuroblasts yet is able to drive *UAS-Imp*^{RNAi} at sufficient levels to maintain quiescence. T2NBs are proliferative in the embryo, then go quiescent, and normally resume proliferation in 12-30h old larvae. We propose that *pnt-ga4* is expressed in the embryo type 2 neuroblasts where it drives *UAS-Imp*^{RNAi} which persists into larval stages due to perdurance of Gal4 and Imp^{RNAi}, thus extending quiescence. As Imp^{RNAi} levels begin to rise (due to lack of *pnt-Gal4 UAS-Imp*^{RNAi} expression) the neuroblasts resume proliferation. We see no evidence for a second wave of quiescence due to re-expression of *pnt-Gal4*.

We quantified Imp levels in both quiescent and proliferative T2NBs to see how they varied and saw no change. We also wanted to compare Syp levels to Imp levels in quiescent and proliferative T2NBs. Syp is required for the entrance into quiescence and decommissioning (Yang et al., 2017a), but it was unknown what Syp levels are in T2NBs nearing the end of quiescence early in larval life. We compared Syp levels in proliferating T2NBs to quiescent T2NBs but found that Syp levels were significantly lower than Imp levels, consistent with their cross-repressive regulation. Interestingly, Syp levels in quiescent T2NBs were higher than Syp levels in proliferative T2NBs, showing a correlation between high Syp levels and neuroblast quiescence, and consistent with earlier work showing Syp is required to elevate levels of nuclear Prospero and initiate neuroblast decommissioning (Yang et al., 2017).

Materials and Methods

Fly genotypes

; UAS-myr::GFP; pointed-Gal4

; ; UAS-Imp^{RNAi}

UAS-Imp ; sco/cyo

Antibodies and immunostaining

We used the following antibodies: chicken GFP (Abcam, Eugene, OR, 1:1000), rabbit Imp (McDonald lab, UT Austin, 1:1000), rabbit Syp (Desplan lab, NYU, 1:1000), rat Deadpan (Dpn: Abcam, Eugene, OR, 1:20) rabbit Cyclin E (CycE: Santa Cruz Biotech, #1C209, 1:500), guinea pig Asense (Wang lab, Duke 1:500), and secondary antibodies were from Thermofisher Eugene OR used at manufacturer's recommendation. All larvae were raised at 25°C and

dissected in Hemolymph Like buffer 3.1 (HL3.1) (NaCl 70mM, KCl 5mM, $CaCl_2$ 1.5mM, $MgCl_2$ 4mM, sucrose 115mM, HEPES 5mM, $NaHCO_3$ 10mM, and Trehalose 5mM in double distilled water). Larvae were grown to specified time points, dissected, mounted on poly-D-lysine coated slips (Neuvitro, Camas, WA), and incubated for 30 minutes in 4% paraformaldehyde solution in Phosphate Buffered Saline (PBS) with 1% Triton-X (1% PBS-T) at room temperature. Larval brains were washed twice with 0.5% PBS-T and incubated for 1-7 days at 4°C in a blocking solution of 1% goat serum (Jackson ImmunoResearch, West Grove, PA), 1% donkey serum (Jackson ImmunoResearch, West Grove, PA), 2% dimethyl sulfoxide in organosulfur (DMSO), and 0.003% bovine serum albumin (BSA) (Fisher BioReagents, Fair Lawn, NJ Lot #196941). Larval brains were incubated overnight at 4°C in a solution of primary antibodies in 0.5% PBS-T. Larval brains were washed for at least 60 minutes in 0.5% PBS-T at room temperature, and then incubated overnight at 4°C in a solution of secondary antibodies in 0.5% PBS-T. Brains were washed in 0.5% PBS-T for at least 60 minutes at room temperature. Brains were dehydrated by going through a series of 10-minute washes in 30%, 50%, 70%, and 90% EtOH, and two rounds of 10 minutes in 100% EtOH and two rounds of 10 minutes in xylene (MP Biomedicals, LLC, Saolon, OH, Lot# S0170), then mounted in dibutyl phthalate in xylene (DPX; Sigma-Aldrich, cat. no. 06522). Brains sat in DPX for at least 48 hours at 4°C or 72 hours (48 hours at room temperature and 24 hours at 4°C) before imaging.

Imaging and statistical analysis

All Imp data were collected with identical confocal settings; all Syp data were collected with identical confocal settings. Fluorescent images were collected on Zeiss LSM 800. T2NBs were counted using the cell counter plugin in FIJI (https:://imagej.net/software/fiji/). Imp pixel

density in each T2NB was calculated in FIJI. In FIJI, T2NBs were manually selected in a 2D plane at the largest cross section of the T2NB with the polygon lasso tool, and the area and Raw Integrated Density (RID) was measured. The nucleus of each T2NB went through the same analysis steps. Imp is cytoplasmic and measuring fluorescence in the nucleus functioned as background subtraction. Imp levels were normalized to cell area using the equation: (Cell $Body^{RID}$ – $Nucleus^{RID}$) / (Cell $Body^{Area}$ – $Nucleus^{Area}$). Two-tailed student t-tests were used to compare two sets of data. *p<0.05; **p<0.01; ***p<0.001; ****p<0.0001. All graphs and statistical analysis were done in Prism (GraphPad Software, San Diego, CA). Note that we were unable to quantify Imp fluorescence in quiescent T2NBs in Imp^{RNAi} flies because quiescent T2NBs cannot be distinguished from quiescent Type 1 neuroblasts.

Figure production

Images for figures were taken in FIJI. Figures were assembled in Adobe Illustrator (Adobe, San Jose, CA). Any changes in brightness or contrast were applied to the entire image.

Acknowledgements

We thank Noah Dillon and Gonzalo Morales Chaya for comments on the manuscript, and Adam Fries for help with developing a fluorescent analysis method.

Bridge:

In this chapter I discussed Imp's role in T2NB exit from quiescence. Under normal Imp expression, all T2NBs have exited quiescence by 36h ALH, while loss of Imp delays T2NB exit until 72h ALH. Overexpression of Imp caused no change in T2NB exit from quiescence. I showed that knocking down or overexpressing Imp levels in T2NBs did not eliminate the Imp expression gradient, but instead shortened or lengthened the expression gradient in T2NBs. I was able to conclude that a base level of Imp is required for T2NB timely exit from quiescence.

In Chapter III I will show that Imp is expressed in a high-to-low gradient in all T2NBs, while Syp expression is T2NB specific. I also characterize the Imp and Syp expression patterns in INPs, as well as showing that Imp expression peaks in old INPs throughout neurogenesis. I further show that Imp is required in old INPs to generate proper central complex neuron (E-PG and PF-R) morphology.

CHAPTER III

IMP IS EXPRESSED IN INPS AND NEWBORN NEURONS WHERE IT REGULATES NEUROPIL TARGETING IN THE CENTRAL COMPLEX

Reproduction with permission from Munroe, JA and Doe, CQ. 2023. *Neural Development*

Introduction

Across the animal kingdom a functioning brain and nervous system allows animals to perform complex behaviors. Here we use *Drosophila melanogaster* as a model to understand how the neural diversity in the brain is generated. The *Drosophila* brain develops from neural stem cells, called neuroblasts (NBs) (Doe, 2017). There are two types of NBs: Type 1 NBs (T1NBs) undergo asymmetrical division to produce ganglion mother cells (GMCs) that divide to produce a pair of neurons (Skeath & Thor, 2003); there are about 100 type 1 NBs per larval brain lobe. Type 2 NBs (T2NBs) have a more complex lineage, undergoing a series of asymmetric divisions to produce smaller Intermediate Neural Progenitors (INPs); each INP subsequently undergoes 4-5 molecularly asymmetric divisions to produce a series of GMCs, and finally each GMC produces a pair of post-mitotic sibling neurons (Bello et al., 2008; Boone & Doe, 2008; Bowman et al., 2008); there are 16 lineages per brain (Figure 3.1C, Supp. Video 3.1). Thus, each T1NB lineage produces ~100 neurons, whereas each T2NB lineage produces 500+ neurons (Ito et al., 2013; Riebli et al., 2013; Yu et al., 2013). In addition, T1 and T2NBs are molecularly distinct: T1 NBs are Asense (Ase)+ Pointed (Pnt)-negative, whereas T2NBs are Pnt+Ase- (Bowman et al., 2008; Zhu et al., 2011). Both types of NBs are positive for the pan-NB marker Deadpan (Dpn). Interestingly, both T2NBs and outer radial glial cells (oRGs) in the primate neocortex have a cell lineage containing INPs (Hansen et al., 2010).

Progeny of T2NBs are major contributors to the intrinsic neurons of the central complex (CX), an evolutionarily conserved brain region in all insects assayed to date (Boyan & Reichert, 2011), and has been proposed to be similar to the basal ganglia in humans (Strausfeld & Hirth, 2013). The CX is critical for celestial navigation in both walking and flying behaviors (Franconville et al., 2018; Hulse et al., 2021; Seelig & Jayaraman, 2013; Turner-Evans & Jayaraman, 2016; Warren et al., 2019). The CX is a collection of six neuropils, or areas of dense synaptic connections. These neuropils are the protocerebral bridge (PB), fan-shaped body (FB), ellipsoid body (EB), noduli (N), gall (G), and round bodies (RB) (Turner-Evans & Jayaraman, 2016) (Figure 3.1). Different types of neurons connect different combinations of these neuropils. Here, we focus on two types of CX neurons: PF-Rs (25-30 neurons) and E-PGs (35-40 neurons) (Sullivan et al., 2019; Wolff et al., 2015).

T2NBs are formed in the embryonic brain (Álvarez & Díaz-Benjumea, 2018; Walsh & Doe, 2017), undergo several divisions, and then both T2NBs and INPs undergo a period of quiescence (Chell & Brand, 2010; Lai & Doe, 2014; Munroe et al., 2022). They exit quiescence 12-36h after larval hatching (ALH; subsequently all larval ages are given as ALH) (Munroe et al., 2022). As T2NBs divide and age, they express different temporal factors in a process called temporal patterning. Two of these factors are the RNA-binding proteins insulin-like growth factor-II mRNA-binding protein (Imp), and Syncrip (Syp) (Ren, Yang, et al., 2017; Syed et al., 2017). These two RNA-binding proteins are found in opposing temporal gradients within T1 and T2NBs throughout larval stages (Ren, Yang, et al., 2017; Syed et al., 2017) (Figure 3.1). Imp has high expression early in T2NBs (0-60h), whereas Syp has an opposite expression pattern, late in T2NBs (60-120h) (Liu et al., 2015; Ren, et al., 2017; Syed et al., 2017). In addition, Imp and Syp have opposing roles in regulating NB proliferation: Imp promotes NB proliferation by stabilizing

Myc and Chinmo (Samuels et al., 2020), whereas Syp promotes T2NB entrance into quiescence (Riebli et al., 2013). Furthermore, the Imp/Syp gradients are essential for the proper progression of early and late temporal transcription factors (TTFs) in the T2NBs (Ren, et al., 2017; Syed et al., 2017).

Newborn INPs (nINPs) will mature to become a young INP (yINPs) and continue to age to become a mid INP (mINPs), then old INPs (oINPs). As INPs age, they go through a series of 4-6 divisions, each division resulting in a pair of newborn neurons (nNeurons) or glial cells (Figure 3.1B) (Bayraktar & Doe, 2013; Bello et al., 2008; Boone & Doe, 2008; Sullivan et al., 2019; Syed et al., 2017). These neurons will go on to populate the adult *Drosophila* central complex (CX) (Sullivan et al., 2019; Walsh & Doe, 2017). The CX, located in the central brain, consists of six neuropils interconnected by different types of neurons and is largely generated from T2NBs (Figure 3.1A) (Ren, et al., 2017; Riebli et al., 2013; Syed et al., 2017). These CX neurons, named for the neuropils they connect, include the two populations of neurons known as E-PGs and P-FRs. There are 35-40 E-PGs with dendrites in the EB and axons in the PB and G, while there are 25-30 PF-Rs with dendrites in the PB and FB and axonal outputs in the RB (Figure 3.1C) (Ren, et al., 2017; Sullivan et al., 2019a; Syed et al., 2017; Walsh & Doe, 2017; Wolff et al., 2015). E-PGs and PF-Rs are generated from early T2NBs, when Imp expression is high, and oINPs (Figure 3.1B) (Sullivan et al., 2019). Importantly, nothing is known about Imp or Syp expression within INP lineages. Here we focus on the expression of Imp and Syp in INPs, and on determining their function in specifying neuronal identity and morphology. We ask: Are Imp and Syp expressed in INPs? Do newborn INPs have the same Imp/Syp levels as their parental NB? Do Imp/Syp form opposing gradients within INP lineages? And lastly, what is the role of Imp in INPs for specifying neuronal identity and morphology?

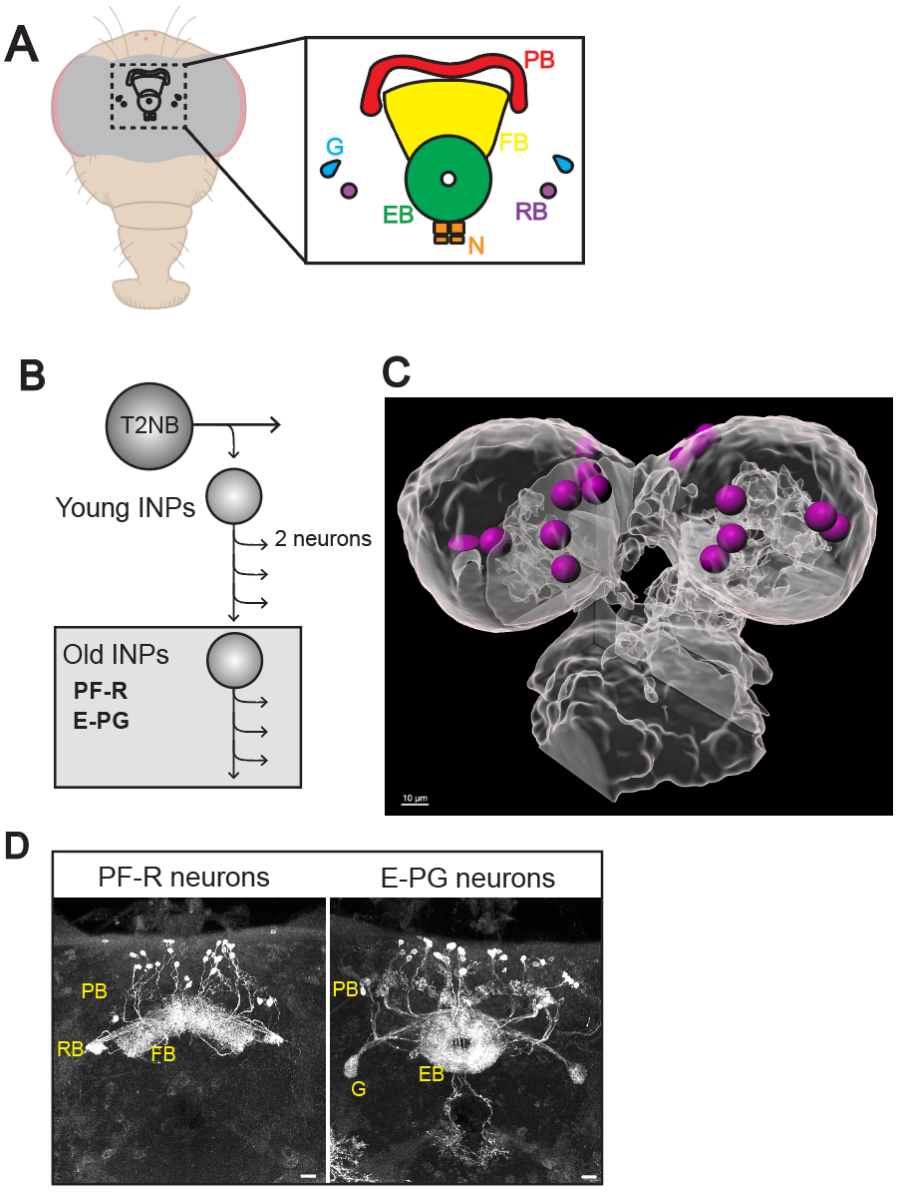

Figure 3.1. The central complex E-PG and PF-R neurons arise from T2NBs.
(A) The central complex consists of six neuropils: protocerebral bridge (PB, red), fan-shaped body (FB, yellow), ellipsoid body (EB, green), noduli (N, orange), round body (RB, purple), and gall (G, blue).
(B) T2NB neuroblast division pattern. E-PG and PF-R neurons arise from old INPs.
(C) Still frame from Supplemental Video 3.1. T2NBs identified by pnt-Gal4 UAS-GFP and represented as magenta spheres to show position in the 48h ALH central brain. Dorsal view, anterior up. Scale bar 10um.
(D) Maximum intensity projections of confocal imaged PF-R and E-PG neurons in the adult *Drosophila* brain. Scale bar 20µm.

Results

Imp/Syp levels are the same in newborn INPs and T2NBs

We first wanted to know if Imp or Syp expression is present in INPs, and if their initial levels are equivalent to their the parental T2NB at time of INP birth. To target young cells within the INP lineage (nINPs and yINPs) and compare Imp/Syp expression to T2NBs we used 12E09-Gal4>UAS-GFP. 12E09-Gal4 targets the entire INP lineage starting at yINPs in DM1-6 T2NBs but does not mark parental T2NBs or nINPs. We used Pointed (Pnt) antibody staining, which labels T2NBs, and found that Pnt expression carried over into nINPs, and thus could be used as a marker for those cell types (Zhu et al., 2011) (Figure 3.2, Supp. Figure 3.1). T2NBs are identified as Pnt+ GFP-, large size, and location; nINPs are Pnt+ GFP- cells in contact with T2NBs (Figure 3.2A-F). Imp and Syp fluorescence levels were measured in T2NBs and nINPs at 48h, 72h, and 96h (Figure 3.2G, H). Imp levels are high in both T2NBs and nINPs at 48h, and low in T2NBs and nINPs at 72h and 96h (Figure 3.2G). At all timepoints there is no difference in Imp or Syp expression between T2NBs and nINPs at any timepoint (Figure 3.2G, H;).

Although our focus here is on Imp and Syp in INPs, we collected data on T2NB expression as part of our comparison between T2NB/nINP levels. We confirmed that all 8 T2NBs had a high-to-low Imp gradient (Figure 3.2I) as previously reported (Ren, et al., 2017; Syed et al., 2017). Surprisingly, we found NB-specific expression of Syp. We confirm that DL1 has a low-to-high gradient, opposing that of Imp, as previously reported (Ren, et al., 2017), as do DM1-3 (Figure 3.2J,K). In contrast, Syp expression in DM5,6 levels stay similar over time, while DM4 and DL2 have an unexpected high-to-low Syp expression gradient (Figure 3.2J,K), matching that of Imp (Figure 3.2I). We also wanted to measure Syp expression at 24h, however at this timepoint some T2NBs are still quiescent and are Pnt-, making them only identifiable as either more medial or more lateral. We used Pnt-Gal>UAS-myr::GFP to target proliferative T2NBs and

categorized them as either medial or lateral. We were able to see that lateral T2NBs had slightly higher Syp levels at 24 than medial T2NBs (Supp. Figure 3.2). However, at 24h Syp levels in T2NBs were universally much lower than 48h.

We conclude nINPs have the same initial Imp and Syp levels as their parental T2NB. Additionally, we find that that Imp levels in all T2NBs follow a high-to-low temporal gradient, while Syp levels differ across T2NBs, with some co-expressed with Imp in a high-to-low temporal gradient.

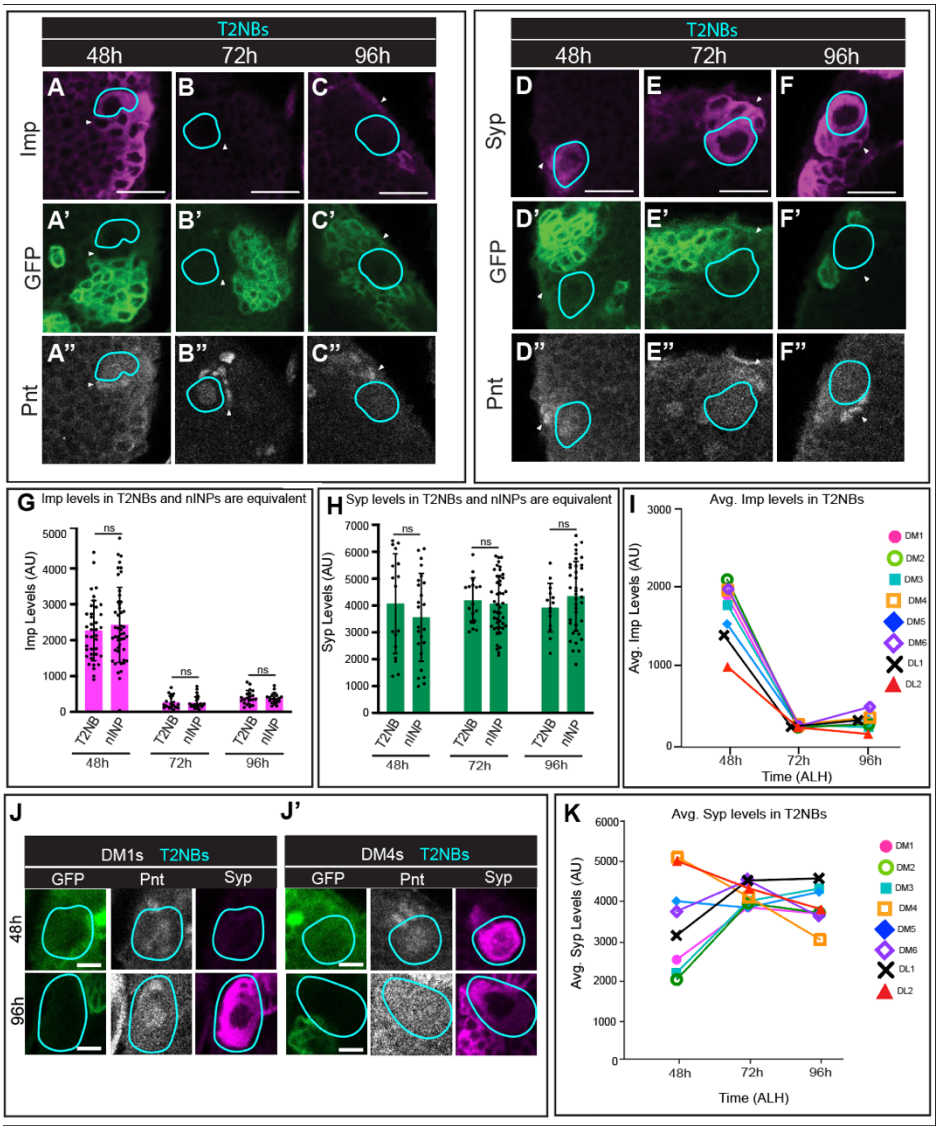

Figure 3.2. Imp/Syp levels are the same in newborn INPs and T2NBs.

(A-F) T2NBs (cyan circles; Pnt+ GFP-) and nINPs (yellow circles, Pnt+ GFP-, contacting T2NBs) at 48h (A), 72h (B), and 96h (C). All timepoints have equivalent Imp (A-C) and Syp (D-F) values between T2NBs and nINPs. 12E09>GFP marks the INP lineage starting at young INP stage. Scale bar 5µm.

(G-H) Quantification of Imp (G) and Syp (H) fluorescent levels in T2NBs and newborn INPs shows no significant differences at 48h, 72h, and 96h. Each point is a single T2NB or nINP, with all 8 T2NBs included n = 3-5 brains per timepoint. Student t-tests were used to compare T2NBs and nINPs at each timepoint. *p<0.05; **p<0.01; ***p<0.001; ****p<0.0001.

(I,K) Quantification of average Imp (I) and Syp (J) levels in individual DM1-6 and DL1-2 T2NBs. Note that all T2NBs have a high-low gradient, whereas Syp shows a neuroblast-specific pattern of expression. n = 3-5 brains per timepoint.

(J) T2NBs (cyan circles; Pnt+ GFP-) at 48h and 96h in DM1 (J) and DM4 (J'). DM1 expresses Syp in a low-to-high expression gradient at 48h to 96h. DM4 Syp expression is the opposite high-to-low expression, similar to Imp. Scale bar 5µm.

Imp is expressed in a high-to-low gradient in INPs at 48h

Having confirmed Imp levels are equivalent in nINPs and T2NBs, we next wanted to know if Imp/Syp expression would follow the same opposing temporal gradients seen in T2NBs (Ren, et al., 2017; Syed et al., 2017). We characterized markers for four stages of INP development, in combination with an early INP driver line (12E09-Gal4) or a late INP driver line (16B06-Gal4). yINPs are Pnt+ GFP+ and border nINPs; mINPs are Grainy head (Grh)+ GFP+; oINPs are Scarecrow (Scro)+ GFP+ Elav-; and nNeurons are Elav+ GFP+ Scro- (Figure 3.3; summarized in Supp. Figure 3.1).

We next quantified Imp levels throughout the INP lineage and into nNeurons at 48h, 72h, and 96h (Figure 3.3). At 48h Imp form a high-to-low gradient in the aging INPs, with a slight increase in oINPs (Figure 3.3A-E). At 72h and 96h Imp is mostly absent (similar to T2NB levels (Ren, et al., 2017; Syed et al., 2017); but still shows an uptick of expression in oINPs (Figure 3.3F-M). We conclude that in L1 larvae (48h) Imp is detected in a high-to-low gradient early in the INP lineage, whereas L2 and L3 larvae (72-96h) have much lower levels of Imp in aging INPs, matching that of T2NBs at those stages, summarized in Figure 3.3N.

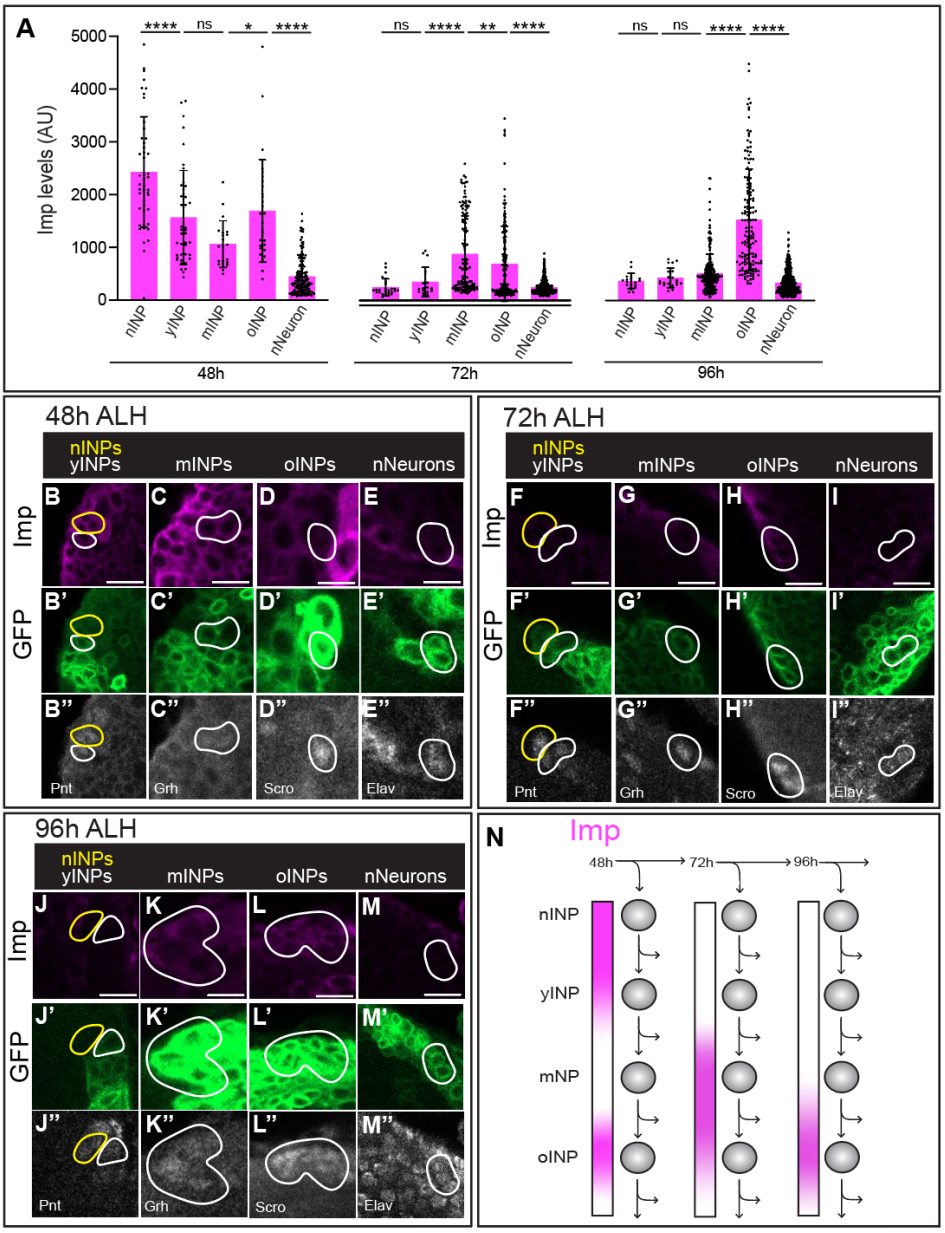

Figure 3.3. Imp forms a high-low gradient in 48h INPs.

(A) Quantification of Imp fluorescence in nINPs, yINPs, mINPs, oINPs and nNeurons at 48h, 72h, and 96h. Note that Imp forms a high-low gradient in INPs at 48h; later timepoints show INP age-specific expression. Each point represents a single INP, n = 3 – 5 brains per timepoint. ANOVA analysis was used to compare all cell types at each timepoint. *p<0.05; **p<0.01; ***p<0.001; ****p<0.0001.

(B-M) Confocal images of Imp levels in aging INPs at 48h (B-E), 72h (F-I), and 96h (J-M). See Figure S1 for INP staging criteria. 12E09>GFP marks the INP lineage beginning at yINPs. Scale bar 5µm.

(N) Summary.

Syp forms a high-to-low gradient in aging INPs

We utilized the same genetics and staining methods to quantify Syp expression levels throughout the INP lineage and in nNeurons at 48h, 72h, and 96h. At all three timepoints Syp is detected in a high-to-low gradient (Figure 3.4). With the exception of DM4 and DL2, Syp is expressed at higher levels in T2NBs and in newborn INPs at the L2 and L3 larval stages (72-96h; Figure 3.4A, F-M) (Ren, et al., 2017; Syed et al., 2017). Interestingly, we find that both Imp and Syp form high-to-low gradients early in the INP lineage in L1 (48h) larvae; this is in contrast to their robust opposing gradients in T2NBs (Ren, et al., 2017; Syed et al., 2017); summarized in Figure 3.4N.

Since Syp expression is T2NB lineage-specific, we wanted to see if this specificity continued into nINPs. We looked at Syp levels in T2NBs and nINPs in each lineage at 48h to see if Syp expression remained lineage-specific (Supp. Figure 3.3). We saw that Syp lineage specificity continues into newborn INPs, apart from the DL2 lineage (Supp. Figure 3.3). Syp levels in the DL2 lineage decrease in newborn INPs, but only to a small extent.

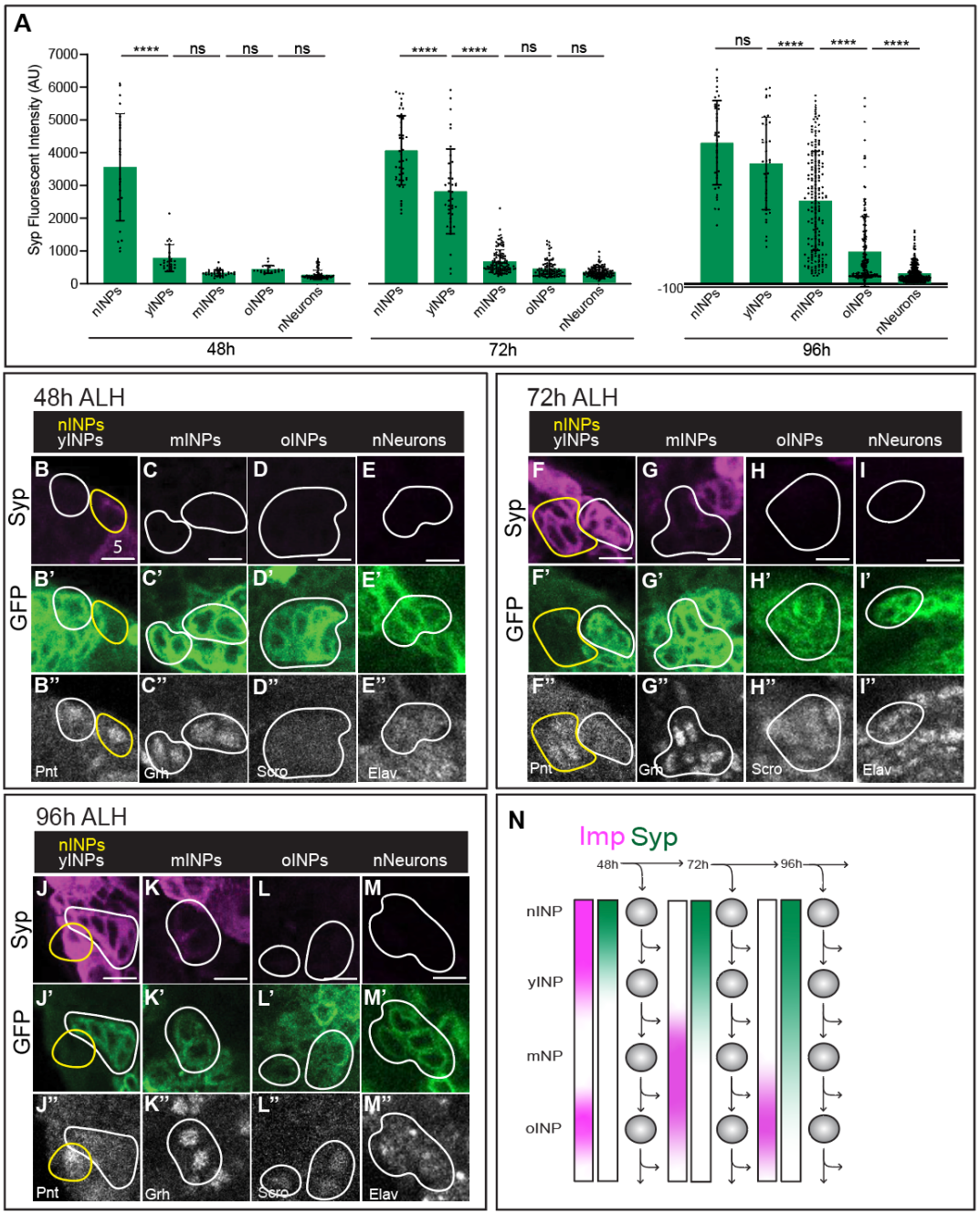

Figure 3.4. Syp forms a high-low gradient in aging INPs.

(A) Quantification of Syp fluorescence in nINPs, yINPs, mINPs, oINPs, and nNeurons at 48h, 72h, and 96h. Syp levels form a high-low gradient in INPs. Each point represents a single INP, n = 3-5 brains per timepoint. ANOVA analysis was used to compare all cell types at each timepoint. *p<0.05; **p<0.01; ***p<0.001; ****p<0.0001.

(B-M) Confocal images of Syp levels in aging INPs at 48h (B-E), 72h (F-I), and 96h (J-M). See Figure S1 for INP staging criteria. 12E09>GFP marks the INP lineage beginning at yINPs. Scale bar 5μm

(N) Summary.

16B06-gal > Imp^{RNAi} decreases Imp levels in oINPs and nNeurons

Imp function in T2NBs has been previously addressed but its function in INPs remain unclear (Ren, et al., 2017; Syed et al., 2017). To determine the role of Imp specifically in INPs, we initially used the 12E09-Gal4 line which is reported to be expressed specifically in INPs (Sullivan et al., 2019). We discovered that 12E09-Gal4 was expressed in embryonic T2NBs (Supp. Figure 3.4), making it unsuitable for INP-specific manipulation of Imp levels. Using 12E09-Gal4 to drive Imp^{RNAi} or Imp overexpression (Imp^{OE}) generated severe defects in PF-R and E-PG targeting to the CX (Supp. Figure 3.4C-E), but we were unable to determine if those phenotypes were due to altered Imp levels in the embryonic neuroblast or INP.

We next turned to the driver line 16B06-Gal4, which we confirm is specifically expressed in oINPs with carryover into nNeurons, with expression continuing into the pupa stages (Figure 3.5A). When we used 16B06-Gal4 to drive expression of Imp^{RNAi}, we observed a decrease in Imp levels in both oINPs and nNeurons at 48h, 72h, and 96h larvae (Figure 3.5B-D, H-J, quantified in 3.5E-G, K-M). In addition, we saw little to no change in oINP cell numbers following any of these manipulations (Supp. Figure 3.5). We conclude that 16B06-Gal4 can be used to specifically reduce Imp levels in oINPs at all stages of larval development, as well as a weaker loss of Imp in nNeurons that is only significant in 72h and 96h larvae. From here we chose to focus only on oINPs using 16B06-Gal4, due to Imp's specific increase at the oINP stage.

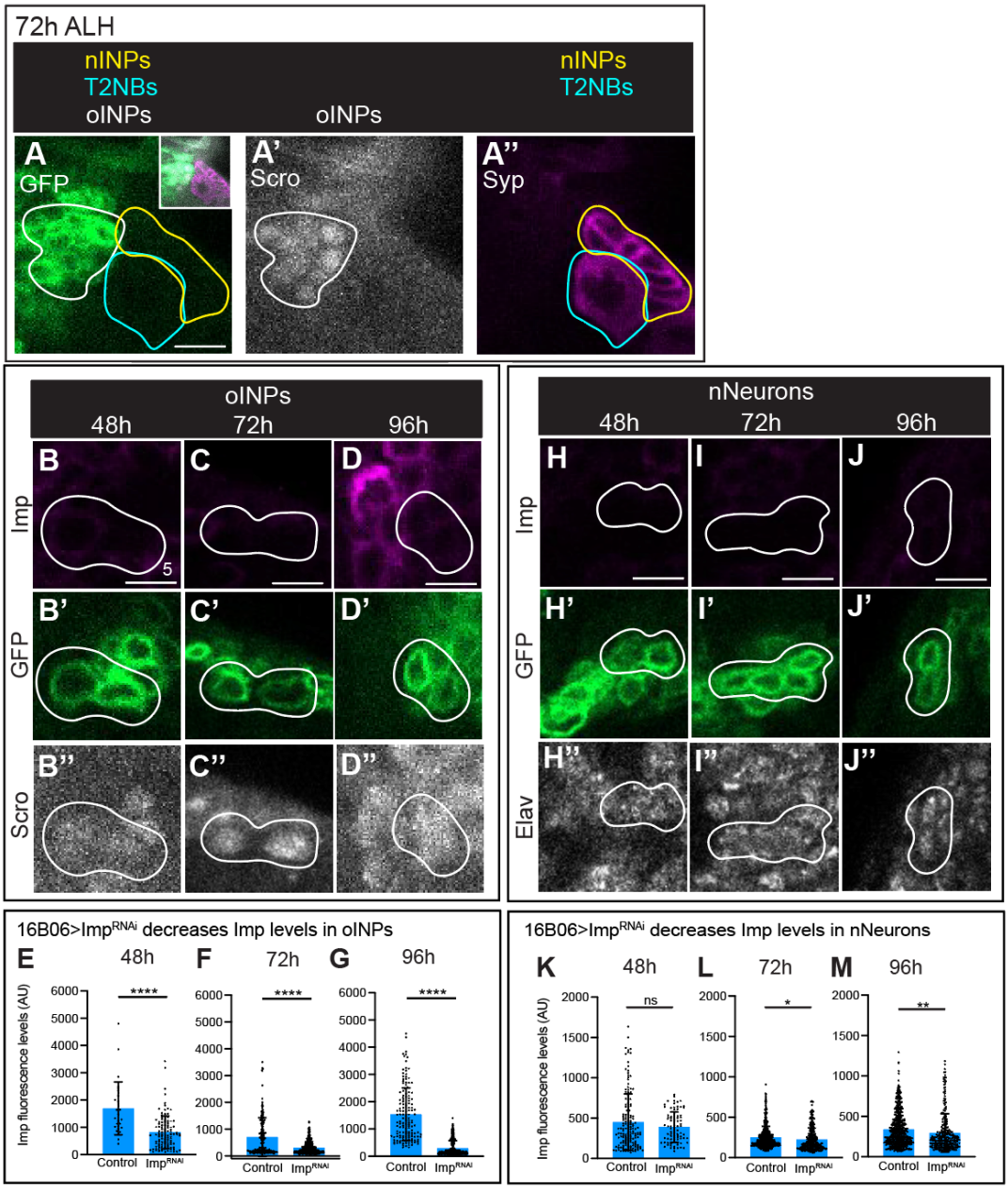

Figure 3.5. 16B06-Gal4>Imp^{RNAi} knocks down Imp in oINPs.

(A) 16B06-Gal4>UAS-GFP UAS-Imp^{RNAi} depletes Imp levels in oINPs, but not T2NBs at 48h (B), 72h (C), and 96h (D). See Figure S1 for INP staging criteria. GFP marks oINPs and nNeurons. Scale bar 5μm.

(B-G) Confocal images of Imp levels in oINPs (B-D), quantified in E-G. Each point is a single oINPs, n = 3-5 brains per timepoint.

(H-M) Confocal images of Imp levels in nNeurons (E-H), quantified in K-M). Each point is a single nNeuron, n = 3-5 brains per timepoint. Student t-tests were used to compare Imp levels at each timepoint. *p<0.05; **p<0.01; ***p<0.001; ****p<0.0001.

16B06-gal > Imp^{OE} decreases Imp levels in oINPs, but increases Imp in nNeurons

Next, we wanted to confirm that 16B06-Gal6>UAS-Imp^{OE} would increase Imp levels. Surprisingly, we found that Imp^{OE} did not increase Imp levels, but counterintuitively decreased Imp levels in oINPs, but caused minor Imp increases in nNeurons (48h and 96h) (Figure 3.6A-F). In addition, we saw little to no change in oINP cell numbers following Imp^{OE} (Supp. Figure 3.5). We hypothesize over-expression of Imp may trigger a homeostatic mechanism that reduces Imp levels (see Discussion). Despite the similarity of both Imp^{RNAi} and Imp^{OE} in decreasing Imp levels, we chose to assay both genotypes for neuronal morphology and connectivity defects, where they generated similar yet distinct phenotypes (see below).

Imp^{RNAi} and Imp^{OE} alter central complex neuropil volume and create ectopic E-PG neuron projections

To decipher the role of Imp in oINPs and nNeurons in regulating neuronal morphology, we used 16B06-Gal4>UAS-Imp^{RNAi} or UAS-Imp^{OE} to alter Imp levels and assayed two neuron populations that are derived from old INPs (Sullivan et al., 2019): E-PG neurons (this section; Figure 3.7) and PF-R neurons (following section; Figure 3.8).

Figure 6. 16B06>ImpOE knocks-down Imp levels in old INPs

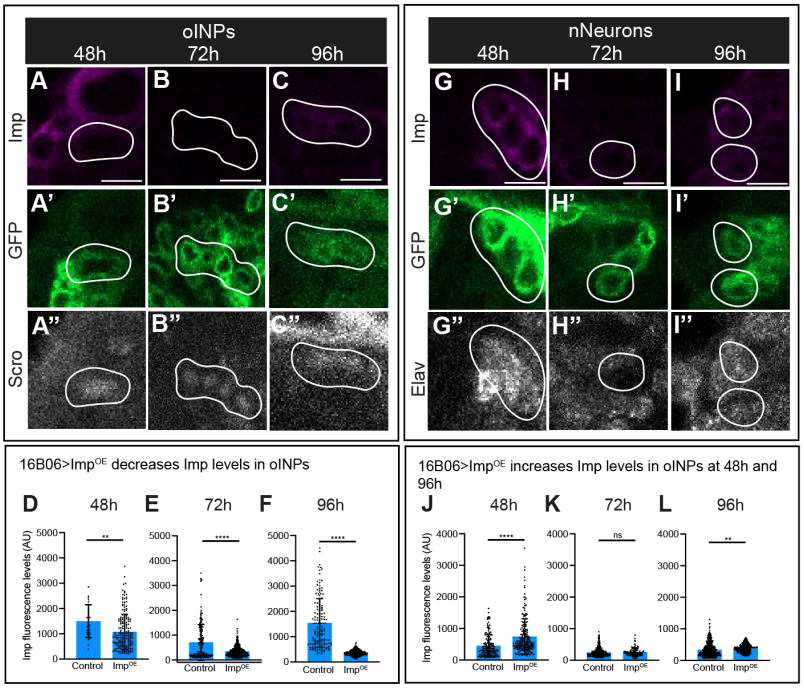

Figure 3.6. 16B06-Gal4>Imp^{OE} knocks down Imp in oINPs.
(A-F) 16B06-Gal4>UAS-GFP UAS-Imp^{OE} depletes Imp levels in oINPs, but not nNeurons at 48h (A), 72h (B), and 96h (C); quantified in D-F. Each point is a single oINPs, n = 3-5 brains per timepoint.
(G-L) 16B06-Gal4>UAS-GFP UAS-Imp^{OE} increases Imp levels in nNeurons at 48h (G) and 96h (I), but not at 72h (H); quantified in J-L. Each point is a single oINPs, n = 3-5 brains per timepoint. Student t-tests were used to compare Imp levels at each timepoint. *p<0.05; **p<0.01; ***p<0.001; ****p<0.0001.

We used the LexA/LexAop system to visualize adult brain E-PG neurons (60D05-LexA>LexAop-GFP or tdTomato). In controls, E-PG neurons innervate the EB, PB, and G neuropils, shown as a confocal image (Figure 3.7A) and Imaris renderings of each individual neuropil (Figure 3.7A-D'). Quantification of cell number and neuropil volumes is shown in Figure 3.7P-Q. In contrast, Imp^{RNAi} resulted in an enlargement of all three neuropils (Figure 3.7E-H; quantified in 3.7Q), without altering E-PG neuron numbers (Figure 3.7P). Imp^{OE} had a similar phenotype with enlarged EB, PB, and Gall neuropils (Figure 3.7I-L), but differed in exhibiting inappropriate projections into the FB, N, and mushroom body (Figure 3.7I, M-O); the latter normally not innervated by T2NB progeny. There was also a large increase in E-PG neuron

numbers (Figure 3.7P); the relationship of increased neuron numbers and ectopic neuropil targeting is unknown; see Discussion. We conclude that Imp acts in INPs or newborn neurons to promote proper E-PG neuropil targeting within the CX. Differences between Imp^{RNAi} and Imp^{OE} phenotypes may be due to different decreases in Imp levels, or potentially due to transient increases in Imp levels prior to homeostatic reduction in Imp levels.

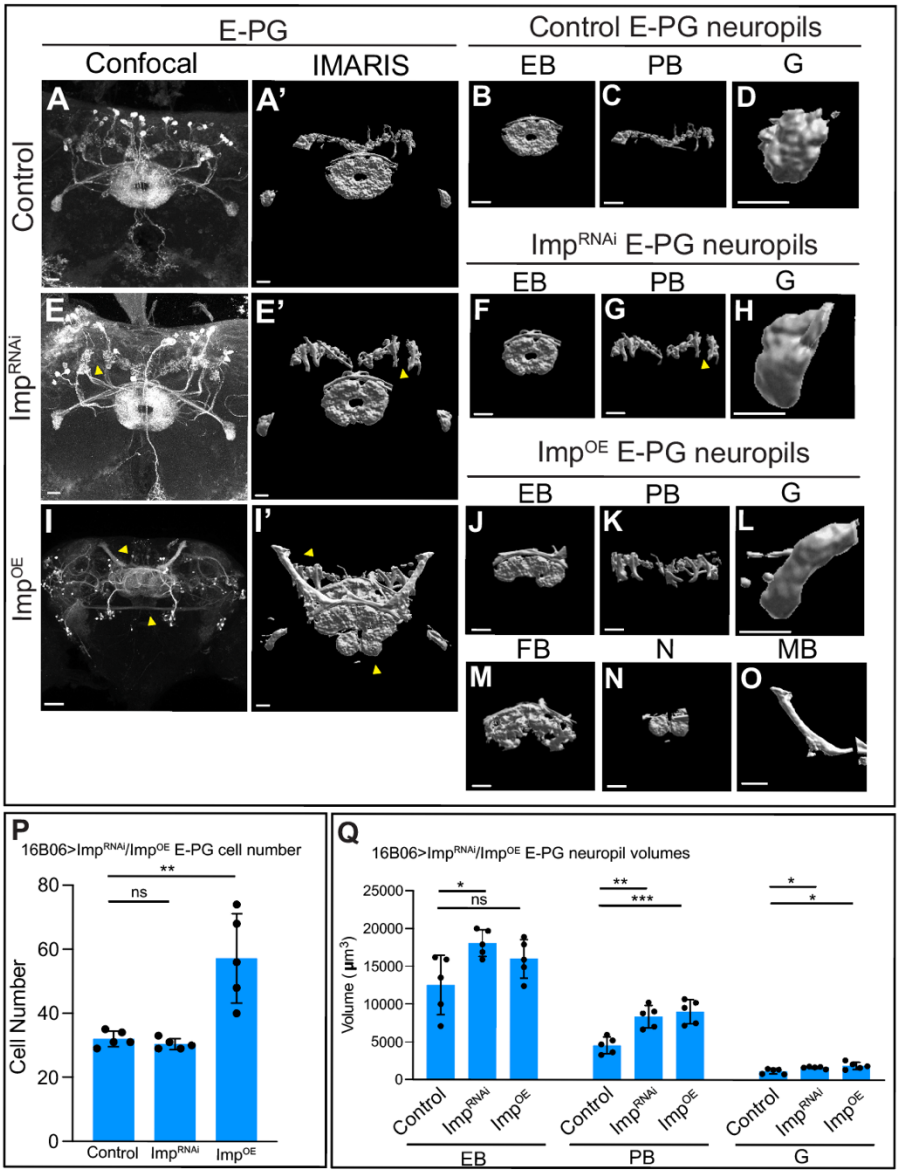

Figure 3.7. Imp^{RNAi} and Imp^{OE} alter E-PG neuropil targeting.
(A-D) Control confocal maximum intensity projection of E-PG neurons (A) and corresponding IMARIS rendering each targeted neuropil (A'-D). Scale bar 20µm (A-C) or 10µm (D).
(E-H) Imp^{RNAi} confocal maximum intensity projection of E-PG neurons (E) and corresponding IMARIS rendering each targeted neuropil (E'-H). Scale bar 20µm (E-G) or 10µm (H).
(I-O) Imp^{OE} confocal maximum intensity projection of E-PG neurons (I) and corresponding IMARIS rendering each targeted neuropil (I'-O); note that Imp^{OE} results in E-PG neurons generating ectopic projections to the fan-shaped body (FB), noduli (N), and mushroom body (MB). Scale bar 20µm (J, K, M, N) or 10µm (L, O).
(P,Q) Quantification of cell numbers (P), and neuropil volume (Q); each point represents an adult *Drosophila* brain, n = 3-5 brains in control, Imp^{RNAi}, and Imp^{OE}. Student t-tests were used to compare cell numbers to control. ANOVA analysis was used to compare neuropil volumes back to control. *p<0.05; **p<0.01; ***p<0.001; ****p<0.0001.

Imp^{RNAi} and Imp^{OE} alter central complex neuropil volume and create PF-R neuron mistargeting

We next wanted to see if these results were consistent in PF-Rs, which are also derived from oINPs (Sullivan et al., 2019). We used the LexA/LexAop system to visualize adult brain P-FR neurons (37G12-LexA>LexAop-GFP or tdTomato). In controls, PF-R neurons innervate the PB, FB, and RB neuropils, shown as a confocal image (Figure 3.8A) and Imaris renderings of each individual neuropil (Figure 3.8A'-D). Quantification of cell number and neuropil volumes is shown in Figure 3.8N-O. In contrast, Imp^{RNAi} resulted in varying alterations in the volume of each neuropil: the PB and RB were enlarged, while the FB was reduced (Figure 3.8E-H; quantified in 3.8O), without altering PF-R neuron numbers (Figure 3.8P). Imp^{OE} had a similar phenotype as Imp^{RNAi} in having enlarged EB and reduced FB neuropils (Figure 3.8I-L) but differed in exhibiting inappropriate projections into the Noduli (Figure 3.8M). There were no increases in PF-R neuron numbers (Figure 3.8N). We conclude that Imp acts in INPs or newborn neurons to promote proper PF-R neuropil targeting within the CX.

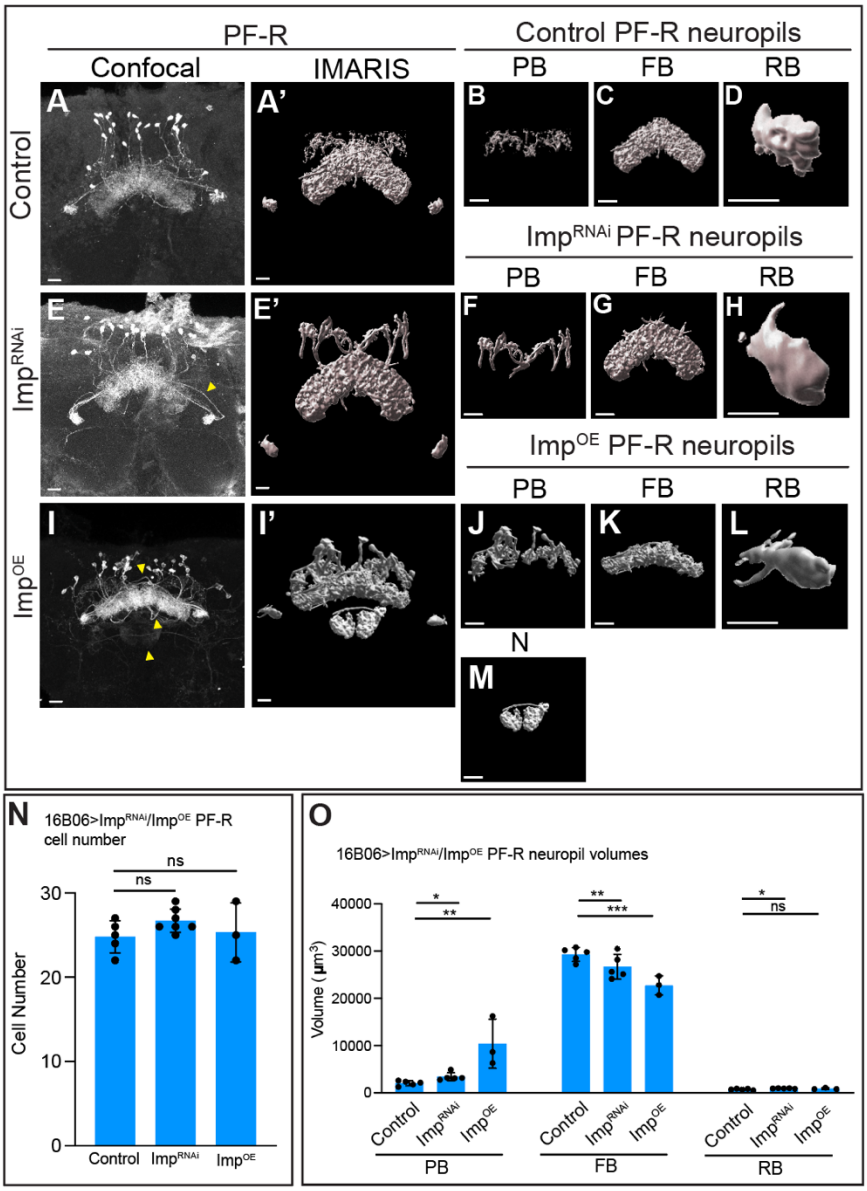

Figure 3.8. Imp^{RNAi} and Imp^{OE} disrupts PF-R neuropil targeting but not cell number.
(A-D) Control confocal maximum intensity projection of PF-R neurons (A) and corresponding IMARIS rendering each targeted neuropil (A'-D). Scale bar 20µm (A-C) or 10µm (D).
(E-H) Imp^{RNAi} confocal maximum intensity projection of PF-R neurons (E) and corresponding IMARIS rendering each targeted neuropil (E'-H). Scale bar 20µm (E-G) or 10µm (H).
(I-O) Imp^{OE} confocal maximum intensity projection of PF-R neurons (I) and corresponding IMARIS rendering each targeted neuropil (I'-M); note that Imp^{OE} results in PF-R neurons generating ectopic projections to the noduli (N). Scale bar 20µm (I-K, M) 10µm (L).
(N,O) Quantification of cell numbers (N), and neuropil volume (O); each point represents an adult *Drosophila* brain, n = 3-5 brains in control, Imp^{RNAi}, and Imp^{OE}. Student t-tests were used to compare cell numbers to control. ANOVA analysis was used to compare neuropil volumes back to control. *p<0.05; **p<0.01; ***p<0.001; ****p<0.0001.

Discussion

Previous research has documented the opposing Imp/Syp gradients in both type 1 and 2 NBs (Liu et al., 2015; Ren, et al., 2017; Sullivan et al., 2019; Syed et al., 2017). However, Imp/Syp expression and function in INPs has not been characterized. Here we show that Imp/Syp expression in T2NBs is the same as newborn INPs. This finding is consistent across all 8 T2NB lineages, no matter the level of Imp/Syp expression. Additionally, we confirmed that all T2NBs express the high-to-low temporal Imp gradient, extending previous work that focused on DL1/DL2 T2NBs, type 1 mushroom body and antennal lobe NB lineages (Ren, et al., 2017). Unlike in mushroom body and antennal lobe NBs (Liu et al., 2015), Syp expression in T2NBs is not always expressed in a low-to-high gradient. Instead, only DL1 and DM1-3 exhibit this familiar Syp gradient, while DM4 and DL2 display an opposite high-to-low expression gradient, more similar to Imp. Separately, DM5 and DM6 each have unique Syp expression pattern: in DM5, Syp remains relatively even at a consistent level throughout larval development; in DM6, Syp peaks at 72h and decreases to a lower level at 48h and 96h. While previous work has described the Imp's role in Syp inhibition, we conclude that additional factors must be regulating Syp expression to allow it to overlap with Imp expression (Liu et al., 2015; Ren et al., 2017; Samuels et al., 2020a; Syed et al., 2017). One hypothesis is the increased levels of Syp in DM4 and DL2 are somehow uncoupled from Imp, preventing Syp-mediated Imp down regulation. An alternate hypothesis stems from the following findings, showing that mammalian SYNCRIP/hnRNPQ (homologous to *Drosophila* Syp) (McDermott et al., 2012) expression can be promoted through long non-coding RNA (lnRNA) NT5E (Zhang et al., 2020). LnRNA NT5E promotes cell proliferation in human pancreatic cancer cell samples during epithelial-mesenchymal transition *in vitro* (Zhang et al., 2020). The lnRNA N5TE genomic location is

close to the Syp locus, and activation of lnRNA NT5E results in Syp activation *in vitro* (Zhang et al., 2020). T2NB lineage-dependent gene expression of lnRNAs located close to Syp could be the cause the variation in Syp levels in each T2NB. Lastly, previous work has shown that co-expression of Imp and Syp in mushroom body NBs (MBNBs) results in a neuronal identity (α'β' neurons) distinct from neurons produced with only high Imp (γ neurons) or high Syp levels (αβ neurons) (Liu et al., 2015). Thus, independent of the mechanism resulting in Imp and Syp overlap, the Imp/Syp co-expression we report in INP lineages may be necessary to specify distinct types of neurons.

At 24h some T2NBs are still in quiescence and T2NBs can only be differentiated at more medial or lateral instead of their specific lineages. At 24h Syp expression is low in medial T2NBs with only a slight increase in lateral T2NBs. Syp levels don't seem to become lineage-specific until 48h into neurogenesis. This further supports the hypothesis of an independent mechanism for Imp and Syp overlap in specific T2NB lineages.

After confirming Imp/Syp expression patterns in T2NBs and validating that Imp/Syp levels are the same in newborn INPs, we found that at 48h, INPs formed a high-to-low Imp gradient. In contrast, at 72h and 96h, Imp showed a peak of expression in old INPs (Figure 3.3A). This brief increase could be due to regulation of Imp by Lin-28, another RNA-binding protein expressed early in T2NB lineages. In *Drosophila* intestinal stem cells, (ISCs) Lin-28 and Imp are both expressed to promote ISC proliferation and regulation regulate of each other (Sreejith et al., 2022). In fact, overexpression of Lin-28 resulted in an increase of Imp expression (Ren et al., 2017; Sreejith et al., 2022; Syed et al., 2017). The old INP Imp peak could also be playing a role in generating gene expression differences between old INPs from young INPs (Bayraktar & Doe, 2013). For example, young INPs express the transcription factor Dichaete (D)

and are negative for the transcription factor Eyeless (Ey), whereas oINPs are the opposite, D- and Ey+ (Bayraktar & Doe, 2013). Another striking difference between young and old INPs is the generation of different types of CX neurons. Young INPs generate P-FN neurons (Sullivan et al., 2019; Walsh & Doe, 2017; Wolff et al., 2015), whereas old INPs generate PF-R and E-PG neurons (Sullivan et al., 2019). The Imp expression peak in old INPs could help distinguish these neuronal identities.

Imp^{RNAi} was able to significantly reduce Imp levels in INPs across all timepoints, with the exception of newborn neurons at 48h ((Figure 3.5E-G, K-M). Surprisingly, Imp^{OE} also significantly decreased Imp levels in INP lineages (Figure 3.6D-F, J-L). We hypothesize that this unexpected drop in Imp levels following Imp^{OE} is caused by tight a homeostatic regulation of Imp levels. For example, the microRNA (miRNA) *let-7* inhibits Imp in the *Drosophila* testis stem cell niche (Toledano et al., 2012); if Imp promotes *let-7* expression it could produce a negative feedback loop that keeps Imp levels low. Traditionally miRNAs bind the 3' UTRs of mRNA targets, but the Imp^{OE} used in this work lacked its normal 3' UTR. Surprisingly, previous work shows that regulation of *let-7* in the 5' UTR does occur (Lytle et al., 2007). Complimentary binding sites from the 3' UTR of *let-7* were added to the 5' UTR of its mRNA target *lin-41* from *C. elegans* (Lytle et al., 2007). When transfected into mammalian cells with endogenous *let-7*, it was sufficient for *lin-41* repression (Lytle et al., 2007). Whether *let-7* or another factor is activated by Imp and then represses Imp levels remains to be determined.

Expression of 16B06-Gal4 was undetectable in T2NBs, which was a prerequisite to characterizing Imp Imp^{RNAi} or Imp^{OE} specifically in INPs. However, this driver was also expressed in newborn neurons, thus limiting our ability to distinguish Imp function in INPs versus neurons. Previous work supports a role for Imp in postmitotic neurons. The mushroom

body is made of up three types of neurons: γ, α'β', and αβ neurons (Liu et al., 2015). Previous research has shown that Imp forms mobile ribonucleoprotein (RNP) granules that are transported to γ axons (Vijayakumar et al., 2019). A mutated form of Imp lacking its prion-like domain (PLD) caused a change in axon morphology through Imp-dependent remodeling (Vijayakumar et al., 2019). ImpΔPLD caused a decrease in γ neuron axon length, and loss of axonal branching (Vijayakumar et al., 2019). This raises the possibility that altered Imp levels in newborn neurons in INP lineages may result in morphological defects.

Imp^{OE} only causes an increase in Imp levels in newborn neurons (Figure 3.6J, L), however this increase in Imp expression does not change the number of newborn neurons (Supp. Figure 3.5B), despite causing an increase in E-PG cell numbers in the adult brain (Figure 3.7P). The increase in E-PG number could be due to the role of Imp in regulating apoptosis. The mammalian paralogue of Imp, IMP-3, prevents cell death after misexpression in lymphoblast cells (Liao et al., 2011), and inhibits apoptosis in human colorectal cancer cells (Di Fusco et al., 2023). We hypothesize that the increased levels of Imp seen in Imp^{OE} in newborn neurons at 48h and 96h (Figure 3.6J, L) could account for the increased E-PG numbers in adults.

Whereas Imp only forms a high-to-low gradient in INPs at 48h, Syp consistently forms a high-to-low gradient in the INP lineages at all timepoints assayed, with the Syp gradient extending longer into the INP lineage at later development stages (Figure 3.4A). This high-to-low Syp gradient in INPs is opposite the low-to-high Syp gradient seen in mushroom body and antennal lobe NB lineages. This is surprising, as Syp is known to promote differentiation in other progenitors. The role of high Syp in young, proliferating INPs is unknown. Perhaps high Syp is required for limiting INP proliferation to 4-6 cell divisions. In addition, the co-expression of Imp and Syp in young INPs may result distinct neuronal identities that are specified by the

combination of Imp and Syp, similar to the α'β'neurons in the mushroom body NB lineages (Liu et al., 2015).

Materials and Methods

Table 3.1. Key Resources

Reagent	**Designation**	**Source**	**Identifiers**	**Additional information**
Species (*D melanogaster*)	12E09-Gal4, 10xUAS-mCD8::GFP	Doe lab	n/a	Early INP driver
Species (*D melanogaster*)	16B06-Gal4, 10xUAS-mCD8::GFP	Doe lab	n/a	Late INP driver
Species (*D melanogaster*)	UAS-Imp^{RNAi}	BDSC	#34977	Imp knockdown
Species (*D melanogaster*)	UAS-Imp	MacDonald lab (UT Austin)	n/a	Imp overexpression
Species (*D melanogaster*)	UAS-myr::GFP	BDSC	#32198	Membrane bound GFP under UAS control
Antibody	Chicken anti-	Abcam (Eugene,	n/a	1:1000

	GFP	OR)		
Antibody	Rabbit anti-Imp	MacDonald lab (UT Austin)	n/a	1:1000
Antibody	Rabbit anti-Syp	Genescript (Piscataway, NJ)	#4060	1:1000
Antibody	Rat anti-Dpn	Abcam (Eugene, OR)	n/a	1:20
Antibody	Rat anti-Grh	Desplan lab (NYU)	n/a	1:500
Antibody	Guinea pig anti-Scro	Genescript (Piscataway, NJ)	#7153	1:200
Antibody	Mouse anti-Elav	DSHB (Iowa City, IA)	9F8A9-CM	1:100
Antibody	Guinea pig anti-Pnt	Genescript (Piscataway, NJ)	#P0111	1:500
Antibody	Rabbit anti-DsRed	Rockland (Pottstown, PA)	#48710	1:500
Antibody, polyclonal	Secondary antibodies	Thermofisher (Eugene, OR)	n/a	1:200 or 1:400 (Dpn and Scro only)

Table 3.1. Key Resources

Fly genotypes used in each figure	**Figure**	**Synopsis**
; 37G12-LexA ; 13xLexAop-myr::GFP ;	Figure 1C	PF-R labeling
; 60D05-LexA ; 13xLexAop-myr::GFP ;	Figure 1C	E-PG labeling
; ; 12E09-Gal4, 10xUAS-mCD8::GFP ;	Figure 2A, B	INP lineage labeling
; ; 12E09-Gal4, 10xUAS-mCD8::GFP ;	Figure 3B-M	INP lineage labeling
; ; 12E09-Gal4, 10xUAS-mCD8::GFP ;	Figure 4B-M	INP lineage labeling
; ; 16B06-Gal4, 10xUAS-myr::GFP ;	Figure 5A	oINP and nNeuron labeling
; ; 16B06-Gal4, 10xUAS-myr::GFP ; x ; ; UAS-Imp^{RNAi}	Figure 5B-J	oINP Imp^{RNAi} and labeling
; ; 16B06-Gal4, 10xUAS-myr::GFP ; x ; ; UAS-Imp^{OE}	Figure 6A-I	oINP Imp^{OE} and labeling
; 60D05-LexA ; x ; 13xLexAop-myr::GFP ; 16B06-Gal4	Figure 7A-D	Control E-PG neurons
; 60D05-Gal4 ; UAS-mCherry^{RNAi} x ; 13xLexAop-myr::GFP ; 16B06-Gal4	Not shown	Control E-PG neurons
; UAS-mCherry ; 60D05-LexA x ; 13xLexAop-myr::GFP ; 16B06-Gal4	Not shown	Control E-PG neurons
; 13xLexAop-myr::GFP ; UAS-Imp^{RNAi} x ; 60D05-LexA ; 16B06-Gal4	Figure 7E-H	oINP Imp^{RNAi}, E-PG labeling

; UAS-Imp ; 20xLexAop-DsRed x ; 60D05-LexA ; 16B06-Gal4	Figure 7I-O	oINP Imp^{OE}, E-PG labeling
; 37G12-LexA ; x ; 13xLexAop-myr::GFP ; 16B06-Gal4	Figure 8A-D	Control PF-R neurons
; 37G12-Gal4 ; UAS-$mCherry^{RNAi}$ x ; 13xLexAop-myr::GFP ; 16B06-Gal4	Not shown	Control PF-R neurons
; UAS-mCherry ; 60D05-LexA x ; 13xLexAop-myr::GFP ; 16B06-Gal4	Not shown	Control PF-R neurons
; 13xLexAop-myr::GFP ; UAS-Imp^{RNAi} x ; 37G12-LexA ; 16B06-Gal4	Figure 7E-H	oINP Imp^{RNAi}, PF-R labeling
; UAS-Imp ; 20xLexAop-DsRed x ; 37G12-LexA ; 16B06-Gal4	Figure 7I-M	oINP Imp^{OE}, PF-R labeling

Antibodies and immunostaining

All larvae and adult *Drosophila* were raised at 25°C and dissected in Hemolymph Like buffer 3.1 (HL3.1) (NaCl 70mM, KCl 5mM, $CaCl_2$ 1.5mM, $MgCl_2$ 4mM, sucrose 115mM, HEPES 5mM, $NaHCO_3$ 10mM, and Trehalose 5mM in double distilled water). Larvae were grown to specified time points, dissected, mounted on poly-D-lysine coated slips (Neuvitro, Camas, WA), and incubated for 30 minutes (adults incubated for 40m) in 4% paraformaldehyde solution in Phosphate Buffered Saline (PBS) with 1% Triton-X (1% PBS-T) at room temperature. Larval brains were washed twice with 0.5% PBS-T (adults brains were washed

twice with 1%PBS-T) and incubated for 2-4 days (adult brains were incubated for 4-10 days) at 4°C in a blocking solution of 1% goat serum (Jackson ImmunoResearch, West Grove, PA), 1% donkey serum (Jackson ImmunoResearch, West Grove, PA), 2% dimethyl sulfoxide in organosulfur (DMSO), and 0.003% bovine serum albumin (BSA) (Fisher BioReagents, Fair Lawn, NJ Lot #196941). Larval brains were incubated for two nights at 4°C in a solution of primary antibodies (see Key Resource Table 3.1) in 0.5% PBS-T. Adult brains were incubated overnight at 4°C in a solution of primary antibodies (see Key Resource Table) in 1% PBS-T. Larval and adult brains were washed for at least 30 minutes in 0.5% PBS-T (adults in 1% PBS-T) at room temperature, and then incubated overnight at 4°C in a solution of secondary antibodies (see Key Resource Table) in 0.5% PBS-T (adults in 1% PBS-T). Larval brains were washed in 0.5% PBS-T (adults in 1% PBS-T) for at least 30 minutes at room temperature. Larval brains were dehydrated by going through a series of 10-minute washes in 30%, 50%, 70%, and 90% EtOH, and two rounds of 10 minutes in 100% EtOH and two rounds of 10 minutes in xylene (MP Biomedicals, LLC, Saolon, OH, Lot# S0170. Adult brains were dehydrated by going through a series of 12-minute washes in 30%, 50%, and 70% EtOH, 15 minutes in 90% EtOH, and two rounds of 18 minutes in 100% EtOH and two rounds of 18 minutes in xylene. Both larval and adult brains were mounted in dibutyl phthalate in xylene (DPX; Sigma-Aldrich, cat. no. 06522). Larval brains sat in DPX for at least 48 hours (72h for adult brains) at room temperature before being imaged or stored at 4°C.

Imaging and statistical analysis

All Imp data was collected with identical confocal settings; all Syp data were collected with identical confocal settings. Fluorescent images were collected on Zeiss LSM 800. Cells

were counted using the cell counter plugin in FIJI (https:://imagej.net/software/fiji/). Imp/Syp pixel density in each cell type was calculated in FIJI. In FIJI, cells were manually selected in a 2D plane at the largest cross section of the cell with the polygon lasso tool, and the area and Raw Integrated Density (RID) was measured. The nucleus of each cell went through the same analysis steps. Imp is cytoplasmic and measuring fluorescence in the nucleus functioned as background subtraction. Imp levels were normalized to cell area using the equation: (Cell Body^{RID} – Nucleus^{RID}) / (Cell Body^{Area} – Nucleus^{Area}). ANOVA or two-tailed student t-tests were used to compare two sets of data. *p<0.05; **p<0.01; ***p<0.001; ****p<0.0001. All graphs and statistical analysis were done in Prism (GraphPad Software, San Diego, CA). Note that we were unable to quantify Imp fluorescence in mitotic cells.

In adult brains, morphology analysis and neuropil volume quantifications for E-PG and PF-R neurons were completed in IMARIS (Oxford Instruments, imaris.oxinst.com). The surfaces tool was used to select individual neuropils.

Table 3.2. Cell Type Identification Markers

Cell type	Identification
T2NB	GFP- Pnt+, location within brain *note that DL1 and DL2 are not labeled with 12E09-Gal4, they were found using the same method.
nINP	GFP- Pnt+, bordering T2NBs
yINP	GFP+ Pnt, bordering nINPs
mINP	GFP+ Grh+ Scro-
oINP	GFP+ Grh- Scro+
nNeuron	GFP+ Scro- Elav+

Figure production

Images for figures were taken in FIJI. Figures were assembled in Adobe Illustrator (Adobe, San Jose, CA). Any changes in brightness or contrast were applied to the entire image.

Acknowledgements

We thank Noah Dillon for comments on the manuscript. We thank the Bloomington Drosophila Stock Center (Bloomington, IN), Developmental Studies Hybridoma Bank (DSHB, Iowa City, IA), Rockland Immunochemicals (Pottstown, PA), Genescript (Piscataway, NJ), ThermoFisher Scientific (Eugene, OR), and Abcam (Eugene, OR) for reagents. We thank the Desplan lab (NYU), Wang lab (Duke University), MacDonald lab (University of Texas at Austin) for resources and reagents.

Bridge:

In chapter III I was able to further characterize Imp and Syp expression patterns in T2NBs, showing that all T2NBs express Imp in a high-to-low gradient, while Syp expression is T2NB dependent. I also showed that Imp and Syp expression in T2NBs is equivalent to newborn INPs. Imp and Syp both form high-to-low gradients throughout the INP lineage, but only Imp increases expression in old INPs. Finally, I was able to show that Imp expression in old INPs is necessary for the proper generation of central complex PF-R and E-PG morphology:

In the next chapter I discuss Imp's minor role in the proper generation of post-mitotic central complex PF-R and P-FN neurons. Increasing or decreasing Imp levels post-mitotically causes only minor defects in neuron morphology. However, these defects are only quantifiable on the population level. I used multi-color flip-out (MCFO) to visual single PF-R and P-FN neurons; however, there is no change in single PF-R or P-FN morphology.

CHAPTER IV

IMP PLAYS A MINOR ROLE POST-MITOTIC ROLE IN GENERATING CENTRAL COMPLEX MORPHOLOGY AT THE POPULATION LEVEL

Introduction

In vertebrates, the basal ganglia plays a major role in sensorimotor behaviors through action selection and recalled associations of past behaviors to familiar stimuli (Fiore et al., 2015; Strausfeld & Hirth, 2013). Damage to the basal ganglia can lead to difficulty in controlling body movement and behavior (Graybiel, 1995; Redgrave et al., 2010; Strausfeld & Hirth, 2013). It has been proposed that the insect central complex (CX) – a highly conserved brain region required for sensorimotor integration, navigation, and sleep (Pfeiffer & Homberg, 2014) – is orthologous to the vertebrate basal ganglia (Fiore et al., 2015; Strausfeld & Hirth, 2013). Further characterization of the development of each brain region is essential for understanding the depth of conservation and the role development plays in the connectivity and function of each structure.

The adult *Drosophila* CX is located in the central brain and plays a major role in celestial navigation, which allows the fly to navigate its environment based on polarized light (Giraldo et al., 2018; Green et al., 2019; Warren et al., 2019). Damage to the CX can cause the animals to be unable to properly navigate their environment (Giraldo et al., 2018; Green et al., 2019; Sullivan et al., 2019; Warren et al., 2019) The CX consists of the four primary neuropils: protocerebral bridge (PB), fan-shaped body (FB), ellipsoid body (EB), and noduli (N); the round body (RB) and gall (G) are also mentioned as peripheral neuropils of the CX (Sullivan et al., 2019; Wolff et al., 2015). These neuropils are interconnected by different types of intrinsic columnar neurons

(Sullivan et al., 2019; Wolff et al., 2015), with two subtypes being PF-R and P-FN neurons (Wolff et al., 2015). PF-Rs have dendrites in the PB and FB and axons in the RB, hence the name PF-R; similarly, the P-FNs have dendrites in the PB and axons targeting the FB and Noduli, hence the name P-FN (Sullivan et al., 2019; Wolff et al., 2015). Here we focus on the PF-R and P-FN neurons due to availability of Gal4 drivers specifically expressed post-mitotically, as detailed below. All intrinsic columnar neurons have distinct morphology and connectivity (Scheffer et al., 2020); yet how each neuron acquires their distinct axon/dendrite morphology is poorly understood.

The intrinsic columnar neurons of the CX arise from four type 2 neuroblasts (T2NBs) on each side of the brain. T2NBs have a division pattern analogous to primate outer radial glial cells (Bayraktar & Doe, 2013; Fietz et al., 2010). Each T2NB divides repeatedly over most of larval life (24-120 hours after larval hatching; ALH) to produce an Intermediate Neuronal Progenitor (INP) that expands neuron number by dividing to generate 8-12 neurons per INP (Bello et al., 2008; Boone & Doe, 2008; Bowman et al., 2008). Larval T2NBs generate a temporal gradient of Insulin-like growth factor-II mRNA-binding protein (Imp), which shifts from high expression to low expression and is in an opposing gradient with the RNA-binding protein Syncrip (Syp) (Ren et al., 2017; Syed et al., 2017). In T2NBs Imp is known to regulate exit from quiescence (Munroe et al., 2022), as well as promoting proliferation through the stabilization of *myc* mRNA in neuroblasts (Samuels et al., 2020). Moreover, the Imp protein gradient is important for specifying neuron identity within mushroom body neuroblasts, with neuroblasts expressing high Imp required for specification of early-born γ neurons (Liu et al., 2015). Similarly, reduced Imp throughout the brain (Medioni et al., 2014; Vijayakumar et al., 2019) or in single post-mitotic neurons (Vijayakumar et al., 2019) shows defects in γ neuron axon/dendrite morphology.

However, in no case has Imp been both reduced and overexpressed in post-mitotic neurons to address its role in axon/dendrite morphology.

Here we focus on the role of Imp in post-mitotic PF-R and P-FN neurons; both are generated by T2NBs early in larval life during the "high Imp" expression window (Sullivan et al., 2019), and Imp levels are maintained in both PF-R and P-FN post-mitotic neurons into adult stages (this work).

Results

Identification of Gal4 drivers specifically expressed in post-mitotic neurons of the CX

We started our search for Gal4 lines specifically expressed in post-mitotic CX columnar neurons by assaying the four intrinsic columnar neuron Gal4 drivers characterized by Sullivan et al (2019). We found that Gal4 drivers labeling adult E-PG and P-EN were expressed in progenitors during larval stages (data not shown) and were excluded from further analysis. In contrast, the lines R37G12-Gal4 and R16D01-Gal4, labeling the PF-R and P-FN neurons, respectively (Figure 4.1A-C), showed expression restricted to larval and adult post-mitotic neurons: both R37G12-Gal4 and R16D01-Gal4 did not express Deadpan (Dpn)+ in progenitors but were labeled by the post-mitotic neuronal marker Elav (Figure 4.1D,E). The lines maintained their specific expression in post-mitotic neurons from 48-96h after larval hatching (ALH) (Figure 4.1D,E; quantified in 4.1F-G). We conclude that our PF-R and P-FN Gal4 drivers are specifically expressed in post-mitotic neurons.

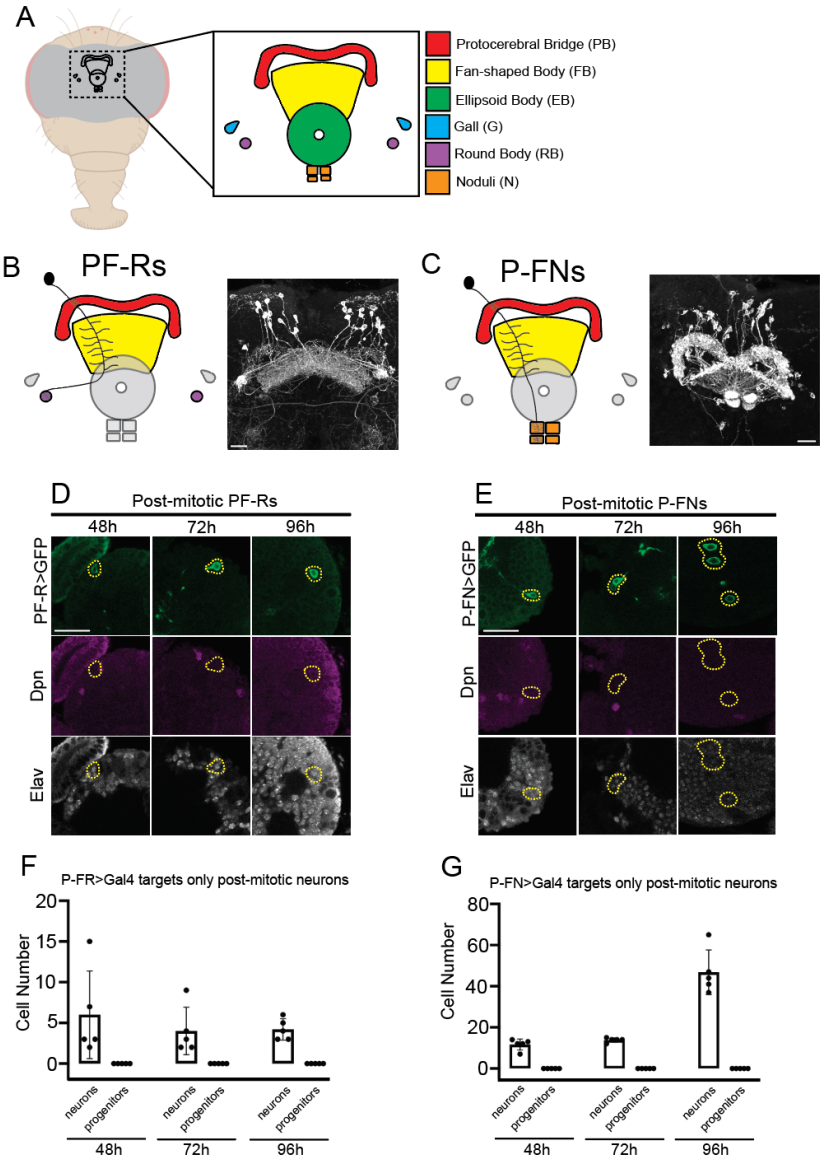

Figure 4.1. PF-R and P-FN drivers target only post-mitotic neurons in *Drosophila* larvae
(A) Schematic of the adult *Drosophila* central complex.
(B,C) PF-R and P-FN neuron morphology. (B) PF-R single neuron schematic (left) and PF-R-Gal4 driving GFP expression in the full central complex; maximum intensity projection shown (right). (C) P-FN single neuron schematic (left) and P-FN-Gal4 driving GFP expression in the full central complex; maximum intensity projection shown (right).
(D,E) PF-R and P-FN Gal4 driving GFP (green) reveals expression restricted to post-mitotic neurons (Elav+; white) but not neuroblast or INP progenitors (Deadpan-; magenta). Yellow dashed lines mark cell bodies. Scale bar, 20μm.
(F,G) Quantification of number of neurons (GFP+ Elav+ Dpn-) and progenitors (GFP+ Elav- Dpn+) cells at 48, 72, and 96h ALH for post-mitotic PF-Rs (left) and P-FNs (right). n = 5 brains per time point.

Imp^{RNAi} reduces Imp levels, while Imp^{OE} increases Imp levels

To assay the effect of decreasing or increasing Imp levels in post-mitotic neurons, we used double *UAS-Imp^{RNAi}* transgenes (Imp^{RNAi}) or a single *UAS-Imp* transgene (Imp^{OE}) driven by either R37G12-Gal4 or R16D01-Gal4 to target PF-R or P-FN neurons. We verified that Imp^{RNAi} reduced Imp levels, and Imp^{OE} increased Imp levels in PF-R neurons (Figure 4.2A-C; quantified in 4.2D) and in P-FN neurons (Figure 4.2E-G; quantified in 4.2H). Thus, Imp^{RNAi} and Imp^{OE} can be used to determine the role of Imp levels in post-mitotic neurons.

Increasing or decreasing Imp levels does not change PF-R or P-FN neuronal number

Altering Imp levels in post-mitotic neurons may be toxic or promote apoptosis. Thus, we next counted the total number of adult PF-R and P-FN neurons in control, Imp^{RNAi}, and Imp^{OE}. We found no difference in neuron numbers in any of the genotypes (Figure 4.2I,J). We conclude that decreasing or increasing Imp protein levels has no effect on neuronal survival.

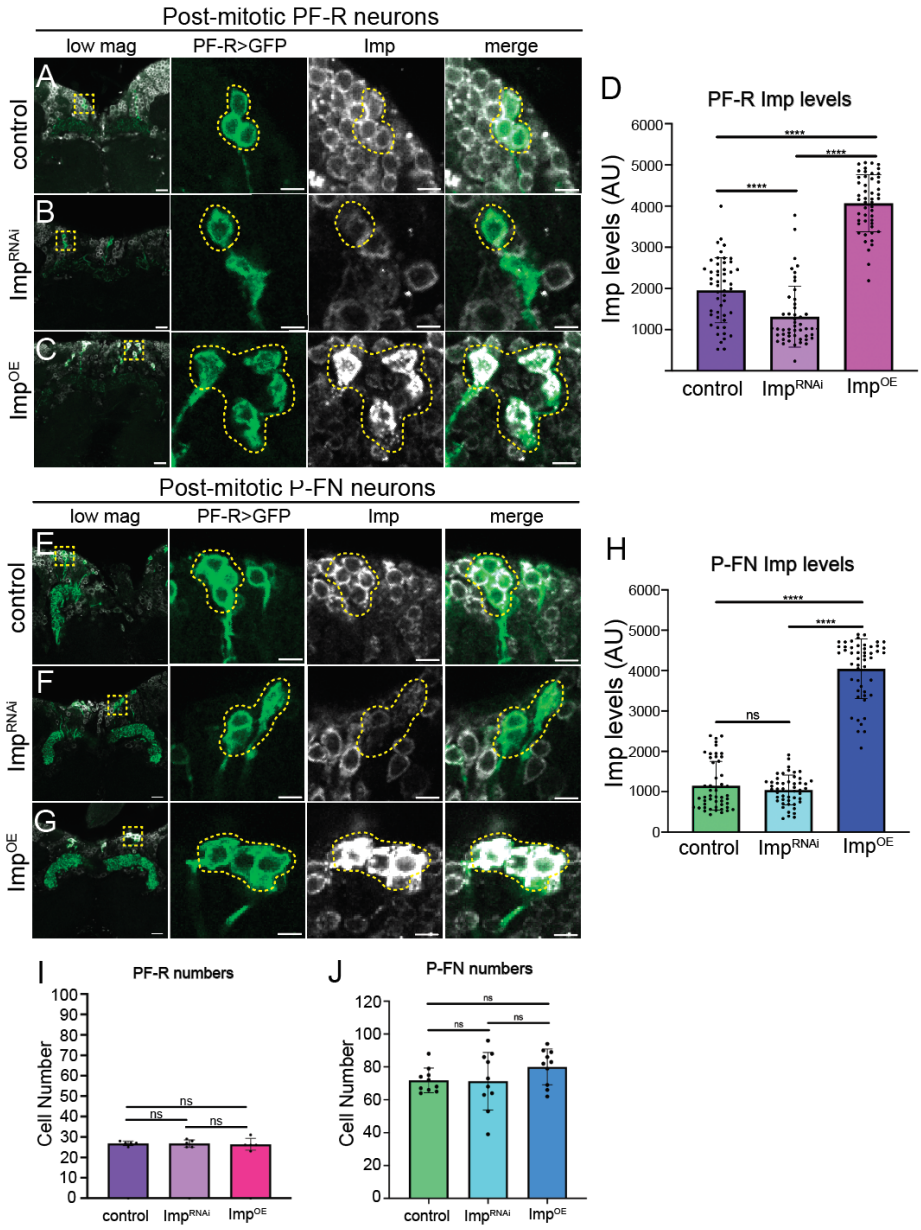

Figure 4.2. PF-R and P-FN cell numbers do not change with Imp^{RNAi} or Imp^{OE}
(A-C) Imp levels in PF-R neurons. (A) Control, (B) Imp^{RNAi} and (C) Imp^{OE} in post-mitotic PF-Rs confocal images showing Imp levels. Dashed yellow box in low mag image marks zoom-in of cell bodies to visualize Imp levels. Low mag and zoom-in scale bars, 20µm. n = 5
(D) Quantification. n = 5 brains, 10 cells measured/brain.
(E-G) Imp levels in P-FN neurons. (E) Control, (F) Imp^{RNAi} and (G) Imp^{OE} in post-mitotic P-FNs confocal images showing Imp levels. Dashed yellow box in low mag image marks zoom-in of cell bodies to visualize Imp levels. Low mag and zoom-in scale bars, 20µm. n = 5
(H) Quantification. n = 5 brains, 10 cells measured/brain.
(I,J) Quantification of PF-R and P-FN neuron numbers. (I) PF-R cell numbers in control, Imp^{RNAi} and Imp^{OE}. n = 5. (J) P-FN cell numbers in control, Imp^{RNAi} and Imp^{OE}. n = 5

Imp is required in PF-R and P-FN post-mitotic neurons for proper CX morphology

We next wanted to determine whether changing Imp levels in PF-R and P-FN post-mitotic neurons caused alterations in their CX neuropil targeting. We assayed for Imp levels in control, Imp^{RNAi}, and Imp^{OE} for PF-R and P-FN neurons in the adult. To determine the effect of Imp knock-down or overexpression on proper neuropil targeting, we calculated the neuropil volume using FIJI. Surprisingly, we found that Imp^{OE} resulted in a smaller neuropil volume for all neuropils in both PF-R and P-FN neurons (Figure 4.3A,B,D; quantified in 4.3C). Decreases in neuropil size are subtle in PF-R PB and RB, but statistically significant. Imp^{OE} in P-FN neurons decreased N volume and resulted in a morphological defect that caused P-FN targeting to the N to appear in multiple smaller pieces. In contrast, Imp^{RNAi} had little effect on neuropil volume, showing a significant decrease only in the FB for P-FN neurons (Figure 4.3A,B,D; quantified in 4.3E). The synapse marker Bruchpilot (Brp) was used to measure synapse expression levels. In both Imp^{RNAi} and Imp^{OE} we saw no change synapse expression in any neuropil for PF-R (Figure S4.1A-C) and P-FN neurons (Figure S4.1D-F).

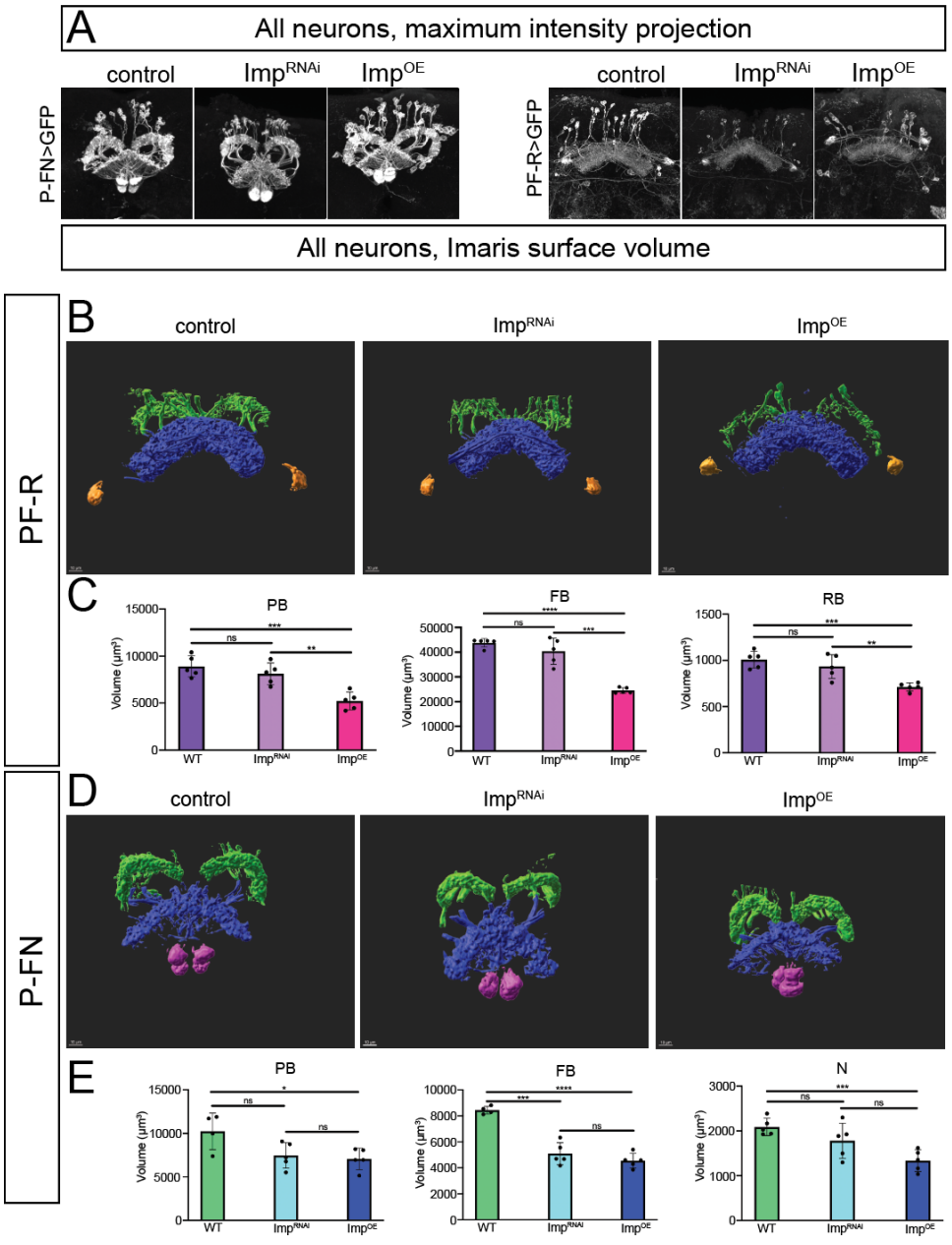

Figure 4.3. Imp^{OE} causes a decrease in all PF-R and P-FN neuropil volume
(A) Maximum intensity projection confocal images of PF-R (top row) and P-FN (bottom row) neurons in control, Imp^{RNAi}, or Imp^{OE} conditions. Scale bar, 20µm.
(B) IMARIS surface reconstructions of PF-R neurons in control, Imp^{RNAi}, or Imp^{OE} conditions. PB (green), FB (blue) RB (orange). Scale bar, 10µm.
(C) Quantification of PF-R neuropil volumes. n = 5
(D) IMARIS surface reconstructions of P-FN neurons in control, Imp^{RNAi}, or Imp^{OE} conditions. PB (green), FB (blue), N (magenta). Scale bar, 10µm.
(F) Quantification of P-FN neuropil volumes. n = 5

Imp does not play a major role in post-mitotic PF-R and P-FN neurite morphogenesis.

To determine the effect of altering Imp levels at the single neuron level, we performed multicolor flip out (MCFO) for PF-R and P-FN neurons (Figure 4.4) (Nern et al., 2015). This was done in WT, Imp^{RNAi} and Imp^{OE} in single PF-R and P-FN neurons. This allowed us to measure the volume of single neuron neuropil targeting and the number of branching points in each neuropil. The PF-R population of neurons consist of 25-30 individual neurons and the P-FN population has ~70 neurons. However, unlike the minor changes seen in PF-R and P-FN neuropil volume at the population level, no change was seen in single cell volumes in any neuropil. There was a small increase in Imp^{RNAi} branch points compared to WT in the FB. However, no change was seen in any other neuropil in Imp^{RNAi} and there was no change in Imp^{OE}. Additionally, the MCFO fly line only contained one copy of Imp, while previous experiments used two copies of Imp^{RNAi}.

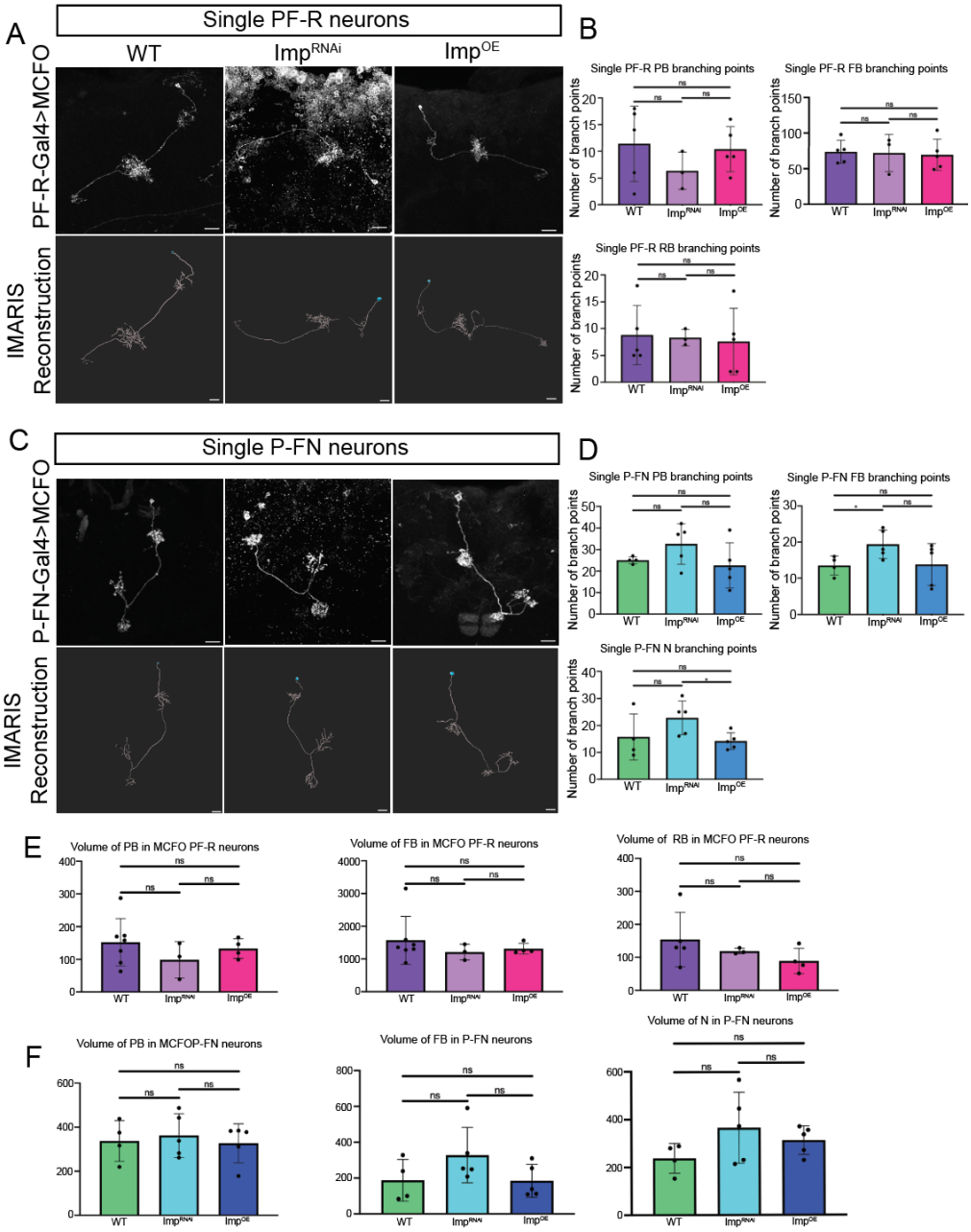

Figure 4.4. Imp^{RNAi} and Imp^{OE} show only minor changes in PF-R and P-FN neuron morphology at the single-cell level.

(A, C) WT, Imp^{RNAi} and Imp^{OE} maximum intensity projections confocal images and IMARIS surface reconstructions of single PF-R (A) and P-FN (C) neurons. Scale bar, 10µm.

(B, D) Number of branch points in WT, Imp^{RNAi}, and Imp^{OE} single PF-R (B) and P-FN (D) neurons. n=3-5 cells.

(E, F) Quantification of PF-R (E) and PF-N (D) single-cell neuropil volumes.

Discussion

In this work we characterized the role of reducing and overexpressing Imp in post-mitotic PF-R and P-FN neurons and assaying axon/dendrite morphology. We found that Imp^{OE} caused a significant increase in Imp levels in both PF-Rs and P-FNs, however Imp^{RNAi} caused a decrease in Imp levels only in PF-R neurons. Though a qualitative difference in P-FN Imp levels can be seen (Figure 4.2F) our quantification of Imp^{RNAi} levels in P-FNs were difficult to interpret. This is due to the formation of Imp ribonucleoprotein (RNP) granules in P-FN cell bodies. RNP granules are formed from mRNA and RNA-binding proteins, such as Imp (Müller-McNicoll & Neugebauer, 2013; Vijayakumar et al., 2019). These RNP granules fluoresce brightly, and complicated Imp measurements in the cell body. WT Imp levels in PF-Rs are nearly double the Imp levels seen in P-FN neurons (Figure 4.3A), which caused Imp RNP granules to skew Imp^{RNAi} measurements in P-FN neurons.

The role of Imp has also been assayed in various central brain neuroblast lineages. Imp knockdown or Imp overexpression in mushroom body neuroblasts (MBNBs) causes a loss or gain of γ neurons respectively (Liu et al., 2015). Additionally, defects in neuronal morphology are seen when Imp is knocked down or overexpressed in antennal lobe neuroblasts (ALNBs) (Ren et al., 2017). These phenotypes include mistargeting and changes in neuron numbers (Ren et al., 2017). However, this work focuses mainly on the presence or absence of cells born within an Imp expression window in progenitors where only the morphology of axons has been characterized (Liu et al., 2015; Ren et al., 2017; Vijayakumar et al., 2019). In our current work we see changes in both axon and dendrite morphology when Imp is knocked down or overexpressed post-mitotically (Figure 4.3B, 4.3D).

Previous work has shown that reducing Imp levels leads to defects in axon/dendrite morphology in γ neurons of the mushroom body -- either following global reduction or in single post-mitotic neurons using the MARCM technique (Liu et al., 2015; Medioni et al., 2014; Ren et al., 2017; Vijayakumar et al., 2019). Our current works shows that Imp plays a role in both axon and dendrite morphology post-mitotically, with a significant decreased in neuropil volume seen in both axon and dendrite targets of PF-Rs and P-FNs (Figure 4.3D, 4.3F).

Imp is part of the VICKZ (Vg1/Vera, Imp, CRD, KOC, ZBP-1) family of RBPs that is conserved across species (Nielsen et al., 1999; Yisraeli, 2005). Zipcode binding protein-1 (ZBP-1) is required for transport of mRNA in dendrites and proper dendrite morphology (Eom et al., 2003; Perycz et al., 2011). However, when ZBP-1 was overexpressed, a decrease in dendrite terminal points was seen while there was no change in the number of primary dendrites (Perycz et al., 2011). This is similar to the phenotype we see following Imp overexpression in PF-R and P-FN neurons.

Overexpression of ZBP-1 mutants with the RNA-binding region removed did not change dendrite morphology, although overexpression of full length ZBP-1 lead to increased β-Actin in dendrites and reduction in dendrite arborization (Perycz et al., 2011). This is similar to the phenotype we see in Imp overexpression in PF-R and P-FN neurons: reduced axon/dendrite branching complexity. How might ZBP-1 and Imp overexpression lead to similar phenotypes? Imp and ZBP-1 share several RNA targets, β-actin (Vikessa et al., 2006) and jim (Samuels et al., 2020); Jim has been reported to regulate dendrite morphogenesis (Iyer et al., 2013). Either of these candidates could be targets of Imp during dendrite morphogenesis, which would be a productive direction for future research.

Many different RNA-binding proteins are involved in axonal and dendrite pathfinding (Olesnicky et al., 2014; Ravanidis et al., 2018). The involvement of other RNA-binding proteins could be the reason we see such minor changes in Imp^{RNAi} and Imp^{OE} in PF-R and PF-N morphology on both the population and single-cell level. Other RNA-binding proteins could be compensating for the changes in Imp levels. The neuro-oncological ventral antigen (NOVA) family of RNA-binding proteins (*Drosophila* homologue: pasilla) has ~230 transcript targets that will change in expression level with *Nova*-KO mice, and a large amount of those encode for synaptic proteins (Ravanidis et al., 2018; Seshaiah et al., 2001). Many RNA-binding proteins are required for dendrite morphogenesis in *Drosophila* as well, including *nanos*, *pumilio*, *smaug*, and *glorund* (Olesnicky et al., 2014). Additionally, the lack of morphological changes in MCFO single cells could be due to a small n number (Figure 4.4). MCFO has a very low penetrance, and a difference in volume may only be quantifiable with a larger sample size of single neurons.

Materials and Methods

Fly genotypes

; UAS-myr::GFP ; R37G12-Gal4 (to visualize PF-R neurons)

; UAS-myr::GFP ; R16D01-Gal4 (to visualize P-FN neurons)

; UAS-Imp^{RNAi} ; UAS-Imp^{RNAi}

; UAS-Imp-3xFlag ;

; hs-Flp ; ; MCFO

; hs-Flp ; UAS-Imp^{RNAi} ; MCFO

Fly husbandry

All fly crosses were set up at 25 °C. For all experiments, only 4-10 days old, mated females were dissected. For larval experiments (Figure 4.1D-G) larvae were raised at 25 °C to specified timepoints. Both males and females were dissected.

Staining and antibodies

The following primary antibodies were used: chicken GFP (Abcam, Eugene, OR, 1:1000), rabbit Imp (Paul McDonald, UT Austin, 1:1000), guinea pig Toy (Claude Desplan, NYU 1:1000), guinea pig Runt (Claude Desplan, NYU 1:1000), mouse Bruchpilot 1:50 (Developmental Studies Hybridoma Bank, Iowa City, Iowa, rat Deadpan (Abcam, Eugene, OR 1:20), rat Elav (DHSB 1:500), chicken V5 (1:800), and rabbit HA (1:1000). All secondary antibodies were obtained from Thermofisher, Eugene, OR and used 1:400, at manufacturer's recommendations. All larvae and adult flies were dissected in Hemolymph Like buffer 3.1 (HL3.1) (NaCl 70mM, KCl 5mM, $CaCl_2$ 1.5mM, $MgCl_2$ 4mM, sucrose 115mM, $NaHCO_3$ 10mM, and Trehalose 5mM in double distilled water). Larval and adult dissected brains were mounted on poly-D-lysine coated slips (Neuvitro, Camas, WA) and incubated for 30m (larvae) or 40m (adults) in 4% paraformaldehyde solution in Phosphate Buffered Saline (PBS) with 1% Triton (1% PBS-T) at room temperature. All brain washes and antibody mixes were made in a solution of 0.5% PBS-T for larvae and 1% PBS-T for adults. All brains were washed twice in PBS-T and then incubated for 1-7 days in a blocking solution of 1% goat serum (Jackson ImmunoResearch, Westgrove, PA), 1% donkey serum (Jackson ImmunoResearch, Westgrove, PA), 2% dimethyl sulfoxide in organosulfur (DMSO), and 0.003% bovine serum albumin (BSA) (Fisher BioReagents, Fair Lawn, NJ, Lot #196941). Once removed from blocking solution, all brain

dissections were incubated overnight at 4 °C in a solution of primary antibodies. Brains were then removed from the primary solution and washed for at least 60 minutes PBS-T at room temperature and then incubated overnight at 4 °C in a solution of secondary antibodies in PBS-T. Brains were then removed from the secondary antibody solution and washed in PBS-T for at least 60 minutes at room temperature. Brains then went through a dehydration process that involved a series of EtOH washes. Larval brains went through a sequence of 10 minutes washes in 30%, 50%, 70%, and 90% EtOH, and two rounds of 10-minute washes in 100% EtOH, and two rounds of 10 minutes in xylene (MP Biomedicals, LLC, Saolon, OH, Lot# S0170), then mounted on a slide in dibutyl phthalate in xylene (DPX; Sigma-Aldrich, cat. No. 06522). Adult brains went through a series of 12-minute washes in 30%, 50%, and 70% EtOH, 15 minutes in 90% EtOH, and two rounds of 18-minute washes in 100% EtOH, and two rounds of 18 minutes in xylene then mounted in DPX. Brains sat for at least 48 hours at 4 °C or 72 hours (48 hours at room temperature and 24 hours at 4 °C) prior to imaging.

Multi-color flip-out

Crosses were all kept at 25°C until hatched. Newly hatched flies were collected and heat-shocked in a water bath of 37°C for 15 minutes. Flies were then transferred to a new vial and kept at 25°C. Only mated 4-10 day old females were dissected.

Image generation

All larvae images were taken with identical confocal settings. All Imp data in adult brains was taken with identical confocal settings. All MCFO data were collected with identical confocal settings. Fluorescent images were collected on Zeiss LSM 800.

Statistical analysis

Adult and larval cell bodies were counted using the cell count plugin in FIJI (https://imagej.net/software/fiji/). Imp pixel density in each cell body was calculated in FIJI. Cell bodies were selected in a 2D plane at the largest cross section of the cell body with the polygon lasso tool, and both the area and Raw Integrated Density (RID) of Imp was measured. The nucleus of each cell body went through the same analysis. Imp is cytoplasmic, and the nucleus measurements functioned as background subtraction. Imp levels were then normalized to cell area using the equation: (Cell Body^{RID} – Nucleus^{RID}) / (Cell Body^{Area} – Nucleus^{Area}). Note that Imp levels were difficult to accurately measure due to bright Imp RNP granules. Imp is known to form RNP granules that start in the cell body and transport mRNA to axons (Vijayakumar et al., 2019).

Neuropil volume and Brp fluorescence were measured in FIJI. Each neuropil consisted of many 2D planes, or z-slices. In each z-slice the polygon lasso tool was used to select the neuropil and the area and Brp RID was measured. For each neuropil, each z-slice area measurements were added together to obtain the volume and each z-slice Brp RID measurement was added together. To normalize Brp signal we used the equation: neuropil total RID / neuropil volume. This process was repeated in MCFO data to measure single cell neuropil volume and Brp fluorescence.

IMARIS 9.9.1 (Oxford Instruments, Carteret, NJ) was used to visualize differences in neuropil volumes. The surfaces tool was used to select individual neuropils and reconstruct the neuropil surface area. The filaments tool in IMARIS was also used to reconstruct the skeletons of single cells labeled through MCFO. Branch points and terminal points were labeled and counted.

Two-tailed student t-tests were used to compare two sets of data. *$p<0.05$; **$p<0.01$; ***$p<0.0001$. All graphs and statistical analysis were done in Prism (GraphPad Software, San Diego, CA).

Bridge:

In this chapter I confirmed the genetic Gal4 drivers used (37G12-Gal4 for PF-Rs, 16D01-Gal4 for P-FNs) targeted only post-mitotic neurons to decipher Imp's post-mitotic role. When Imp levels were knocked down or overexpressed in post-mitotic PF-R and P-FN neurons there was no change in cell number and only minor changes see in the PF-R and P-FN morphology on the population level. Using multi-color flip-out (MCFO) allowed me to look at single PF-R and P-FN neurons in WT and Imp^{RNAi} backgrounds. However, we did not see any changes in morphology on the single cell level.

In the final chapter, I summarize the work I have done to further characterize the expression patterns of Imp and Syp throughout the T2NB lineage. I was able to elucidate the role of Imp in generating neural diversity in INPs. Lastly, I discuss possible future directions for this work.

CHAPTER V

CONCLUDING SUMMARY

To create a functional nervous system, neural stem cells must generate the cellular diversity through different neuron morphologies, connectivity, and molecular identities. This diversity is necessary for proper behavior in the adult *Drosophila* is largely generated during development. Temporal patterning of neural stem cells plays a key role in defining this neural diversity in both mammals and *Drosophila*, reviewed in Doe et al. (2017) and Pollington et al. (2023) . In *Drosophila*, T2NBs expand this neural number and diversity through temporal patterning and the generation of INPs (Bayraktar & Doe, 2013; Sullivan et al., 2019; Syed et al., 2017; Walsh & Doe, 2017). Two of these factors are the RNA-binding proteins Imp and Syp which are expressed in opposing temporal gradients (Ren et al., 2017; Syed et al., 2017). During neurogenesis in larval life, T2NBs shift from high-to-low Imp expression and low-to-high Syp expression (Figure 5.1) (Ren et al., 2017; Syed et al., 2017). Imp, expressed early, promotes proliferation (Samuels et al., 2020a; Yang et al., 2017a), while Syp, expressed later, promotes T2NB decommissioning at the end of larval life (Yang et al., 2017a). Previous work shows that Imp and Syp are critical in different sets of neuroblasts to define early- and late-born progeny (Liu et al., 2015; Ren et al., 2017). During neurogenesis T2NBs will generate a large number and diverse number of cells, across both the Imp and Syp expression windows, that will populate the adult *Drosophila* central complex (Sullivan et al., 2019; Syed et al., 2017; Walsh & Doe, 2017; Wolff et al., 2015). My research has worked to further characterize Imp's role in T2NB exit from quiescence in early neurogenesis, the Imp and Syp expression patterns in intermediate neural progenitors, what role Imp plays in INPs to generate different types of CX neurons, and Imp's potential post-mitotic role in CX neurons (Figure 5.1).

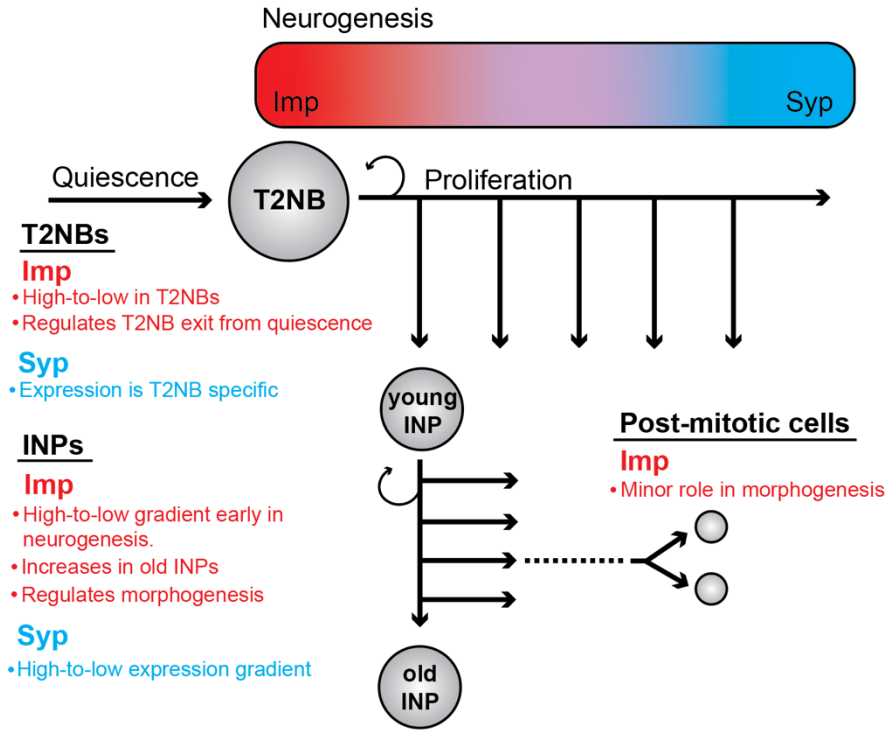

Figure 5.1. Summary schematic. Summarizes Imp and Syp expression in T2NBs and INPs, as well as the role of Imp in generating neural diversity throughout the T2NB lineage.

The Imp expression gradient in T2NBs shifts from high-to-low expression, with its highest expression at 24h ALH and reaching low levels by 60h ALH (Munroe et al., 2022; Syed et al., 2017). This high level of Imp is necessary in T2NBs for timely exit from quiescence (Munroe et al., 2022). In wild type larval brains, all 16 T2NBs have exited quiescence and begun proliferating by 36h ALH, but if Imp is knocked down all 16 T2NBs will not exit quiescence until 72h ALH (Munroe et al., 2022). This work expands on Imp's known roles in regulating proliferation and differentiation in early T2NBs (Samuels et al., 2020a; Yang et al., 2017)

Once T2NBs exit quiescence and begin proliferation they will start to generate INPs to pairs of neurons that populate the central complex. As INPs divide they age from young to old, and change their molecular identity, with young and old INPs each producing specific types of

CX neurons (Bayraktar & Doe, 2013; Sullivan et al., 2019)I have been able to show that Imp expression in T2NBs is consistently high-to-low across all T2NB lineages, while Syp expression is T2NBs specific, and these Imp and Syp levels are equivalent in newborn INPs (Munroe, accepted). In certain T2NB lineages high levels of Imp and Syp are co-expressed early in development. This could suggest a novel interaction between Imp and Syp, which are known to down-regulate each other (Liu et al., 2015; Ren et al., 2017; Syed et al., 2017). While Syp expression in the INP lineage consistently shifted from high-to-low, Imp expression increased in old INPs (Munroe, accepted), potentially due to up-regulation via Lin-28 which is also expressed early in T2NBs (Sreejith et al., 2022; Syed et al., 2017). Both Lin-28 and Imp are expressed in Drosophila intestinal stem cells and upregulate each other (Sreejith et al., 2022). I showed that Imp expression is required in old INPs to generate neural diversity in the CX (Munroe, accepted). Imp expression persists into post-mitotic neurons, where it seems to play a minor role in proper neurite morphogenesis (Munroe, unpublished). Analysis on behavior and functionality of these CX neurons when Imp has been knocked-down or mis-expressed either post-mitotically or in INPs would be a logical next step for this research.

Previous work has shown that E-PG neurons in the CX are required for celestial navigation behavior in the adult fly (Giraldo et al., 2018; Seelig & Jayaraman, 2013; Sullivan et al., 2019; Warren et al., 2019). *Drosophila* will follow an arbitrary heading (menotaxis), and when presented with a moving target the animal will adjust its heading relative to the visual stimulus, such as polarized light (Giraldo et al., 2018; Seelig & Jayaraman, 2013; Warren et al., 2019). This change in heading is occurs with an increase in activity in E-PG neurons (Giraldo et al., 2018; Seelig & Jayaraman, 2013; Warren et al., 2019). When E-PG neurons are silenced, then the fly will only direct it's heading directly to the source of light (Giraldo et al., 2018;

Warren et al., 2019). Impaired flight behavior can also be seen when disruptions occur during E-PG neurogenesis (Sullivan et al., 2019). The TF Eyeless (Ey) is expressed only old INPs, but not younger INPs stages (Bayraktar & Doe, 2013; Sullivan et al., 2019). Ey knock-down results in morphological defects in E-PG neurons and loss of cell number, as well as impairing flight (Sullivan et al., 2019). My work has shown that Imp and Syp are both expressed throughout INP lineages (Munroe, accepted). This finding, in combination with previous research, demonstrates the possibility that changes in the CX due to loss or overexpression of Imp could be seen at the behavioral level.

Though much has been characterized about Imp's expression patterns in T2NBs, very little is known about its mRNA targets within this lineage. In mushroom body neuroblasts (MBNBs), Imp targets and stabilizes Myc mRNA and regulates MBNB growth and proliferation period (Samuels et al., 2020a). Imp could potentially be playing the same role regulating T2NB lifespan. In both MBNBs and T2NBs, loss of Syp expression causes an extended expression of the TF Chinmo (Liu et al., 2015; Syed et al., 2017), meaning Chinmo mRNA could be a direct target for Syp in both NB lineages. Finally, in MBNBs and a subset of T2NBs, Imp and Syp target and repress each other (Liu et al., 2015; Ren et al., 2017; Syed et al., 2017). However, my work has shown that in T2NBs Imp and Syp down regulation of each other is lineage specific (Munroe, accepted). The DM4 and DL2 T2NB lineages have both high Imp and Syp expression in T2NBs and newborn INPs early in neurogenesis (Munroe, accepted). How Imp/Syp regulation could be T2NB lineage specific is not understood.

The T2NB lineage is key for proper neural development of the *Drosophila* central brain. Mis-regulation of these neural progenitors can result in the incorrect number and type of cells and result in behavioral phenotypes in adult *Drosophila* (Sullivan et al., 2019; Syed et al., 2017).

The RNA-binding protein Imp, conserved in both mammals and *Drosophila*, plays several key roles in the T2NB lineage (Samuels et al., 2020a; Yisraeli, 2005). The proper level of Imp expression is required to regulate proliferation in T2NBs and the generation of neural diversity in INPs (Munroe et al., 2022; Munroe, accepted). The neural progenitors, outer radial glial cells (oRGs), in primates are similar to T2NBs in that they also generate intermediate progenitors to expand neural number (Hansen et al., 2010; Pollen et al., 2015). This research suggests that the intrinsic, temporal regulation required in *Drosophila* T2NBs and its following lineage via Imp could be occurring in oRGs in humans.

APPENDEX A

SUPPLEMENT TO CHAPTER III

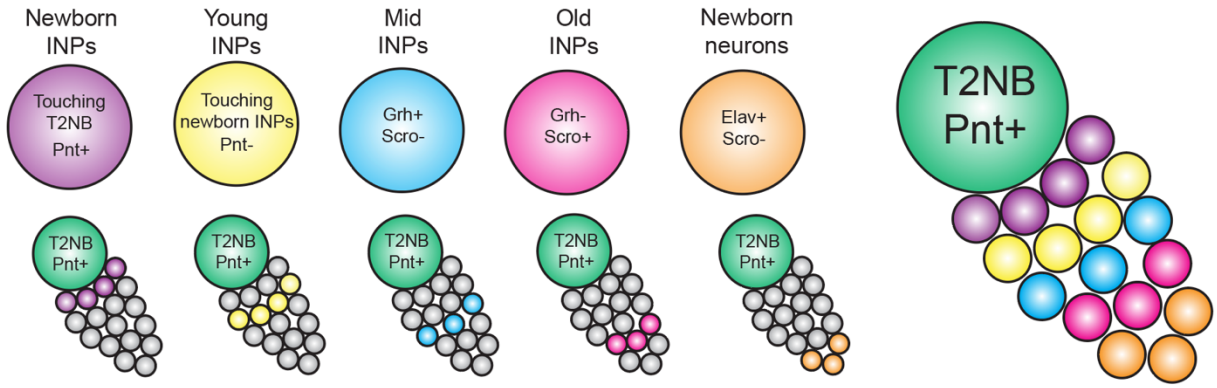

Supplemental Figure 3.1. INP staging criteria.
Schematic showing markers that define different stages in INP lineage progression. T2NBs (green, GFP- Pnt+); nINPs contact the parental NB (purple, GFP- Pnt+); yINPs (yellow, GFP+ Pnt+) border nINPs; mINPs (blue, GFP+ Grh+ Scro-); oINPs (pink, GFP+ Grh- Scro+); and nNeurons (orange, GFP+ Elav+ Scro-). GFP was driven in nINPs, yINPs, mINPs and oINPs with 12E09-Gal4, and in oINPs and nNeurons with 16B06-Gal4.

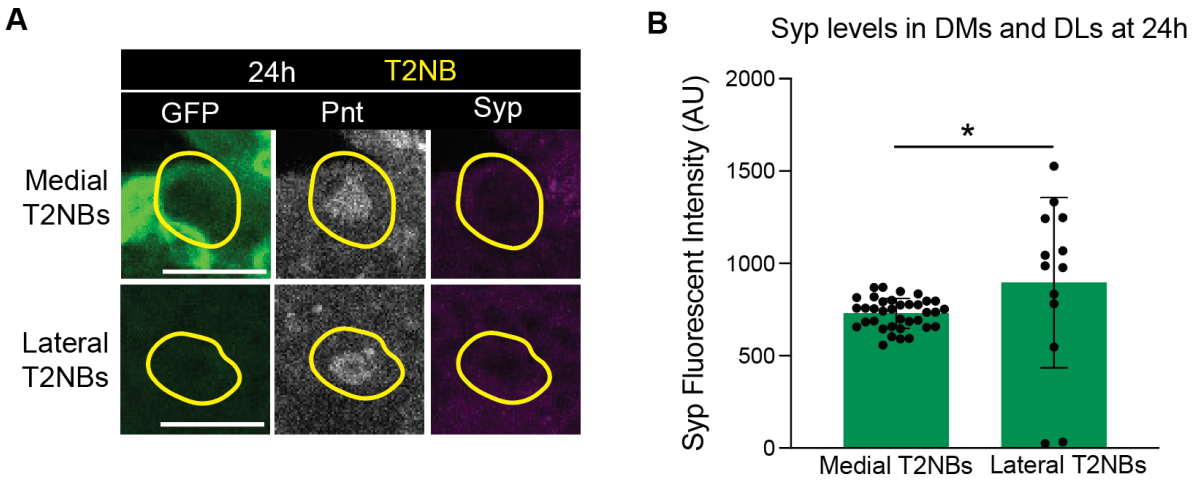

Supplemental Figure 3.2. At 24h T2NB lineages can only be characterized as medial and lateral.

(A) 12E09>UAS-GFP at 24h targets proliferative T2NBs (GFP+, Pnt+ yellow circles). Scale bar 5μm.

(B) Quantification of Syp levels in medial and lateral T2NBs at 24h. n = 5 brains. Student t-tests were used to compare medial cells to lateral cells. *p<0.05; **p<0.01; ***p<0.001; ****p<0.0001.

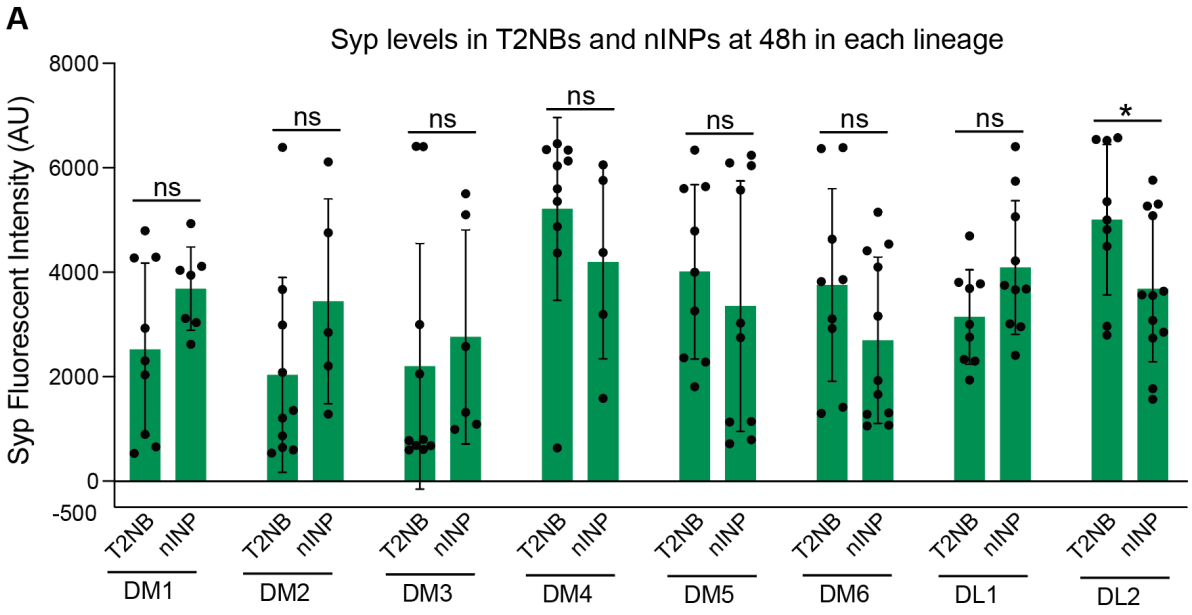

Supplemental Figure 3.3. Lineage specific Syp levels in T2NBs and nINPs is equivalent except for DL2.

(A) Quantification of Syp levels in T2NBs and nINPs in each specific lineage. n = 5 brains. Student t-tests were used to compare medial cells to lateral cells. *p<0.05; **p<0.01; ***p<0.001; ****p<0.0001.

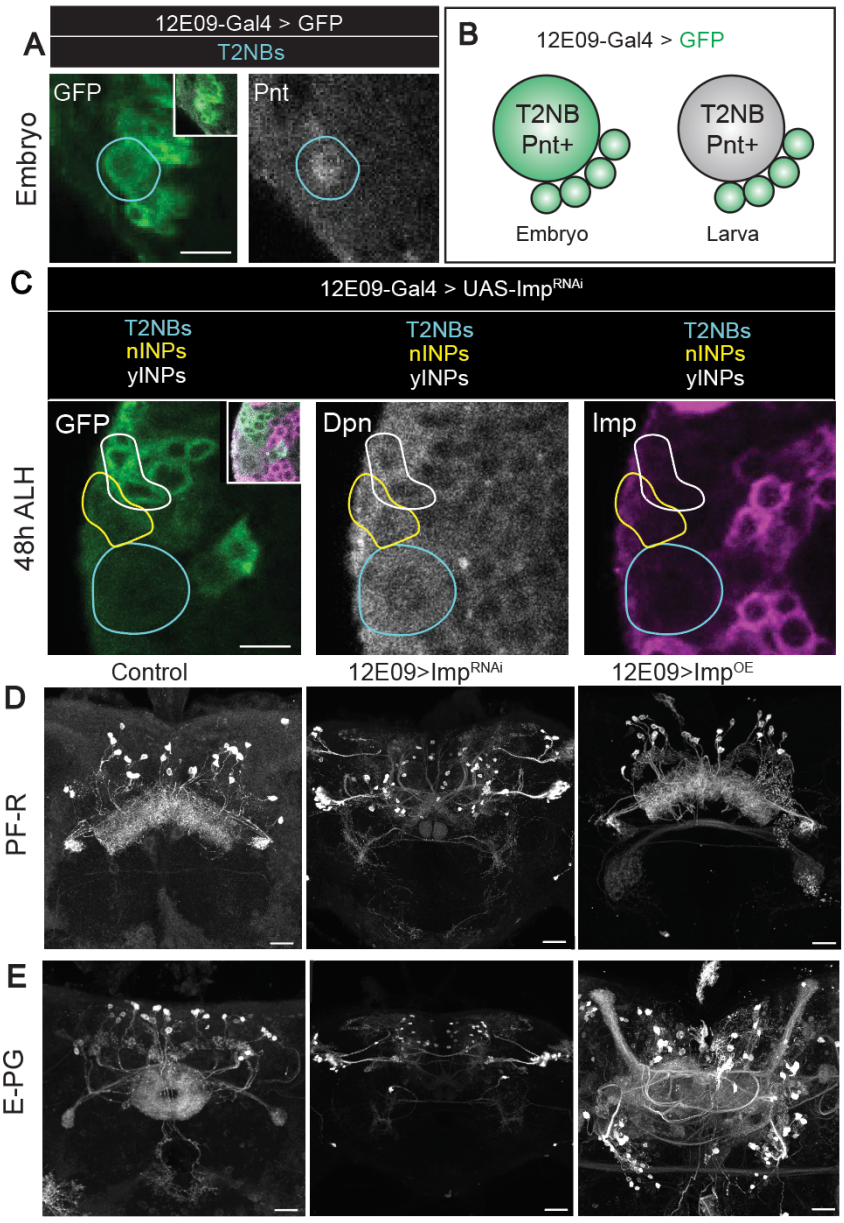

Supplemental Figure 3.4. 12E09-Gal4 is expressed in embryonic T2NBs and is required for PF-R and E-PG neuron morphology.

(A) 12E09-Gal4>UAS-GFP in embryonic T2NBs. T2NBs (GFP+ Pnt+, cyan circles). Scale bar 5μm.

(B) Schematic of 12E09-Gal4 expression in embryonic and larval T2NBs and n/yINPs.

(C) 12E09-Gal4>UAS-Imp^{RNAi} turns on earlier in development. T2NBs (cyan circles, GFP- Dpn+), nINPs (yellow circles, GFP- Dpn+), and yINPs (white circles, GFP+ Dpn-) show a loss of Imp at 48h in T2NBs. Scale bar 5μm.

(D-E) Confocal maximum intensity projections of control, Imp^{RNAi} and Imp^{OE} in PF-R and E-PG neurons. n = 5, scale bar 20μm.

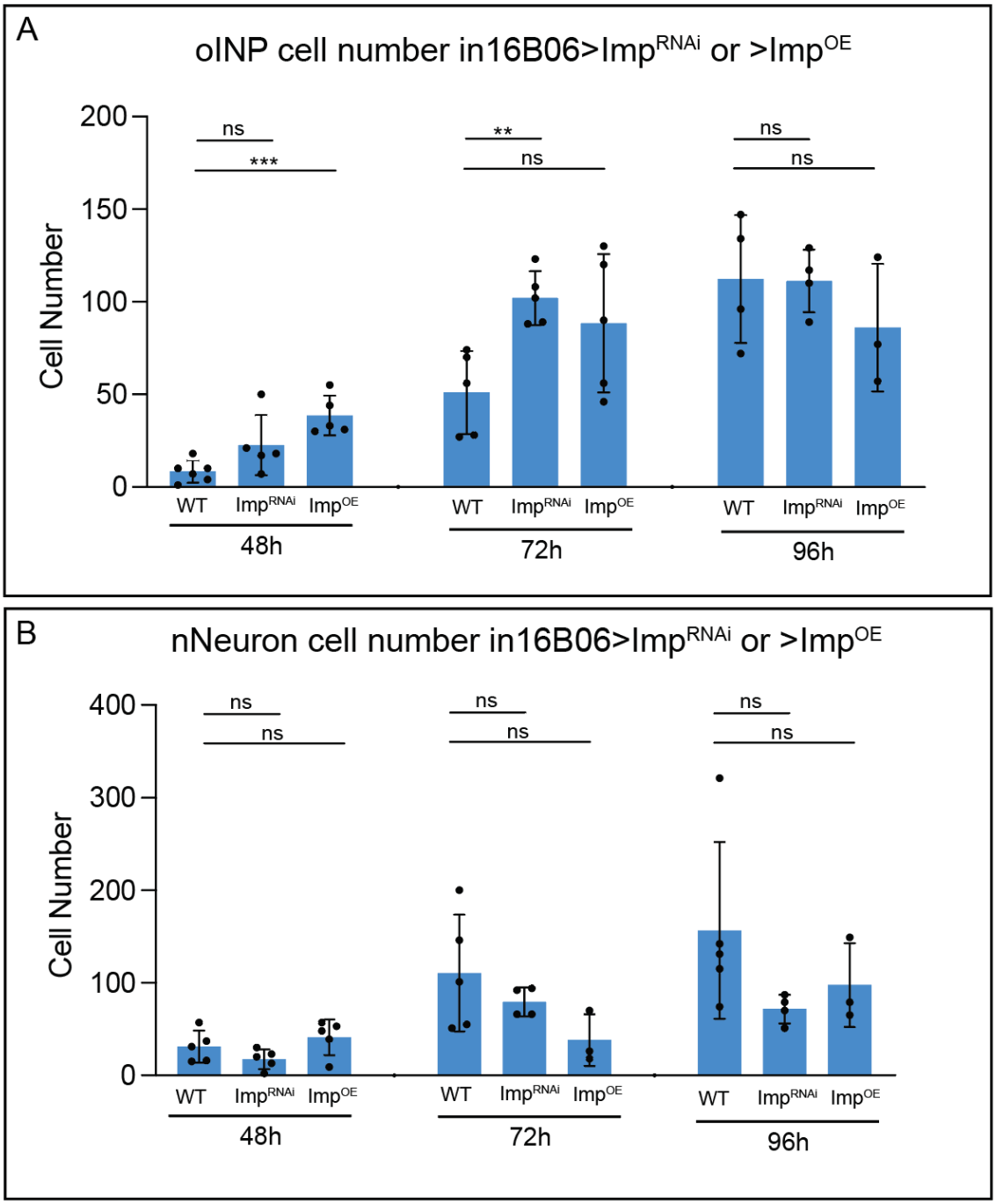

Supplemental Figure 3.5. 16B06>Imp^{RNAi} causes an increase in cell number at 48h and 72h.
(A-B) Number of oINPs (A) and nNeurons (B) in control, Imp^{RNAi} and Imp^{OE}. Each point is an oINP (A) or nNeuron (B). n = 3-5 brains. Student t-tests were used to compare cell numbers to control. *p<0.05; **p<0.01; ***p<0.001; ****p<0.0001.

Supplemental Video 3.1. Imaris reconstruction of T2NBs in a larval brain. Imaris reconstruction of a 60h larval brain (clear) showing location of T2NBs (magenta). Scale bar 20µm.

APPENDIX B

SUPPLEMENT TO CHAPTER IV

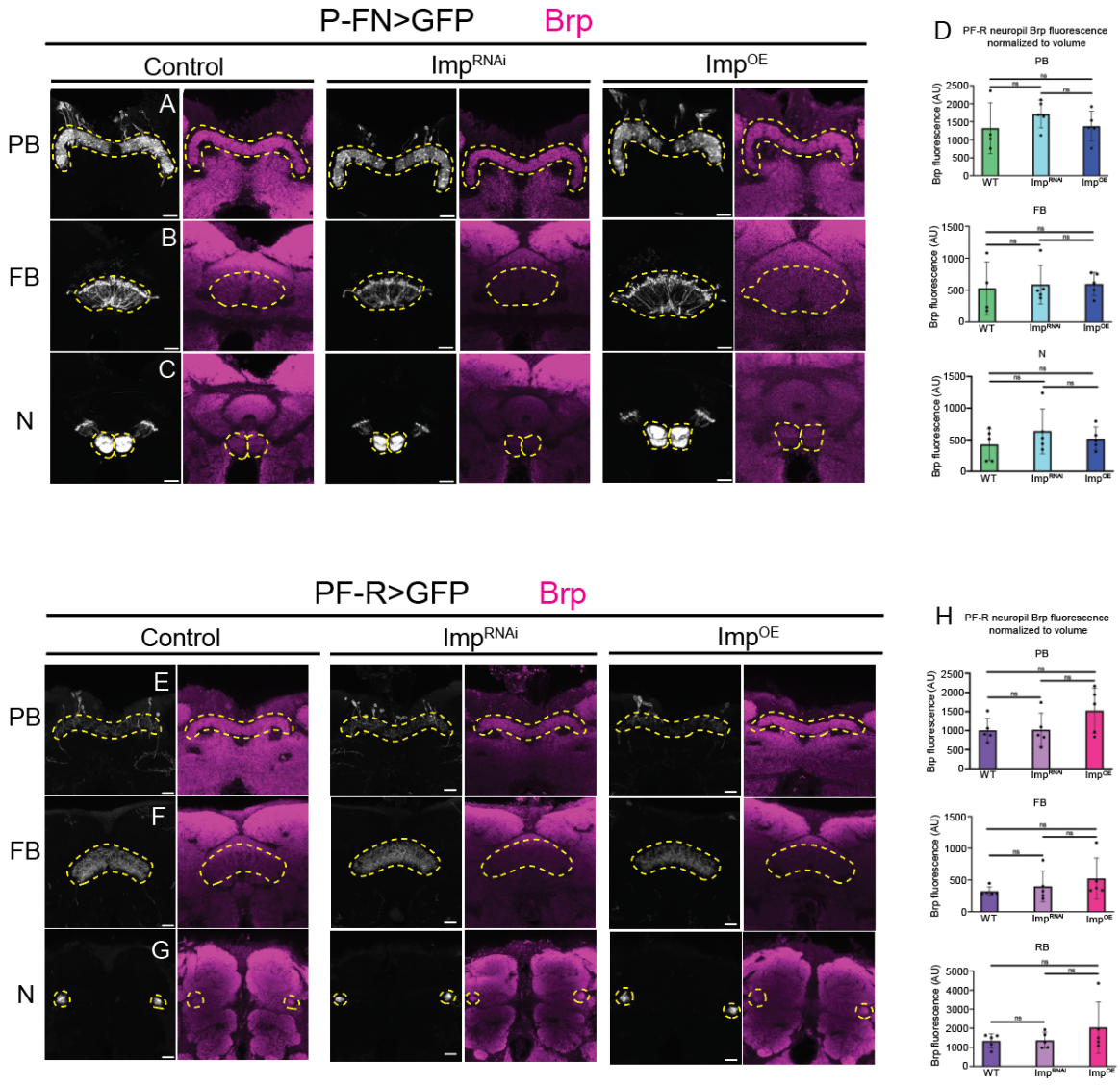

Supplemental Figure 4.1. Brp expression levels do not change in Imp^{RNAi} or Imp^{OE}.
(A-C) P-FN neuropils (A) PB, (B) FB, (C) N confocal images and Brp antibody fluorescence. (D-F) PF-R neuropils (D) PB, (E) FB, (F) RB confocal images and Brp antibody fluorescence. Yellow dashed lines mark each neuropil.

References

Abdusselamoglu, M. D., Eroglu, E., Burkard, T. R., & Knoblich, J. A. (2019). The transcription factor odd-paired regulates temporal identity in transit-amplifying neural progenitors via an incoherent feed-forward loop. *eLife*, *8*, e46566. https://doi.org/10.7554/eLife.46566

Álvarez, J. A., & Díaz-Benjumea, F. J. (2018). Origin and specification of type-II neuroblasts in the *Drosophila* embryo. *Development*, dev.158394. https://doi.org/10.1242/dev.158394

Bayraktar, O. A., & Doe, C. Q. (2013). Combinatorial temporal patterning in progenitors expands neural diversity. *Nature*, *498*(7455), 449–455. https://doi.org/10.1038/nature12266

Bello, B. C., Izergina, N., Caussinus, E., & Reichert, H. (2008). Amplification of neural stem cell proliferation by intermediate progenitor cells in Drosophila brain development. *Neural Development*, *3*(1), 5. https://doi.org/10.1186/1749-8104-3-5

Boone, J. Q., & Doe, C. Q. (2008). Identification of *Drosophila* type II neuroblast lineages containing transit amplifying ganglion mother cells. *Developmental Neurobiology*, *68*(9), 1185–1195. https://doi.org/10.1002/dneu.20648

Bowman, S. K., Rolland, V., Betschinger, J., Kinsey, K. A., Emery, G., & Knoblich, J. A. (2008). The Tumor Suppressors Brat and Numb Regulate Transit-Amplifying Neuroblast Lineages in Drosophila. *Developmental Cell*, *14*(4), 535–546. https://doi.org/10.1016/j.devcel.2008.03.004

Boyan, G. S., & Reichert, H. (2011). Mechanisms for complexity in the brain: Generating the insect central complex. *Trends in Neurosciences*, *34*(5), 247–257. https://doi.org/10.1016/j.tins.2011.02.002

Chell, J. M., & Brand, A. H. (2010). Nutrition-Responsive Glia Control Exit of Neural Stem Cells from Quiescence. *Cell*, *143*(7), 1161–1173. https://doi.org/10.1016/j.cell.2010.12.007

Choksi, S. P., Southall, T. D., Bossing, T., Edoff, K., De Wit, E., Fischer, B. E., Van Steensel, B., Micklem, G., & Brand, A. H. (2006). Prospero Acts as a Binary Switch between Self-Renewal and Differentiation in Drosophila Neural Stem Cells. *Developmental Cell*, *11*(6), 775–789. https://doi.org/10.1016/j.devcel.2006.09.015

Di Fusco, D., Di Grazia, A., Di Maggio, G., Segreto, M. T., Iannucci, A., Maresca, C., De Stefano, A., Sica, G., Stolfi, C., Monteleone, G., & Monteleone, I. (2023). A novel tumour enhancer function of Insulin-like growth factor II mRNA-binding protein 3 in colorectal cancer. *Cell Death & Disease*, *14*(4), 243. https://doi.org/10.1038/s41419-023-05772-6

Dillard, C., Narbonne-Reveau, K., Foppolo, S., Lanet, E., & Maurange, C. (2017). Two distinct mechanisms silence *chinmo* in *Drosophila* neuroblasts and neuroepithelial cells to limit their self-renewal. *Development*, dev.154534. https://doi.org/10.1242/dev.154534

Doe, C. Q. (2017). *Temporal Patterning in the Drosophila CNS*. 25.

Eom, T., Antar, L. N., Singer, R. H., & Bassell, G. J. (2003). *Localization of a β-Actin Messenger Ribonucleoprotein Complex with Zipcode-Binding Protein Modulates the Density of Dendritic Filopodia and Filopodial Synapses*.

Fietz, S. A., Kelava, I., Vogt, J., Wilsch-Bräuninger, M., Stenzel, D., Fish, J. L., Corbeil, D., Riehn, A., Distler, W., Nitsch, R., & Huttner, W. B. (2010). OSVZ progenitors of human and ferret neocortex are epithelial-like and expand by integrin signaling. *Nature Neuroscience*, *13*(6), 690–699. https://doi.org/10.1038/nn.2553

Fiore, V. G., Dolan, R. J., Strausfeld, N. J., & Hirth, F. (2015). Evolutionarily conserved mechanisms for the selection and maintenance of behavioural activity. *Philosophical Transactions of the Royal Society B: Biological Sciences*, *370*(1684), 20150053. https://doi.org/10.1098/rstb.2015.0053

Franconville, R., Beron, C., & Jayaraman, V. (2018). Building a functional connectome of the Drosophila central complex. *eLife*, *7*, e37017. https://doi.org/10.7554/eLife.37017

Giraldo, Y. M., Leitch, K. J., Ros, I. G., Warren, T. L., Weir, P. T., & Dickinson, M. H. (2018). Sun Navigation Requires Compass Neurons in Drosophila. *Current Biology*, *28*(17), 2845-2852.e4. https://doi.org/10.1016/j.cub.2018.07.002

Givon, L. E., Lazar, A. A., & Yeh, C.-H. (2017). Generating Executable Models of the Drosophila Central Complex. *Frontiers in Behavioral Neuroscience*, *11*, 102. https://doi.org/10.3389/fnbeh.2017.00102

Graybiel, A. M. (1995). The basal ganglia. *Trends in Neurosciences*, *18*(2), 60–62.

Green, J., Vijayan, V., Mussells Pires, P., Adachi, A., & Maimon, G. (2019). A neural heading estimate is compared with an internal goal to guide oriented navigation. *Nature Neuroscience*, *22*(9), 1460–1468. https://doi.org/10.1038/s41593-019-0444-x

Guan, W., Bellemin, S., Bouchet, M., Venkatasubramanian, L., Guillermin, C., Laurençon, A., Kabir, C., Darnas, A., Godin, C., Urdy, S., Mann, R. S., & Enriquez, J. (2022). Post-transcriptional regulation of transcription factor codes in immature neurons drives neuronal diversity. *Cell Reports*, *39*(13), 110992. https://doi.org/10.1016/j.celrep.2022.110992

Hakes, A. E., & Brand, A. H. (2020). Tailless/TLX reverts intermediate neural progenitors to stem cells driving tumourigenesis via repression of asense/ASCL1. *eLife*, *9*, e53377. https://doi.org/10.7554/eLife.53377

Hansen, D. V., Lui, J. H., Parker, P. R. L., & Kriegstein, A. R. (2010). Neurogenic radial glia in the outer subventricular zone of human neocortex. *Nature*, *464*(7288), 554–561. https://doi.org/10.1038/nature08845

Hobor, F., Dallmann, A., Ball, N. J., Cicchini, C., Battistelli, C., Ogrodowicz, R. W., Christodoulou, E., Martin, S. R., Castello, A., Tripodi, M., Taylor, I. A., & Ramos, A. (2018). A cryptic RNA-binding domain mediates Syncrip recognition and exosomal partitioning of miRNA targets. *Nature Communications*, *9*(1), 831. https://doi.org/10.1038/s41467-018-03182-3

Homem, C. C. F., Reichardt, I., Berger, C., Lendl, T., & Knoblich, J. A. (2013). Long-Term Live Cell Imaging and Automated 4D Analysis of Drosophila Neuroblast Lineages. *PLoS ONE*, *8*(11), e79588. https://doi.org/10.1371/journal.pone.0079588

Hulse, B. K., Haberkern, H., Franconville, R., Turner-Evans, D., Takemura, S., Wolff, T., Noorman, M., Dreher, M., Dan, C., Parekh, R., Hermundstad, A. M., Rubin, G. M., & Jayaraman, V. (2021). A connectome of the Drosophila central complex reveals network motifs suitable for flexible navigation and context-dependent action selection. *eLife*, *10*, e66039. https://doi.org/10.7554/eLife.66039

Isshiki, T., Pearson, B., Holbrook, S., & Doe, C. Q. (2001). Drosophila Neuroblasts Sequentially Express Transcription Factors which Specify the Temporal Identity of Their Neuronal Progeny. *Cell*, *106*(4), 511–521. https://doi.org/10.1016/S0092-8674(01)00465-2

Ito, M., Masuda, N., Shinomiya, K., Endo, K., & Ito, K. (2013). Systematic Analysis of Neural Projections Reveals Clonal Composition of the Drosophila Brain. *Current Biology*, *23*(8), 644–655. https://doi.org/10.1016/j.cub.2013.03.015

Iyer, E. P. R., Iyer, S. C., Sullivan, L., Wang, D., Meduri, R., Graybeal, L. L., & Cox, D. N. (2013). Functional Genomic Analyses of Two Morphologically Distinct Classes of Drosophila Sensory Neurons: Post-Mitotic Roles of Transcription Factors in Dendritic Patterning. *PLoS ONE*, *8*(8), e72434. https://doi.org/10.1371/journal.pone.0072434

Kanning, K. C., Kaplan, A., & Henderson, C. E. (2010). Motor Neuron Diversity in Development and Disease. *Annual Review of Neuroscience*, *33*(1), 409–440. https://doi.org/10.1146/annurev.neuro.051508.135722

Lai, S.-L., & Doe, C. Q. (2014). Transient nuclear Prospero induces neural progenitor quiescence. *eLife*, *3*, e03363. https://doi.org/10.7554/eLife.03363

Lee, T., Lee, A., & Luo, L. (1999). Development of the *Drosophila* mushroom bodies: Sequential generation of three distinct types of neurons from a neuroblast. *Development*, *126*(18), 4065–4076. https://doi.org/10.1242/dev.126.18.4065

Lewitus, E., Kelava, I., & Huttner, W. B. (2013). Conical expansion of the outer subventricular zone and the role of neocortical folding in evolution and development. *Frontiers in Human Neuroscience*, *7*. https://doi.org/10.3389/fnhum.2013.00424

Liao, B., Hu, Y., & Brewer, G. (2011). RNA-binding Protein Insulin-like Growth Factor mRNA-binding Protein 3 (IMP-3) Promotes Cell Survival via Insulin-like Growth Factor II Signaling after Ionizing Radiation. *Journal of Biological Chemistry*, *286*(36), 31145–31152. https://doi.org/10.1074/jbc.M111.263913

Liu, Z., Yang, C.-P., Sugino, K., Fu, C.-C., Liu, L.-Y., Yao, X., Lee, L. P., & Lee, T. (2015). Opposing intrinsic temporal gradients guide neural stem cell production of varied neuronal fates. *Science*, *350*(6258), 317–320. https://doi.org/10.1126/science.aad1886

Lu, B., & Vogel, H. (2009). Drosophila Models of Neurodegenerative Diseases. *Annual Review of Pathology: Mechanisms of Disease*, *4*(1), 315–342. https://doi.org/10.1146/annurev.pathol.3.121806.151529

Lytle, J. R., Yario, T. A., & Steitz, J. A. (2007). Target mRNAs are repressed as efficiently by microRNA-binding sites in the 5′ UTR as in the 3′ UTR. *Proceedings of the National Academy of Sciences*, *104*(23), 9667–9672. https://doi.org/10.1073/pnas.0703820104

Mattar, P., Ericson, J., Blackshaw, S., & Cayouette, M. (2015). A Conserved Regulatory Logic Controls Temporal Identity in Mouse Neural Progenitors. *Neuron*, *85*(3), 497–504. https://doi.org/10.1016/j.neuron.2014.12.052

Maurange, C., Cheng, L., & Gould, A. P. (2008). Temporal Transcription Factors and Their Targets Schedule the End of Neural Proliferation in Drosophila. *Cell*, *133*(5), 891–902. https://doi.org/10.1016/j.cell.2008.03.034

McDermott, S. M., Meignin, C., Rappsilber, J., & Davis, I. (2012). *Drosophila* Syncrip binds the *gurken* mRNA localisation signal and regulates localised transcripts during axis specification. *Biology Open*, *1*(5), 488–497. https://doi.org/10.1242/bio.2012885

Medioni, C., Ramialison, M., Ephrussi, A., & Besse, F. (2014). Imp Promotes Axonal Remodeling by Regulating profilin mRNA during Brain Development. *Current Biology*, *24*(7), 793–800. https://doi.org/10.1016/j.cub.2014.02.038

Müller-McNicoll, M., & Neugebauer, K. M. (2013). How cells get the message: Dynamic assembly and function of mRNA–protein complexes. *Nature Reviews Genetics*, *14*(4), 275–287. https://doi.org/10.1038/nrg3434

Munroe, J. A., Syed, M. H., & Doe, C. Q. (2022). Imp is required for timely exit from quiescence in Drosophila type II neuroblasts. *PLOS ONE*, *17*(12), e0272177. https://doi.org/10.1371/journal.pone.0272177

Nern, A., Pfeiffer, B. D., & Rubin, G. M. (2015). Optimized tools for multicolor stochastic labeling reveal diverse stereotyped cell arrangements in the fly visual system. *Proceedings of the National Academy of Sciences*, *112*(22). https://doi.org/10.1073/pnas.1506763112

Nielsen, J., Christiansen, J., Lykke-Andersen, J., Johnsen, A. H., Wewer, U. M., & Nielsen, F. C. (1999). A Family of Insulin-Like Growth Factor II mRNA-Binding Proteins Represses Translation in Late Development. *Molecular and Cellular Biology*, *19*(2), 1262–1270. https://doi.org/10.1128/MCB.19.2.1262

Noctor, S. C., Martínez-Cerdeño, V., Ivic, L., & Kriegstein, A. R. (2004). Cortical neurons arise in symmetric and asymmetric division zones and migrate through specific phases. *Nature Neuroscience*, *7*(2), 136–144. https://doi.org/10.1038/nn1172

Olesnicky, E. C., Killian, D. J., Garcia, E., Morton, M. C., Rathjen, A. R., Sola, I. E., & Gavis, E. R. (2014). Extensive Use of RNA-Binding Proteins in *Drosophila* Sensory Neuron Dendrite Morphogenesis. *G3 Genes|Genomes|Genetics*, *4*(2), 297–306. https://doi.org/10.1534/g3.113.009795

Perycz, M., Urbanska, A. S., Krawczyk, P. S., Parobczak, K., & Jaworski, J. (2011). Zipcode Binding Protein 1 Regulates the Development of Dendritic Arbors in Hippocampal Neurons. *Journal of Neuroscience*, *31*(14), 5271–5285. https://doi.org/10.1523/JNEUROSCI.2387-10.2011

Pfeiffer, K., & Homberg, U. (2014). Organization and Functional Roles of the Central Complex in the Insect Brain. *Annual Review of Entomology*, *59*(1), 165–184. https://doi.org/10.1146/annurev-ento-011613-162031

Pollen, A. A., Nowakowski, T. J., Chen, J., Retallack, H., Sandoval-Espinosa, C., Nicholas, C. R., Shuga, J., Liu, S. J., Oldham, M. C., Diaz, A., Lim, D. A., Leyrat, A. A., West, J. A., & Kriegstein, A. R. (2015). Molecular Identity of Human Outer Radial Glia during Cortical Development. *Cell*, *163*(1), 55–67. https://doi.org/10.1016/j.cell.2015.09.004

Pollington, H. Q., Seroka, A. Q., & Doe, C. Q. (2023). From temporal patterning to neuronal connectivity in Drosophila type I neuroblast lineages. *Seminars in Cell & Developmental Biology*, *142*, 4–12. https://doi.org/10.1016/j.semcdb.2022.05.022

Ravanidis, S., Kattan, F.-G., & Doxakis, E. (2018). Unraveling the Pathways to Neuronal Homeostasis and Disease: Mechanistic Insights into the Role of RNA-Binding Proteins and Associated Factors. *International Journal of Molecular Sciences*, *19*(8), 2280. https://doi.org/10.3390/ijms19082280

Redgrave, P., Rodriguez, M., Smith, Y., Rodriguez-Oroz, M. C., Lehericy, S., Bergman, H., Agid, Y., DeLong, M. R., & Obeso, J. A. (2010). Goal-directed and habitual control in the basal ganglia: Implications for Parkinson's disease. *Nature Reviews Neuroscience*, *11*(11), 760–772. https://doi.org/10.1038/nrn2915

Ren, Q., Yang, C.-P., Liu, Z., Sugino, K., Mok, K., He, Y., Ito, M., Nern, A., Otsuna, H., & Lee, T. (2017). Stem Cell-Intrinsic, Seven-up-Triggered Temporal Factor Gradients Diversify Intermediate Neural Progenitors. *Current Biology*, *27*(9), 1303–1313. https://doi.org/10.1016/j.cub.2017.03.047

Riebli, N., Viktorin, G., & Reichert, H. (2013). Early-born neurons in type II neuroblast lineages establish a larval primordium and integrate into adult circuitry during central complex development in Drosophila. *Neural Development*, *8*(1), 6. https://doi.org/10.1186/1749-8104-8-6

Samuels, T. J., Järvelin, A. I., Ish-Horowicz, D., & Davis, I. (2020). Imp/IGF2BP levels modulate individual neural stem cell growth and division through myc mRNA stability. *eLife*, *9*, e51529. https://doi.org/10.7554/eLife.51529

Santangelo, L., Giurato, G., Cicchini, C., Montaldo, C., Mancone, C., Tarallo, R., Battistelli, C., Alonzi, T., Weisz, A., & Tripodi, M. (2016). The RNA-Binding Protein SYNCRIP Is a Component of the Hepatocyte Exosomal Machinery Controlling MicroRNA Sorting. *Cell Reports*, *17*(3), 799–808. https://doi.org/10.1016/j.celrep.2016.09.031

Scheffer, L. K., Xu, C. S., Januszewski, M., Lu, Z., Takemura, S., Hayworth, K. J., Huang, G. B., Shinomiya, K., Maitlin-Shepard, J., Berg, S., Clements, J., Hubbard, P. M., Katz, W. T., Umayam, L., Zhao, T., Ackerman, D., Blakely, T., Bogovic, J., Dolafi, T., … Plaza, S. M. (2020). A connectome and analysis of the adult Drosophila central brain. *eLife*, *9*, e57443. https://doi.org/10.7554/eLife.57443

Seelig, J. D., & Jayaraman, V. (2013). Feature detection and orientation tuning in the Drosophila central complex. *Nature*, *503*(7475), 262–266. https://doi.org/10.1038/nature12601

Seshaiah, P., Miller, B., Myat, M. M., & Andrew, D. J. (2001). Pasilla, the Drosophila Homologue of the Human Nova-1 and Nova-2 Proteins, Is Required for Normal Secretion in the Salivary Gland. *Developmental Biology*, *239*(2), 309–322. https://doi.org/10.1006/dbio.2001.0429

Siletti, K., Hodge, R., Mossi Albiach, A., Lee, K. W., Ding, S.-L., Hu, L., Lönnerberg, P., Bakken, T., Casper, T., Clark, M., Dee, N., Gloe, J., Hirschstein, D., Shapovalova, N. V., Keene, C. D., Nyhus, J., Tung, H., Yanny, A. M., Arenas, E., … Linnarsson, S. (2023). Transcriptomic diversity of cell types across the adult human brain. *Science*, *382*(6667), eadd7046. https://doi.org/10.1126/science.add7046

Skeath, J. B., & Thor, S. (2003). Genetic control of Drosophila nerve cord development. *Curr Opin Neurobiol*, *13*(1), 8–15. https://doi.org/S0959438803000072 [pii]

Sreejith, P., Malik, S., Kim, C., & Biteau, B. (2022). Imp interacts with Lin28 to regulate adult stem cell proliferation in the Drosophila intestine. *PLOS Genetics*, *18*(9), e1010385. https://doi.org/10.1371/journal.pgen.1010385

Strausfeld, N. J., & Hirth, F. (2013). Deep Homology of Arthropod Central Complex and Vertebrate Basal Ganglia. *Science*, *340*(6129), 157–161. https://doi.org/10.1126/science.1231828

Sullivan, L. F., Warren, T. L., & Doe, C. Q. (2019). Temporal identity establishes columnar neuron morphology, connectivity, and function in a Drosophila navigation circuit. *eLife*, *8*, e43482. https://doi.org/10.7554/eLife.43482

Suzuki, T., Kaido, M., Takayama, R., & Sato, M. (2013). A temporal mechanism that produces neuronal diversity in the Drosophila visual center. *Developmental Biology*, *380*(1), 12–24. https://doi.org/10.1016/j.ydbio.2013.05.002

Syed, M. H., Mark, B., & Doe, C. Q. (2017). Steroid hormone induction of temporal gene expression in Drosophila brain neuroblasts generates neuronal and glial diversity. *eLife*, *6*, e26287. https://doi.org/10.7554/eLife.26287

Tang, J. L. Y., Hakes, A. E., Krautz, R., Suzuki, T., Contreras, E. G., Fox, P. M., & Brand, A. H. (2022). NanoDam identifies Homeobrain (ARX) and Scarecrow (NKX2.1) as conserved temporal factors in the Drosophila central brain and visual system. *Developmental Cell*, *57*(9), 1193-1207.e7. https://doi.org/10.1016/j.devcel.2022.04.008

Titlow, J., Robertson, F., Järvelin, A., Ish-Horowicz, D., Smith, C., Gratton, E., & Davis, I. (2020). Syncrip/hnRNP Q is required for activity-induced Msp300/Nesprin-1 expression

and new synapse formation. *Journal of Cell Biology*, *219*(3), e201903135. https://doi.org/10.1083/jcb.201903135

Toledano, H., D'Alterio, C., Czech, B., Levine, E., & Jones, D. L. (2012). The let-7–Imp axis regulates ageing of the Drosophila testis stem-cell niche. *Nature*, *485*(7400), 605–610. https://doi.org/10.1038/nature11061

Tran, K. D., & Doe, C. Q. (2008). Pdm and Castor close successive temporal identity windows in the NB3-1 lineage. *Development*, *135*(21), 3491–3499. https://doi.org/10.1242/dev.024349

Tratnjek, L., Živin, M., & Glavan, G. (2017). Synaptotagmin 7 and SYNCRIP proteins are ubiquitously expressed in the rat brain and co-localize in Purkinje neurons. *Journal of Chemical Neuroanatomy*, *79*, 12–21. https://doi.org/10.1016/j.jchemneu.2016.10.002

Turner-Evans, D. B., & Jayaraman, V. (2016). The insect central complex. *Current Biology*, *26*(11), R453–R457. https://doi.org/10.1016/j.cub.2016.04.006

Vijayakumar, J., Perrois, C., Heim, M., Bousset, L., Alberti, S., & Besse, F. (2019). The prion-like domain of Drosophila Imp promotes axonal transport of RNP granules in vivo. *Nature Communications*, *10*(1), 2593. https://doi.org/10.1038/s41467-019-10554-w

Vikessa, J., Hansen, T., VO, Jonson, L., Borup, R., Wewer, U. M., Christiansen, J., & Nielsen, F. C. (2006). RNA-binding IMPs promote cell adhesion and invapodia formation. *The EMBO Journal*.

Vu, L. P., Prieto, C., Amin, E. M., Chhangawala, S., Krivtsov, A., Calvo-Vidal, M. N., Chou, T., Chow, A., Minuesa, G., Park, S. M., Barlowe, T. S., Taggart, J., Tivnan, P., Deering, R. P., Chu, L. P., Kwon, J.-A., Meydan, C., Perales-Paton, J., Arshi, A., … Kharas, M. G. (2017). Functional screen of MSI2 interactors identifies an essential role for SYNCRIP in myeloid leukemia stem cells. *Nature Genetics*, *49*(6), 866–875. https://doi.org/10.1038/ng.3854

Walsh, K. T., & Doe, C. Q. (2017). Drosophila embryonic type II neuroblasts: Origin, temporal patterning, and contribution to the adult central complex. *Development*, dev.157826. https://doi.org/10.1242/dev.157826

Wang, Y.-C., Yang, J. S., Johnston, R., Ren, Q., Lee, Y.-J., Luan, H., Brody, T., Odenwald, W. F., & Lee, T. (2014). *Drosophila* intermediate neural progenitors produce lineage-dependent related series of diverse neurons. *Development*, *141*(2), 253–258. https://doi.org/10.1242/dev.103069

Warren, T. L., Giraldo, Y. M., & Dickinson, M. H. (2019). Celestial navigation in *Drosophila*. *Journal of Experimental Biology*, *222*(Suppl_1), jeb186148. https://doi.org/10.1242/jeb.186148

Wolff, T., Iyer, N. A., & Rubin, G. M. (2015). Neuroarchitecture and neuroanatomy of the *Drosophila* central complex: A GAL4-based dissection of protocerebral bridge neurons and circuits. *Journal of Comparative Neurology*, *523*(7), 997–1037. https://doi.org/10.1002/cne.23705

Wu, Y.-C., Chen, C.-H., Mercer, A., & Sokol, N. S. (2012). Let-7-Complex MicroRNAs Regulate the Temporal Identity of Drosophila Mushroom Body Neurons via chinmo. *Developmental Cell*, *23*(1), 202–209. https://doi.org/10.1016/j.devcel.2012.05.013

Yang, C.-P., Samuels, T. J., Huang, Y., Yang, L., Ish-Horowicz, D., Davis, I., & Lee, T. (2017). Imp and Syp RNA-binding proteins govern decommissioning of *Drosophila* neural stem cells. *Development*, dev.149500. https://doi.org/10.1242/dev.149500

Yisraeli, J. K. (2005). VICKZ proteins: A multi-talented family of regulatory RNA-binding proteins. *Biology of the Cell*, *97*(1), 87–96. https://doi.org/10.1042/BC20040151

Yu, H.-H., Awasaki, T., Schroeder, M. D., Long, F., Yang, J. S., He, Y., Ding, P., Kao, J.-C., Wu, G. Y.-Y., Peng, H., Myers, G., & Lee, T. (2013). Clonal Development and Organization of the Adult Drosophila Central Brain. *Current Biology*, *23*(8), 633–643. https://doi.org/10.1016/j.cub.2013.02.057

Zhang, P., Cao, M., Zhang, Y., Xu, L., Meng, F., Wu, X., Xia, T., Chen, Q., Shi, G., Wu, P., Chen, L., Lu, Z., Yin, J., Cai, B., Cao, S., Miao, Y., & Jiang, K. (2020). A novel antisense lncRNA NT5E promotes progression by modulating the expression of SYNCRIP and predicts a poor prognosis in pancreatic cancer. *Journal of Cellular and Molecular Medicine*, *24*(18), 10898–10912. https://doi.org/10.1111/jcmm.15718

Zhu, S., Barshow, S., Wildonger, J., Jan, L. Y., & Jan, Y.-N. (2011). Ets transcription factor Pointed promotes the generation of intermediate neural progenitors in *Drosophila* larval brains. *Proceedings of the National Academy of Sciences*, *108*(51), 20615–20620. https://doi.org/10.1073/pnas.1118595109